POLITECNICO

MILANO 1863

Investigation on the effect of Benzoyl Peroxide on the synthesis of polyynes via Pulsed Laser Ablation in Liquid

TESI DI LAUREA MAGISTRALE IN
MATERIALS ENGINEERING AND NANOTECHNOLOGY
INGEGNERIA DEI MATERIALI E DELLE NANOTECNOLOGIE

Author: **Martino Cambiaggio**

Student ID: 945062
Advisor: Prof. Carlo S. Casari
Co-advisors: Pietro Marabotti
Academic Year: 2020-21

Abstract

In this thesis work, I investigate the effect of a radical initiator (Benzoyl Peroxide - BPO) on the synthesis of polyynes via Pulsed Laser Ablation in Liquid (PLAL). The ablations were performed by ablating with 1064 nm, 532 nm and 355 nm lasers for 15 min a solid graphite target in different solvents: methanol, ethanol, isopropyl alcohol and acetonitrile. I ablated solutions with increasing concentrations of Benzoyl Peroxide in isopropyl alcohol with 1064 nm and 532 nm and I discovered an increase in the concentration of polyynes with respect to the pure solvent for increasing BPO concentrations. Ablations with 532 nm were enhanced more than 1064 nm ablations, leading to higher gain in the polyynes concentration. The presence of BPO was also shown to have a greater effect on longer polyynes than shorter ones, reaching for the 20-atoms hydrogen-capped polyyne a concentration up to 180% of the one in pure solvent. This effect was shown both for hydrogen-capped and methyl-capped polyynes. By ablating 5 mM solutions of BPO in the other alcohols the same effect was shown: the presence of BPO led to higher concentration of polyynes and favoured longer chains. On the contrary, ablations in acetonitrile shown an opposite effect: the concentration of polyynes was decreased for 532 nm ablations, while was increased for 1064 nm. Cyano-capped polyynes were favoured by the presence of BPO for both wavelengths (1064 nm and 532 nm), and the concentration 16-atoms cyano-capped polyyne ($HC_{16}CN$) was found to be 310% of the concentration in pure acetonitrile for 532 nm ablations and even larger for 1064 nm. Longer ablation times (30 min and 120 min) were also considered. By considering all the parameter I investigated, I managed to obtain 24- and 26-atom long hydrogen-capped polyynes.

Keywords: Carbon atomic wires, polyynes, Pulsed Laser Ablation in Liquid, HPLC, benzoyl peroxide, alcohols

Abstract in lingua italiana

I Carbon atomic wires (CAWs) sono una famiglia di molecole caratterizzate da una catena lineare di soli atomi di carbonio ibridizzati sp. Rappresentano alcune delle strutture più piccole e confinate possibili e teoricamente dovrebbero avere proprietà rimarchevoli. Catene lineari di carbonio-sp sono state osservate attorno alle stelle nella polvere interstellare. Negli ultimi decenni, molti metodi chimici e fisici sono stati impiegati con successo per la sintesi di CAWs. Tra questi ho impiegato l'ablazione a laser pulsato in liquido (Pulsed Laser Ablation in Liquid - PLAL) come metodo di sintesi in questa tesi. Dalla trattazione teorica emergono due possibili isomeri di catene lineari di carbonio: il cumulene, composto unicamente da doppi legami, e la poliina, caratterizzata dall'alternanza di legami singoli e tripli. In questa tesi ho indagato l'effetto di un iniziatore radicalico (Perossido di Benzoile - BPO) sulla sintesi di poliine via PLAL. Le ablazioni sono state fatte impiegando diverse lunghezze d'onda del laser (1064 nm, 532 nm e 355 nm) a 15 min e ablando un target di grafite in diversi solventi: metanolo, etanolo, isopropanolo e acetonitrile. Ho quindi ablato soluzioni con concentrazione crescente di Perossido di Benzoile in isopropanolo a 1064 nm e 532 nm e ho scoperto un aumento della concentrazione di poliine rispetto al solvente puro per concentrazioni di BPO crescenti. Il miglioramento della produzione a 532 nm si è visto essere maggiore che a 1064 nm, portando le ablazioni a 532 nm ad avere aumenti maggiori della concentrazione di poliine. La presenza del BPO ha anche mostrato di avere effetti maggiori sulle catene più lunghe rispetto alle più corte, per esempio la concentrazione della poliina idrogenata lunga 20 atomi è risultata essere il 180% della concentrazione in solvente puro. L'effetto del BPO è stato individuato sia per le catene idrogenate sia per le catene terminate con un gruppo metile. Lo stesso effetto è stato mostrato ablando in soluzioni 5 mM di BPO e altri alcool: la presenza del BPO ha portato a concentrazioni più alte di poliine e ha favorito le catene più lunghe. Al contrario, ablazioni in acetonitrile hanno mostrato un effetto opposto: la concentrazione di poliine era inferiore nelle ablazioni a 532 nm con BPO, mentre è stato visto un aumento per ablazioni a 1064 nm. Le concentrazioni delle ciano-poliine sono state incrementate dalla presenza del BPO a entrambe le lunghezze d'onda del laser (1064 nm e 532 nm) e in ablazioni a 532 nm la concentrazione della ciano-poliina lunga 16 atomi di carbonio

(HC$_{16}$CN) è risultata essere il 310% della concentrazione in acetonitrile puro. Inoltre ho considerato tempi di ablazione più lunghi (30 min e 120 min). Considerando tutti i parametri studiati, sono riuscito a ottenere poliine idrogenate lunghe 24 e 26 atomi di carbonio.

Parole chiave: Carbon atomic wires, nanofili di carbonio, poliine, ablazione a laser pulsato in liquido, HPLC, perossido di benzoile, alcoli

Contents

Introduction

In the field of nanotechnology, carbon-based nanostructures take on great importance for research and technological applications. Carbon nanomaterials as graphene, carbon nanotubes and fullerenes show outstanding properties and represent some of the most confined possible structures. The great variety of carbon-based nanostructure is possible thanks to sp^3, sp^2 and sp hybridization of carbon atoms. Contrary to sp^3 and sp^2 carbon, the existence of a solid allotropic form of sp carbon is still under debate. Instead, linear sp carbon compounds were observed in space and have been synthesized through several chemical and physical methods. These linear compounds are also called Carbon Atomic Wires (CAWs) and represent the most confined 1D materials, with a diameter of a single atom. Theoretically, CAWs should show remarkable properties, suitable for applications in electronics, optics and mechanics. However, stability is an open issue, since CAWs undergo easily degradation processes as crosslinking and oxidation. Hence, due to their instability, the synthesis and applications of CAWs are not trivial. The theoretical description of CAWs starts from the infinite chain model, which describes an infinite linear chain of sp carbon atoms. According to this framework, two different structures are possible: cumulene, whose carbon atoms are bound through consecutive double bonds, and polyyne, which features the alternation of single and triple bonds. Regarding real finite CAWs, it is found that polyynes are the stable isomer when considering long chains, due to Peierls' distortions. Instead, shorter chains are more strongly affected by the effects of endgroups, which can induce both structures and provide further properties. Chemical synthesis methods synthesize CAWs through chemical reactions, which allow to control the structure and terminations of the chains. However, chemical methods are not feasible for industrial scale-up. Physical methods, instead, represent a cheaper route and do not require complex reagents. Pulsed Laser Ablation in Liquid (PLAL) is based on the interaction of a pulsed laser with a target in a liquid environment. Due to the presence of the liquid an out-of-equilibrium plasma is formed, which promotes the formations of sp-carbon chains. In PLAL synthesis the most concentrated chains are usually hydrogen-capped polyynes. Although few other terminations are reported in literature, PLAL synthesis has not allowed a great control over the terminations yet. PLAL was the

employed method for the synthesis of polyynes in this thesis work.

In this thesis work several material and laser parameters were studied to build a better framework of the method. Since the mechanism of growth of polyynes is supposed to involve radical clusters, I investigated the effect of a radical initiator (Benzoyl Peroxide) on the synthesis of polyynes via PLAL. In this way I wanted to investigate the parameters that govern the chain growth and the termination, trying to obtaining more concentrated and longer chains. Moreover, by employing Benzoyl Peroxide I tried to understand the effect of reactive molecules on the synthesis of CAWs.

This work is structured as follows:

Chapter 1: an overview on carbon hybridization and on the main carbon-based nanostructure is given, followed by a theoretical description of CAWs and by a summary of the synthesis and characterization methods.

Chapter 2: the process of pulsed laser ablation in liquid is described thoroughly, highlighting the physics of the process and the role of the main parameters. Then, the state of the art of the synthesis of polyynes via PLAL is presented.

Chapter 3: the materials and experimental methods employed in this thesis work are presented. I also describe the main properties of Benzoyl Peroxide.

Chapter 4: the experimental results are described. In the first part I consider experiments performed only with a single solvent and discuss the effects I observed. In the second part I consider experiment with three further solvents, comparing the results.

1 | Carbon atomic wires

Carbon atomic wires (CAWs) are a family of molecules characterized by linear chains made only of carbon atoms linked together. They represent some of the smallest and most confined linear structures. Theoretically CAWs should show astonishing properties [1, 2]. In nature, carbon atomic wires are found to be part of interstellar dust, as confirmed by many astrophysical observations [3–5], and they have been also isolated in some plants [6]. CAWs synthesis is not trivial, and synthesis attempts date back to the end of nineteenth's century [5]. In 1869 Glaser reported the synthesis of diphenylbutadiyne [7] and few years later in 1885 also Baeyer tried to synthesize linear forms of carbon [5]. However, only in 1963 Sladkov and Kudryavtsev reported the synthesis of eight different CAWs through chemical synthesis [8]. In 1985, while looking for short linear carbon chains [2] and trying to understand *"the mechanisms by which long-chain carbon molecules are formed in interstellar space and circumstellar shells"* [9], Kroto and Smalley discovered instead fullerenes [9]. This serendipitous discovery gave new interest for carbon-based nanostructures and *"marked the beginning of a new era of synthetic carbon allotropes"* as stated by Hirsch [10].

Over the last 35 years, since the discovery of the C_{60} fullerene [9], several carbon nanostructures were discovered, including carbon nanotubes (discovered by Iijima in 1991 [11]) and graphene (studied by Geim and Novoselov in 2004 [12]). These carbon-based nanomaterials show outstanding properties, which lead to their applications in many different fields, such as electronics, optics and mechanics [10]. The capability of carbon in forming conducting and semiconducting materials leads to the possibility of employing carbon nanostructures as substitutes of silicon-based electronics [10]. The interest in carbon nanostructures arise also from the great availability of carbon in nature [13]. Indeed, carbon is the sixth most common element in the universe and the fourth one in our solar system [13]. Moreover, carbon is also commonly found bound to many other elements forming more than half-a-million organic compounds [14].

The research in carbon atomic wires has been also favoured by this renewed interest, and several different synthesis techniques have been studied by researchers. Nowadays,

linear carbon chains are synthesized in liquid by means of chemical reactions or physical techniques [1, 5]. Recently, Tykwinski and co-workers managed to synthesize the longest wire ever obtained with a length of 48 atoms [15]. CAWs were also observed in mixed structures, for example suspended between graphene flakes or encapsulated in carbon nanotubes [1, 5, 16].

In this chapter, a general framework on carbon hybridization and a description of the main carbon-based nanostructure is given. Then, I will present a description of carbon atomic wires, their properties and an overview on synthesis and characterization techniques.

1.1.   Carbon hybridization and allotropes

The versatility of carbon originates from the number of chemical bonds it can sustain (from one to four) and, hence, from its capability to produce long chains and networks between other elements and itself. Carbon features four electrons in its outer shell and its electronic configuration is $1s^2 \, 2s^2 \, 2p^2$, which theoretically should allow to form only two chemical bonds. However, this is not the case and an explanation is given using the Valence Bond theory (VB) [17, 18]. VB theory states that by linearly combining atomic orbitals new hybrid orbitals can be generated, introducing new possible symmetries in the electronic distribution around the atom. These new hybrid orbitals can be imagined as the result of constructive and destructive interference between electron wavefunctions [18]. The configurations that result from this process are sp^3, sp^2 and sp, which are obtained combining the 2s orbital with three, two and one 2p orbitals, respectively. sp^2 and sp carbon maintain one or two non-hybrid 2p atomic orbitals, respectively. Hence, when interacting with other atoms carbon can form different bonds building up molecules with different geometries. It is worth noting that carbon hybrid orbitals arise only from the interaction between distinct atoms.

In this framework, carbon-carbon bonds are obtained by the overlap of atomic and hybrid orbitals, that produces two type of molecular orbitals (MOs): σ and π molecular orbitals. The overlap of atomic orbitals in the region between two atomic nuclei produces a σ MO, which is directed along the internuclear axis which connects the two atoms involved in the bond. σ orbitals between carbon atoms are formed by the overlap of hybrid orbitals. π molecular orbitals, instead, are formed by the overlap side-by-side of p atomic orbitals and hence are not localized in the internuclear region. Therefore, double and triple bonds can be made by 2p orbitals of carbon which are not involved in the hybridization, forming π-bonds [17]. In the framework of Linear Combination of Atomic Orbitals theory (LCAO), double and triple bonds generate also the phenomenon called conjugation: π-bonds delo-
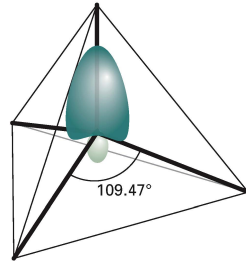
Figure 1.1: A sp^3 orbital with its characteristic tetrahedron symmetry [18].
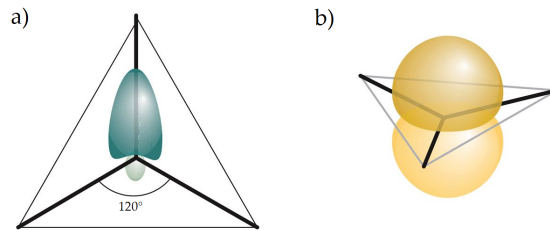

Figure 1.2: a) A sp^2 hybrid orbital placed in the trigonal planar geometry. b) The remaining 2p orbitals that are perpendicular to the plane [18].

calize the involved electrons over the affected part of the molecule. The delocalization of π electrons is responsible of many electronic properties of conjugated molecules, such as their electrical conductivity.

The sp^3 hybridization (see Fig. 1.1) results in four identical hybrid orbitals, each of them pointing to the vertex of a tetrahedron and separated by an angle of 109.47° [18], which grants the largest possible distance between atoms. This hybridization allows four single-bonds and produces only σ molecular orbitals. Examples of sp^3 carbon are the alkanes, such as methane or ethane. Diamond is the sp^3-hybridized allotropic form of carbon, sp^3 hybridization allows a tridimensional FCC crystalline lattice. Diamond is an insulator (electrical resistivity$\rho= 10^{18}$ Ωm [14]) due to the fact that all σ bonds do not allow delo-calization of electrons, which produces a large optical bandgap (5.5 eV) [13]. Conversely, the strong sp^3 bonds lend an extremely high thermal conductivity (2200 W/mK) due to the efficient lattice vibrations transport (i.e. phonons) and make diamond the hardest material ever synthesized (10 Mohs) [13].

On the other hand, sp^2 hybridization (see Fig. 1.2) produces three identical hybrid orbitals placed on a planar trigonal symmetry with angles of 120°. This configuration allows the formation of three σ and one π molecular orbital (Fig. 1.3.a). An example of sp^2-hybridized carbon material is graphene, which is a single layer of carbon atoms disposed exactly as depicted previously with a planar-trigonal symmetry. This produces an highly conjugated system due to the delocalized electrons. Graphite is the crystalline form of sp^2
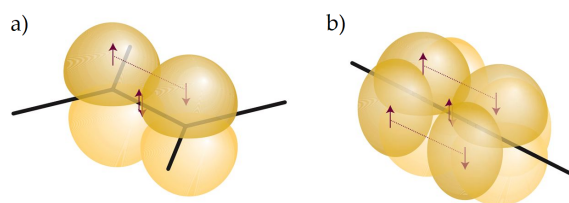
Figure 1.3:   a) The formation of a π orbital by the overlap of two 2p orbitals between two sp^2 carbon. b) Two couple of 2p orbitals in sp hybridization form two π orbitals. Arrows represent the spin of electrons (up or down) [18].

carbon, and it is made up by stacked graphene layers. Each layer is bound to the others through weak intermolecular forces generated by the interaction of π electrons of each layer. Due to the conjugation of each layer, graphite is a zero gap semiconductor, resulting in the absorption of all visible photons and hence in a grey-black appearance. Graphite has a strong anisotropic behaviour in many of its properties due to its crystalline structure. For example, mechanical strength is high in the direction parallel to the graphene planes, while it is low in the perpendicular direction. Also electronic transport is highly anisotropic: indeed the electrical conductivity is much higher in the direction parallel to the graphene layers than to the perpendicular one [13].

Lastly, sp hybridization produces only two hybrid orbitals in a linear configuration with a bond angle of 180°, leaving two p-orbitals free to make π-bonds. This allows to produce two double-bonds or an alternation of single- and triple-bonds (Fig. 1.3.b). Triple-bonds are characterized by the largest bond energy among covalent bonds, but they are more prone to react with other species due to the higher concentration of electrons around the two carbon atoms. An example of an sp carbon compound is acetylene $H-C\equiv C-H$, where the two carbon atoms are connected via a triple bond. Contrary to sp^3 and sp^2 carbon, a crystalline sp carbon allotrope has not been discovered yet, although its existence has been theorized as described later [1].

1.2.   Carbon Nanostructures

Carbon presents also a plethora of possible nanostructures with remarkable properties. Indeed, as pure carbon it forms many nanostructures with different hybridization whose dimensionality can range from zero-dimensional systems (fullerenes, carbon clusters and nanodiamonds), to one-dimensional (carbon nanotubes and carbon atomic wires), and two-dimensional system as graphene [1, 19]. Carbon nanostructures feature quantum confinement along at least one dimension, which in conjunction with hybridization give
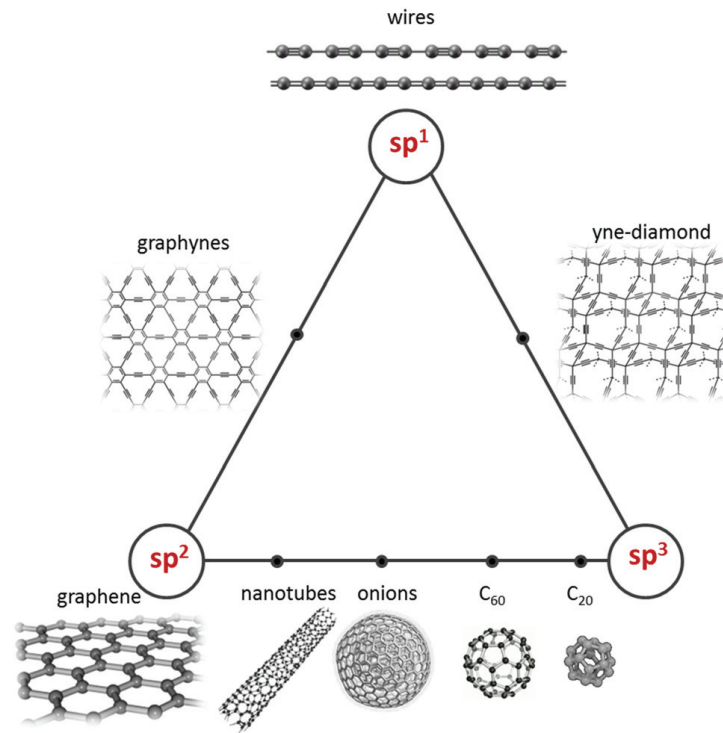
Figure 1.4: Ternary diagram of carbon nanostructures, according to their hybridization [1].

rise to outstanding properties [1, 10].

Hybridization can also be used to classify carbon nanostructures as shown in Fig. 1.4 [5]. Graphene is for example an allotrope made up completely by sp^2 carbon, while nanodiamonds are sp^3 carbon. Since its planar nature, pure sp^2 carbon cannot form curved structures, hence carbon nanotubes or fullerenes are often classified as in between sp^2 and sp^3 in the triangular diagram [5]. Mixed sp^2-sp planar structures (graphyne) and rings can be found in the path from sp^2 to sp carbon. Along the third edge, thus mixing sp-sp^3hybridization, we found yne-diamond [5]. Lastly, carbon atomic wires occupy the sp vertex [1]. In this section the main carbon nanostructures are presented, while in the next section CAWs are described more in detailed.

1.2.1. Graphene

Graphene is a single layer of carbon atoms arranged in a honeycomb lattice as shown in Fig. 1.5. It is a carbon allotrope made up by only sp^2 carbon, which ensures a planar structure. Since its thickness is exactly an atom, it experiences a strong quantum confinement along this dimension, while the other two direction parallel to the sp^2 bonds are unconfined, and thus it is an example of a real 2D material. The strong π-conjugation combined
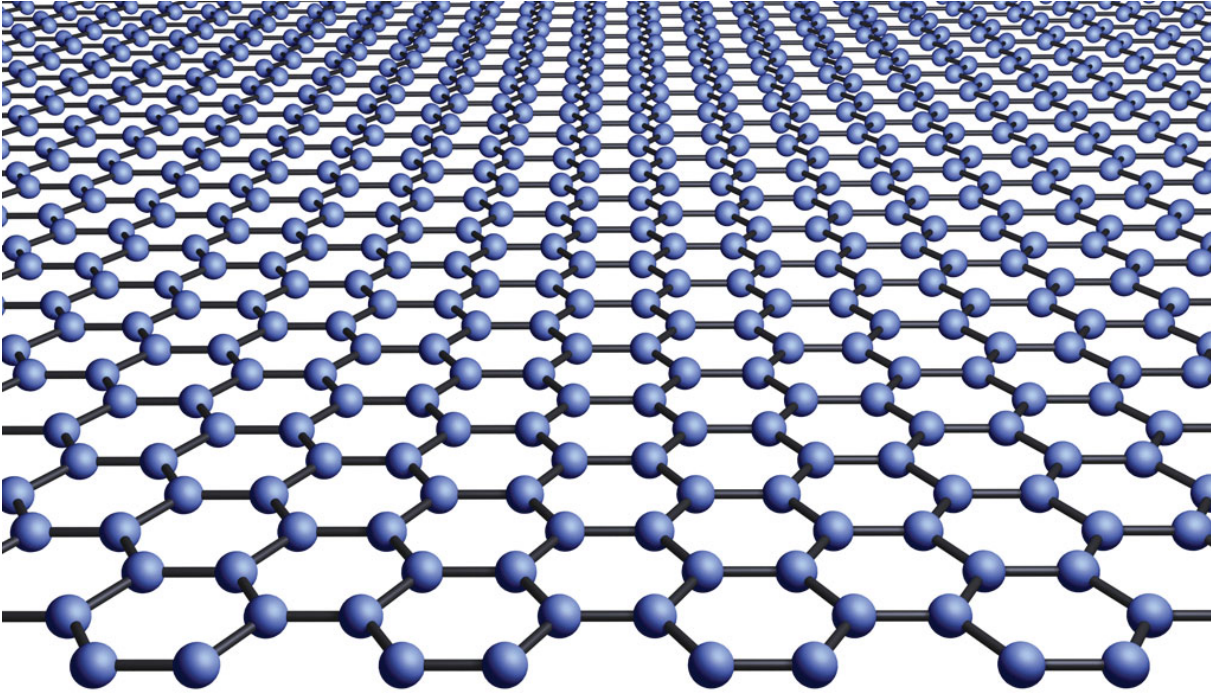
Figure 1.5:   The honeycomb lattice structure of a graphene sheet [20].

with quantum confinement leads to some remarkable electronic, optical and mechanical properties. Graphene is a zero-gap material with high electron mobility and ambipolar behaviour [1, 21], due to the presence of Dirac cones between valence and conduction bands [1, 13]. It was shown that electrons and holes have almost the same mobility, with values ranging between 1×10^3-$1 \times 10^5 \, cm^2/Vs$ [22], although in some particular configuration electron mobility over $200\,000 \, cm^2/Vs$ were achieved [23]. Graphene has a very low optical absorption which makes it almost transparent. These properties make graphene an actractive candidate for electronic and optoelectronic applications and energy storage. A widely studied application of graphene are field effect transistors (FETs) [24], in which the graphene sheet can be also modified to act as a semiconductor. This latter behaviour can be obtained by introducing a more strong confinement along a further dimension in the graphene sheet, opening the bandgap, and leading to a semiconducting behaviour. For example, graphene nanoribbons are nanomaterials obtained by reducing one dimension obtaining a ribbon [25].

Graphene has a breaking strength of approximately $40 \, N/m$, a value 200 times larger than the one of structural steel, but it may also be stretched up to 20% of its length and its Young modulus is around $1 \, TPa$ [13, 17, 21]. These mechanical properties make graphene a good candidate as a filler for innovative nanocomposites. Moreover, graphene shows an in-

credibly high thermal conductivity and it is also impermeable to gases [17, 21]. Graphene is interesting not only for its appealing properties but also for graphene-based nanostructures and as a starting point for the study of 2D materials. For example, graphene oxide, which has been recently synthesized, can be further functionalized or reduced to get back graphene and it is one of the most used compound to produce graphene-like materials on a large scale [13].

1.2.2. Fullerenes

Fullerenes are stable carbon clusters made up by quasi-sp^2 hybridized atoms disposed in closed cage structures. Ideally, a fullerene could be visualized as a graphene sheet closed into a closed cage geometry, and thus some distortion in chemical bonds is needed to close completely the carbon cage (Fig. 1.6). For this reason, the hybridization of carbon atoms in fullerenes is not pure sp^2 but is commonly indicated as quasi-sp^2. The word *fullerene* is often referred to the Buckminsterfullerene or C_{60}, a molecule with 60 carbon atoms disposed in the vertex of a truncated icosahedron, (also called bucky-ball), made of twenty hexagons and twelve pentagons [9, 19]. However, fullerenes may be also smaller and larger molecules, e.g. C_{70}, C_{76}, C_{78}, C_{80}, ... [19] (see Fig. 1.7). C_{20} is the smallest possible fullerene [26], made by 12 pentagons, which is far from the honeycomb lattice peculiar of sp^2 carbon. This distorted geometry leads to stability problems, and many authors consider C_{20} a metastable configuration, which may rearrange in other C_{20} isomers [27]. Fullerenes feature quantum confinement on all the three directions (mean radius $\approx$ 1 nm), which makes them 0D systems.

Fullerenes from C_{60} on are stable and can generate crystal structures through weak Van der Waals forces (e.g. the fullerite) [19]. Fullerenes are easily processable since they are normally soluble in hydrocarbons, and they can also be functionalized attaching substituent on the external surface of the cage. Moreover, hetero atoms, small molecules or fullerenes can be caged inside large fullerenes, obtaining the so-called endohedral fullerenes [17, 28]. The functionalization of fullerenes allows to give specific properties to the cages, for example increasing the solubility or some physical properties. Indeed, electronic transport properties can be enhanced as, for example functionalized C_{60} is used as electron acceptor in solar cells (as PCBM) [10].

1.2.3. Carbon Nanotubes (CNTs)

Carbon Nanotubes (CNTs) are made up by quasi-sp^2 carbon in closed cage structures as fullerenes, but rolled up into a cylindrical geometry. CNTs are an example of a structure
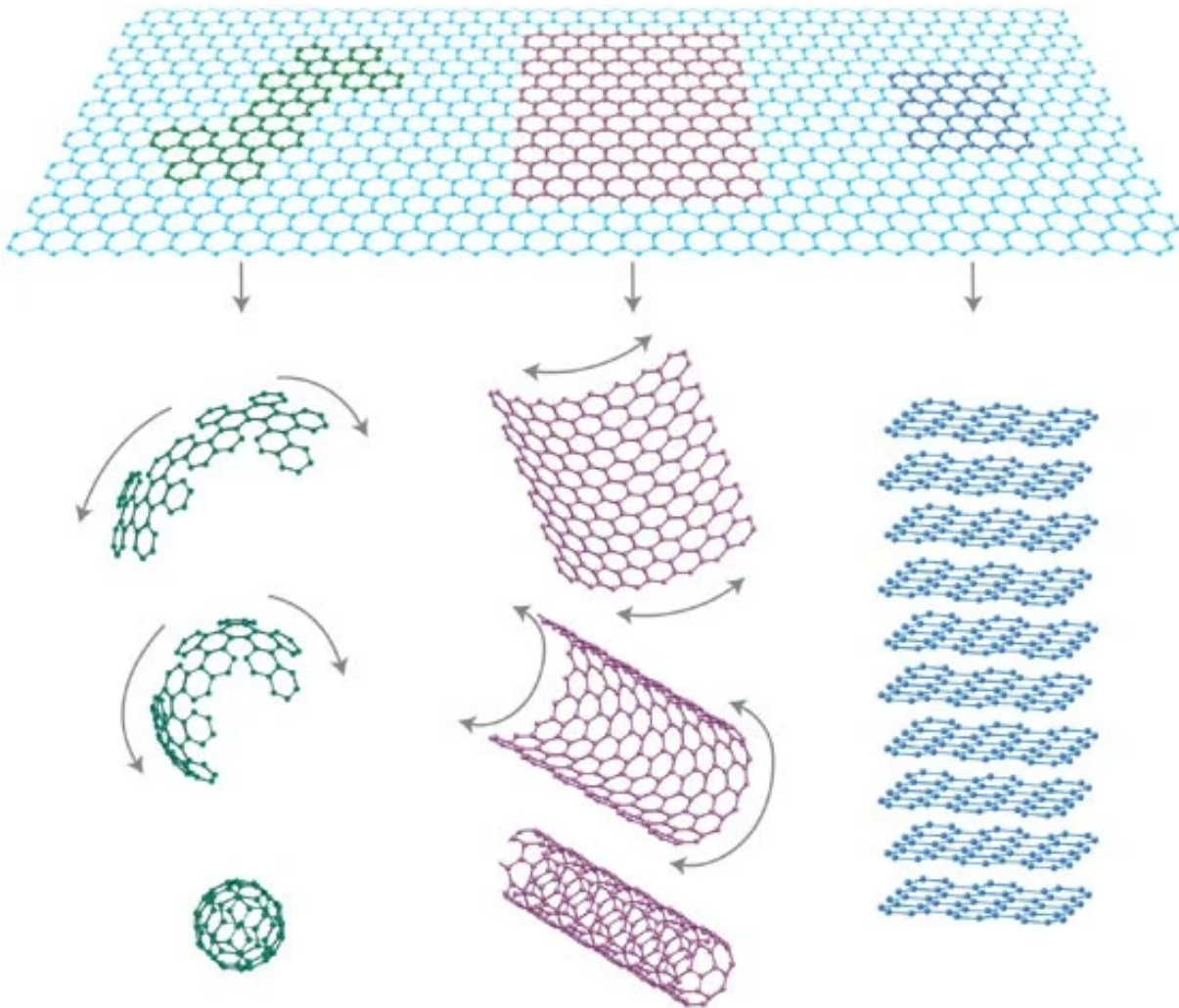
Figure 1.6:   Graphene may be imagined as the building block for many carbon nanostructure, i.e. fullerenes (a) and carbon nanotubes (b). Instead, many layers of graphene stacked together produce a fraction of graphite (c) [12].
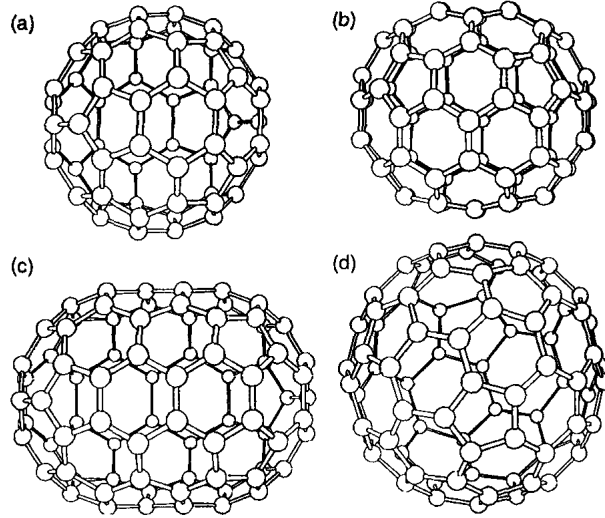
Figure 1.7: Different fullerenes: a) the icosahedral Buckminsterfullerene C60, b) C70 and c-d) C80 in two different configurations [19].

confined in two dimensions, i.e. along the radial directions, and therefore, they represent truly 1D systems. Carbon nanotubes are a wide family consisting not only of single-walled tubes but also of tubes made by concentric cylinders, and therefore we have single-walled nanotubes (SWNTs) and multi-walled nanotubes (MWNTs), respectively.

As for fullerenes, CNTs can be visualized as a graphene plane rolled up (Fig. 1.6), which can be closed by two end caps at each termination (usually some sort of half fullerene). The planar sp^2 structure is therefore distorted, leading to a quasi-sp^2 hybridization. In the geometrical description of CNTs, the chiral vector, that ideally connects the graphene atoms which superimpose when the sheet is rolled up, represents a fundamental quantity for the characterization of CNTs. Moreover, its length is equal to the circumference of the CNT. Thus, the chiral vector can be written $C_h = na_1 + ma_2$, where a_1 and a_2 are the primitive vectors of graphene, while n and m are two integer numbers and define the direction of the chiral vector, as shown in Fig. 1.8. The properties of CNTs can be theoretically derived from the graphene ones and are determined by the chiral vector. Indeed, the CNTs are divided into three types depending on their chirality represented by the indices $(n; m)$: armchair $(n = m)$, chiral$(n \neq m)$ and zig-zag $(m = 0)$ (Fig. 1.9). An important difference between these three classes of CNTs lies in their electrical behaviour: indeed, armchair nanotubes are metallic due to the presence of Dirac's cones in the band structure, while zig-zag nanotubes have both metallic and semiconductor behaviour depending on their chirality. One-dimensional systems such nanotubes have been extensively studied for their transport properties of both electrons and optical excitations,
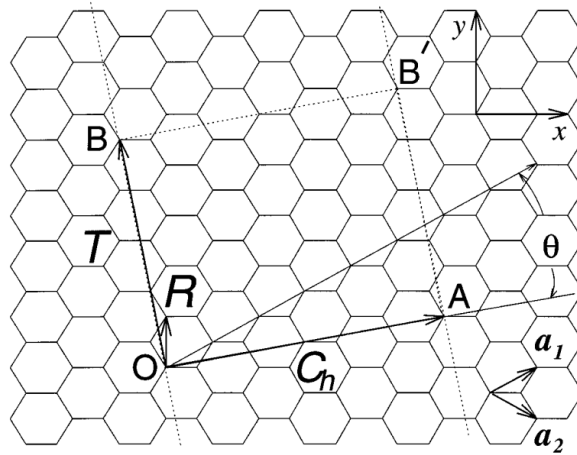
Figure 1.8:   Chiral vector C_h as linear combination of graphene unit vectors a_1 and a_2. [28].
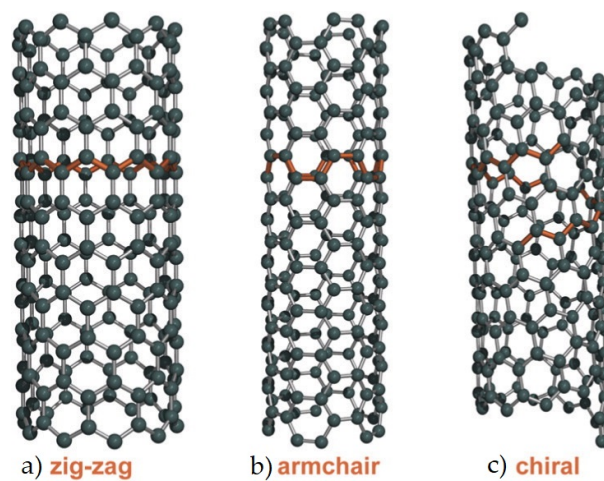

Figure 1.9:   Three configuration of CNTs: a) zig-zag, b) armchair and c) chiral [29].

since at least one unconfined dimension is needed to have appealing transport properties. Thus, 1D systems are the most confined structures which can be used for this purpose [17].

Carbon nanotubes are promising candidates for electronic and optoelectronic applications. They also show many other attractive applications-oriented properties such as their high thermal conductivity, high elastic modulus up to $1\,TPa$ and tensile strength of $100\,GPa$ [13]. Carbon nanotubes have also a high surface area and, therefore, they are largely employed in nanocomposites and in functionalized nanostructured materials [17, 30]. CNTs surface can be functionalized for many applications, for example by attaching graphene flakes in order to further increase the surface area. The space inside the tube can be used to transport substances and protect small molecules. Moreover, other hybrid structures can be produced, for example by inserting fullerenes in nanotubes obtaining the so-called nanobuds [17], or by incapsulating a linear carbon chain within a nanotube [16].

1.3.   Carbon Atom Wires - CAWs

As mentioned before, there exist many compound containing sp-hybridized carbon. However, a pure sp-hybridized carbon allotrope, commonly called carbyne, has not been discovered yet [5]. Thanks to the great interest in carbon nanostructures, the research toward carbynes has increased in the last decades, also driven by its outstanding predicted properties [2]. This elusive carbon crystal is commonly called *carbyne*. However this term is often used to indicate different structures, both a sp-carbon material and an ideal infinite sp-carbon wire [1]. Unfortunately, a bulk carbyne should be very unstable, due to the tendency of sp-carbon to react and crosslink forming sp^2-carbon compounds [2]. This fact led the researcher to question the real existence of a crystalline form made by sp-hybridized carbon only [1]. Carbyne as an ideal infinite sp-carbon wire would represent the perfect 1D material, indeed having a diameter of a single atom. Real finite chains are generally called Carbon Atom Wires (CAWs) and are made up by sp-hybridized carbon atoms.

1.3.1.   The ideal model of carbyne

As a first step, it is worth considering the ideal case of an infinite wire. Due to the sp hybridization, an infinite sp-carbon chain features two different isomers: one containing only double bonds, which is called polycumulene or simply cumulene, and the other characterized by the alternation of single and triple bonds, called polyyne, as shown in Fig. 1.10 [1]. The two 2p orbitals of each carbon atoms form delocalised molecular orbitals as stated by the LCAO theory. Thus, the result is a highly conjugated molecule
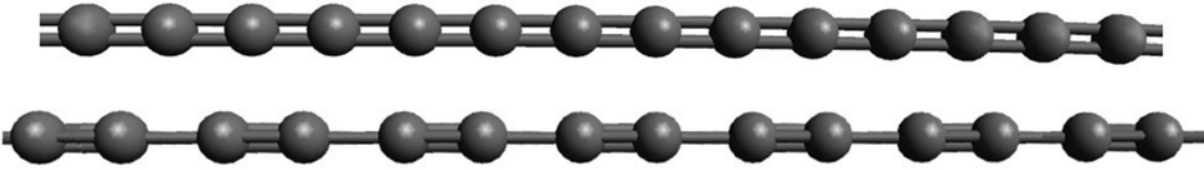
Figure 1.10:   The structures of a cumulene and a polyyne [1].

with delocalized π electrons [1, 5]. Cumulene shows the maximum conjugation due to the uninterrupted sequence of double bonds, which allows to delocalize π electrons over the whole chain. The presence of single bonds, instead, lowers the conjugation of polyyne with respect to the cumulenic one. However, the lengths of bonds in polyyne are affected by the presence of delocalized electrons resulting in shorter single bonds and longer triple bonds compared to other carbon-based materials. As a consequence, cumulenes have a half-filled conduction band, which makes them electrical conductors. On the other hand, the greater electron localization in polyynes opens a gap and therefore polyynes behave as semiconductors. This difference is also clear looking at the crystalline unit cell. In cumulenes, the unit cell has a single atom which contributes with an electron per 2p orbital, thus a half-filled conduction band is obtained, while polyynes have a two atoms basis in their unit cell, which leads to a gap at the edges of the Brillouin zone, a completely filled valence band and an empty conduction band [1, 5]. The difference between cumulene and polyyne is also in the vibrational properties. A homoatomic one-dimensional chain with a single atom in the basis (i.e. cumulene) has only the acoustic branch in the phonon dispersion relation. Polyyne features two atoms per basis, instead, which leads to the presence also of an optical branch [5]. As a consequence, cumulenes are theoretically not optically active, and hence ideal infinite cumulenic chains are not detectable by vibrational spectroscopy [1].

Carbynes can be characterized in terms of their bond length alternation (BLA), which is the mean difference between adjacent carbon bonds in the chain [1]. Since the length of a bond depends on the conjugation, the BLA is also related to the conjugation of the system. Therefore, it is a useful parameter to investigate the structural, but also electronic properties of sp-carbon chains. Indeed, cumulenes have BLA= 0, while polyynes feature BLA$\neq$ 0, thus showing CAWs electronic configuration [1, 5]. The different BLA configurations are the effect of a greater conjugation for cumulenes than for polyynes. Furthermore, increasing the BLA means to reduce the conjugation of the system, and thus increasing the band gap [1].

The two isomers, i.e. cumulene and polyyne, are not equally stable. Indeed, the infinite equalized chain structure (i.e. all equal double bonds) converts in a more energetically
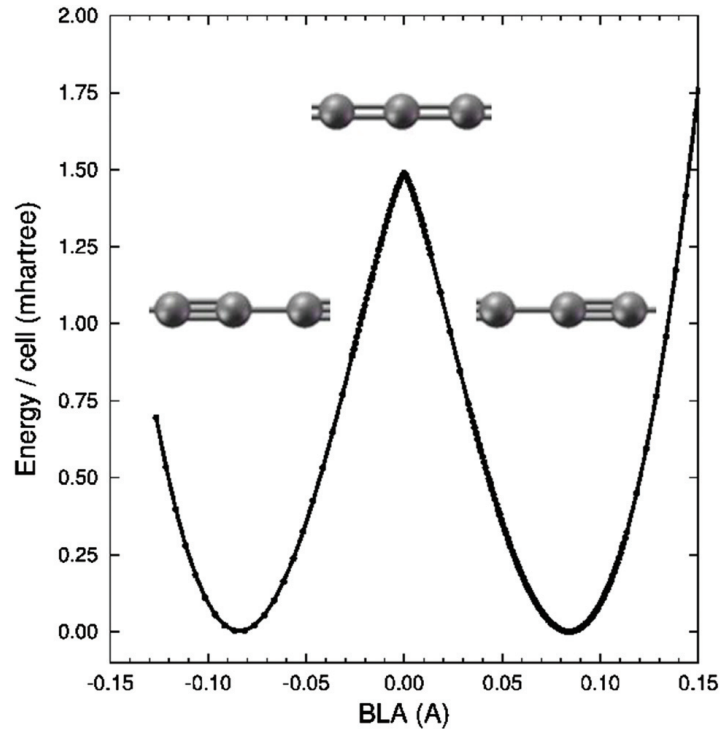
Figure 1.11: The total energy of carbyne compared to their on BLA [1].

stable dimerized chain (i.e. alternated structure) [5]. This phenomenon is called Peierls' distortion and CAWs share it with other polyconjugated materials, such as polyacetylene and polyenes [1]. Hence, due to Peierls' distortions the configuration with less energy, and thus more stable, is the polyynic one, as shown in Fig. 1.11.

Besides the electronic and optical properties, the structure of carbyne provides other remarkable properties. The vibrational structure of carbyne should allow the ballistic transport of phonons up to the micron-scale [2]. Thus, the thermal conductivity of carbynes should also be very high (200 mK/m/K) [2], being up to two orders of magnitude greater than the graphene one. The stiffness of the sp bonds makes CAWs great also for mechanical applications. Indeed, the predicted elastic modulus of carbyne should be 32 TPa [2], which is greater than the one of graphene and CNTs, and would be also one of the largest ever recorded.

1.3.2. Finite carbon atomic wires and effects of terminations

The ideal model of an infinite chain is useful to understand the predicted properties of sp-carbon chains, but it is far from a real system. Indeed, real chains are finite systems and thus they are terminated by atoms or chemical groups (i.e. endgroups). It is worth noting that since finite CAWs are molecules, they show discrete energy levels and the electronic
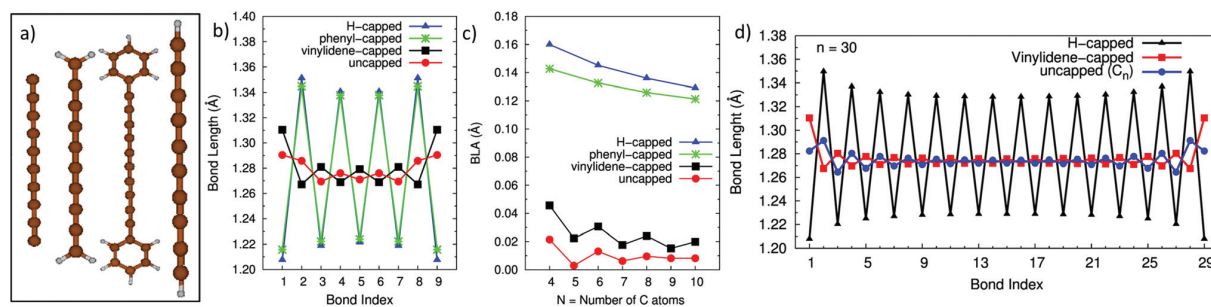
Figure 1.12: a) Four different simulated CAWs, from left to right, uncapped, vinylidene-, phenyl- and hydrogen-capped. b) Bonds length as a function of the termination in the four systems showed in panel a). c) BLA of the previous four CAWs as a function of the number of carbon atoms. d) Bonds length in a long CAW (30 atoms) [1].

band description cannot be used. Hence, the electronic and optical properties are related to specific levels as the HOMO (Highest Occupied Molecular Orbital - i.e. the highest-in-energy MO occupied by electrons) and the LUMO (Lowest Unoccupied Molecular Orbital - i.e. the lowest-in-energy MO not occupied). For example, the difference between the energy of the LUMO and the HOMO corresponds to the energy gap of a semiconducting molecule, and thus to the minimum photon energy which can be absorbed.

A significant effect is given by the length of the chain, which affects the electronic, optical and vibrational properties [1]. A higher number of carbon atoms in the chain corresponds to a greater number of delocalized electrons, and thus to a higher conjugation. Therefore, longer chains have a smaller BLA and a smaller HOMO-LUMO gap [1]. As a consequence, the semiconducting behaviour can be tuned by changing the length of the chain and the absorption spectrum is shifted to longer wavelengths for increasing chain length.

The description of the previous section ascribes to Peierls' distortions the role in determining the structure of an infinite wire [1], however for finite wires Peierls' distortions become relevant only for long chains with more than 37 alkyne units ($[-C\equiv C-]_n$ hence more than 74 carbon atoms) [15]. For shorter CAWs endgroups have a stronger influence on the structure of the chains and on the vibrational and electronic properties [1]. The chemical nature of terminations imposes certain bonds to the first carbon atom of the chain, determining a cumulenic or polyynic structure. If a endgroup makes a single bond with the first carbon, the chain is a polyynic one, while if it makes a double bond instead, the favoured structure would be a cumulene (see Fig. 1.12) [1, 31]. Hence, endgroups determine the extent of the semiconducting behaviour. Moreover, terminations modulate the BLA and, as a consequence, the HOMO-LUMO gap and the absorption spectrum [1]. Therefore, it is possible to tune CAWs properties by simply changing length and ter-

minations, leading to a huge number of combinations. Hydrogen-capping is the simplest termination of polyynes, whereas that of cumulene is two hydrogens. Moreover, methyl and nitrogen terminations were obtained by many authors [32–34]. More complex and bulkier endgroups were successfully attached to CAWs through chemical methods instead as, for example, phenyl, biphenyl, dinaphtyl and super-trityl terminations [1, 35–37].

The main problem of carbon atomic wires is their poor stability [1, 2, 5]: indeed, the presence of more energetic π orbitals makes polyynes and cumulenes very reactive and prone to degrade in more stable sp^2 carbon structures. This occurs also through the interaction between different chains, which can lead to crosslinking and reorganization processes into sp^2 carbon [1, 32]. Endgroups can improve the stability of chains as bulky groups can increase the steric hindrance between chains, hence reducing the interaction among them [1, 2, 35, 38, 39]. By exploiting this principle, Tykwinski and co-workers successfully synthesized 44 and 48 atoms long polyynes [15, 39]. To reduce crosslinking phenomenon another strategy is exploited in literature: nanocomposite are produce by embedding the chains in solid matrices, which reduces the interaction between wires. For example, CAWs were inserted in polymers such as PVA [40, 41] or in silica gels [42]. Another strategy employed in literature to stabilize CAWs is to embed the wires inside a nanotube [16, 43]. By exploiting this strategy Shi and co-workers managed to obtain the longest CAWs ever synthesized reaching a length of 6000 carbon atoms [16].

Stability of CAWs is also related to other processes as oxidation and hydrogenation. Oxidation of CAWs simply happens due to oxidizing agents, while hydrogenation is due to the highly unsaturated nature of the chains, which can bond with atomic hydrogen and break the sp hybridization. Air promotes oxidation of chains, while liquids are safer environments because they reduce chain-chain interactions and oxidation, and thus the solubility of oxygen in a solvent is a key parameter for sp-carbon stability [32, 44].

1.3.3.   CAWs Synthesis Techniques

Carbon atomic wires can be synthesized by several techniques, which are mainly grouped in two categories: chemical synthesis and physical synthesis methods.

Chemical Synthesis

Chemical synthesis methods involve the exploitation of several chemical reactions to synthesize sp-carbon wires. Nowadays, chemical methods follow two strategies: the synthesis of CAWs through polymerization processes, as condensation of acetylenic units, or the dimerization of ethynil groups (also called Glaser reaction) [1]. The first approach can

synthesize sp-chains in a single step, however the result is a broader length-distribution of chains, while Glaser reaction targets a CAW with a precise length and termination instead [1]. Several different terminations other than hydrogen have been successfully produced by chemical methods, producing polyyne with bulkier end-groups, such as phenyl, biphenyl or dinaphtyl groups [36, 37, 45]. Chemical synthesis offer higher control over the process and the final result, allowing to obtain longer chains with respect to physical methods. Furthermore, due to the possibility to select bulky terminations, the products tend to be more stable. Indeed, Tykwinski and Gao obtained the 48 atoms long polyyne through a chemical synthesis [15]. Using Cadiot-Chodkiewicz reaction conditions, Cataldo and co-workers managed to synthesize polyyne with a single-step method [36].

However, chemical synthesis techniques have some drawbacks. Indeed chemical techniques are difficult to be scaled up to industrial production, are expensive and may use toxic solvents and reagents. Moreover, they involve complex chemical reactions, consisting of many steps, and need a great number of compounds and thus a purification steps is necessary in order to get to the final product. Furthermore, each polyyne needs its own reaction, making it challenging to find appropriate reactions.

Physical Synthesis

Physical synthesis methods consist in the synthesis of CAWs through the production of a carbon vapour or of a plasma [1]. Carbon clustering is then induced by the fast quenching of the plasma (or the vapour) to induce strong out-of-equilibrium conditions [1]. Due to the higher stability of polyyne with respect to cumulene, via physical methods it is easier to produce polyynes [1]. Physical methods have quite simple setups, are faster and can be used with safer and eco-friendly materials (graphite, water, ethanol, . . .). For these reasons, physical methods are easier to be scaled up for an industrial production, which makes them interesting to be further studied [1]. A main drawback of physical techniques is the low control on the products, which means that many different polyynes are synthesized during the process, and also a lot of other carbon-based structures and molecules are synthesized simultaneously, which is detrimental for analysis and stability [46]. Another important drawback is the lower concentration of synthesized polyynes with respect to chemical methods, that can be a problem for their characterization (e.g. Raman) and further applications.

The most common physical techniques used for this purpose are Submerge Arc Discharge in Liquid (SADL) and Pulsed Laser Ablation in Liquid (PLAL). Both exploit the formation of a plasma and the presence of a liquid phase to bring the system out of equilibrium by quenching the plasma. Solvent has an important role in both methods, since it con-

fines the plasma, but also may act as a secondary source of carbon and provide chain terminations [32]. Indeed, when PLAL or SADL are performed with organic solvents the production is enhanced due to the contribution of carbon atoms of the solvent [34].

SADL produces polyynes by using two electrodes immersed in a solvent and by imposing a high voltage on the two electrodes that generates an arc discharge between them [1, 47]. The electrodes are usually made of graphite, even if other materials have been used, such as titanium [48] or copper [49]. Due to the plasma formation, carbon atoms are etched from the graphite and atomized from the solvent molecules and build up sp-carbon chains.

PLAL involves a similar process, but the plasma is generated by a highly energetic pulsed laser usually focused on a target [1]. Common targets are made of graphite, but also other materials are employable such as polymers or metals. However, many other parameters affect the process, in the next chapter a more in depth description of PLAL process is given.

1.3.4.   Characterization methods

Many different methods can be used to characterize CAWs and here the most relevant are presented. Due to the peculiar vibrational properties of CAWs, Raman spectroscopy is one of the most used characterization tool for sp-carbon chains. Raman and Surface Enhanced Raman Spectroscopy (SERS) allow to identify lengths and terminations of CAWs, since the vibrational properties of CAWs are intrinsically connected to their structure due to the π-conjugation [1]. UV-Vis absorption spectroscopy, instead, is a typical technique used to determine the absorption spectra of CAWs, investigate their optical properties as their HOMO-LUMO gap and gather their concentration in solutions [32]. High Performance Liquid Chromatography (HPLC) is employed to detect, separate and collect each species contained in a solution, hence it is a fundamental step to purify and analyse CAWs synthesized by physical synthesis methods [32].

Raman and Surface-Enhanced Raman spectroscopy

Raman spectroscopy is a widespread and powerful technique, which exploits inelastic scattering of monochromatic light to record vibrational transitions of a sample. In Raman spectroscopy, the sample material is exposed to monochromatic electromagnetic radiation, e.g. a laser. In general, an electron from a vibrational state of the electronic ground state is excited by the incident photon to the electronic excited state as in the case of resonant Raman spectroscopy, or a virtual state as in non-resonant Raman. Then, by a radiative relaxation process, the electron relaxes back to a vibrational state which can be different
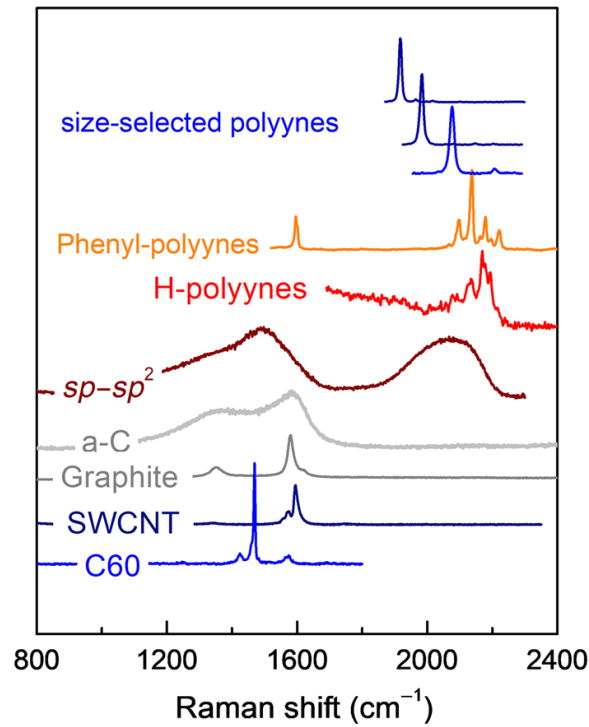
Figure 1.13: Raman spectra of several carbon allotropes and nanostructures, made of differently hybridized carbon atoms [2].

from the starting one [17]. In the latter case, the energy of the emitted (or Raman) photon is different from the incident one. If an electron relaxes back to a vibrational state with higher energy, the process is called Stokes and the emitted photon has an energy lower than the incident one. On the contrary, if the electron from a certain vibrational state relaxes to a less energetic state, the process is called anti-Stokes. Since in Stokes process the final energy level is higher than the starting one, the first level may be also the ground-state. Hence, Stokes process is more probable, since the ground state is more populated due to the temperature dependence of the Fermi-Dirac distribution [17].

The difference in energies between the absorbed and emitted photon is therefore related to the energy of the vibrational transitions. The vibrational structure of a molecule is strongly related to its bonds and local symmetry, and since different molecules differ in their vibrational states, Raman spectrum represents a chemical fingerprint of a molecule.

Indeed, Raman spectroscopy is often used to characterize carbon materials, since it allows to easily recognize the different allotropic forms of carbon by their characteristic vibrational modes (see Fig. 1.13) [31]. This is also true for carbon atomic wires which have a signal related to the collective vibration of all the CC bonds in the chain in the 1800-2200 cm^{-1} range, which is far from the characteristic signals of sp$_2$ and sp^3 carbon.
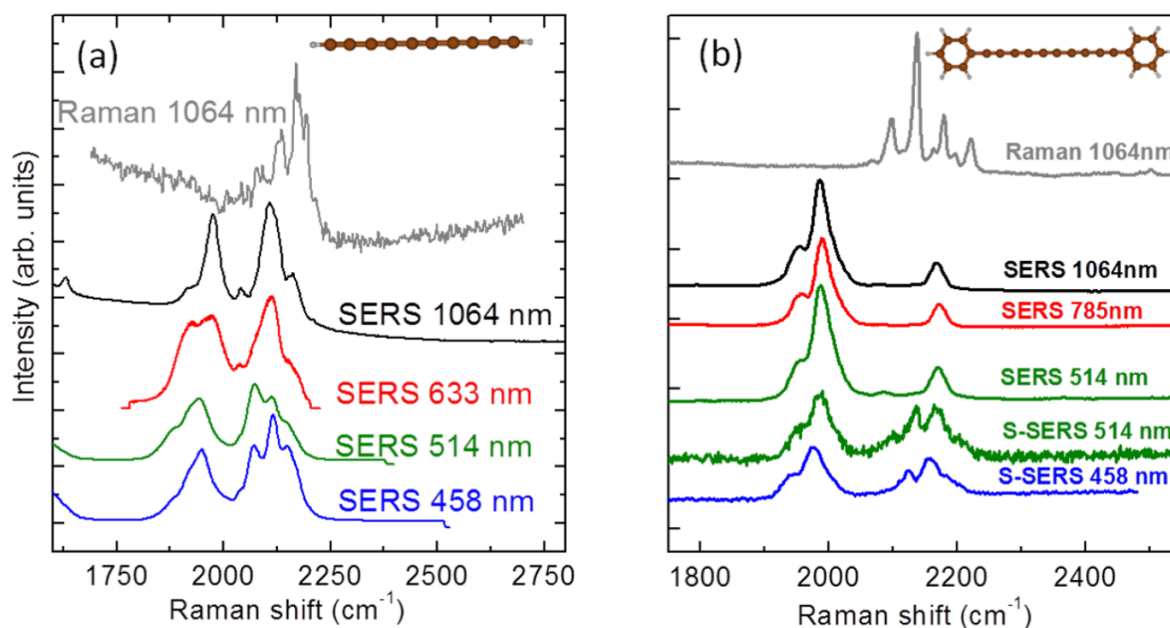
Figure 1.14: Raman and SERS spectra at different laser wavelengths for a) hydrogen-capped and b) phenyl-capped polyynes. For phenyl-polyynes also two surface-SERS (S-SERS) are reported [31].

For this reason, this Raman mode is a fingerprint of sp-hybridization and thus carbon atomic wires. However, if the concentration of the target polyyne is low (approximatively $< 10^{-3}$ M) also the related Raman signal is often too low and not visible.

Therefore, Surface Enhance Raman Spectroscopy (SERS) is largely used to increase the vibrational response of carbon atomic wires. Indeed, SERS exploits the enhancement given by metallic nanoparticles to the Raman signal via the excitation of a localized surface plasmon. As a consequence, the interaction between a molecule and the metallic nanoparticle enhances the Raman signal up to six orders of magnitude. However, SERS spectra are different from the Raman spectra, as shown in Fig. 1.14, resulting in an overall shift and broadening of the peaks and the generation of new features due to the chemical interaction of CAWs with nanoparticles.

UV-Vis absorption spectroscopy

UV-Vis spectroscopy is a widely used technique based on the absorption of electromagnetic radiation in the ultraviolet, visible and near infrared range by the analyte under investigation [17]. The absorption of photons corresponds to optical excitation of electrons to higher electronic states, hence UV-Vis spectroscopy probes the electronic transitions of a material. Indeed, a photon of wavelength λ is absorbed by a material if its energy

($E_{ph} = hc/\lambda$) corresponds at least to the energy gap between the valence and conduction bands, as in the case of a semiconductor ($E_{ph} = E_{gap}$) or between the HOMO and LUMO levels, as in the case of a molecule ($E_{ph} = E_{LUMO-HOMO}$). Normally, an UV-Vis spectrophotometer illuminates the sample through a series of lamps which provide photons with energy ranging from the ultraviolet to the near infrared. Then, photons that match an electronic transition are absorbed by the electrons in the sample. As a result, the absorption spectrum contains a series of peaks at certain wavelengths, each of them is related to a specific electronic transition of the sample. Therefore, by knowing the absorption spectrum, we can get information about the electronic structure of the molecules or nanostructures of the analysed sample. It is worth noting that the same electronic transitions might be common to many molecules. Hence, UV-Vis absorption spectra are not fingerprints of a specific compound, as for Raman spectra.

UV-Vis spectroscopy allows also to get the concentrations of the species in a solution. Indeed, by the intensity of the absorption is possible to calculate the concentration of target molecules. This is stated by the Lambert-Beer law which correlates the absorbed light (A) to the concentration of the absorbing species in a solution (c molar concentration in mol/l) and the optical path inside the sample (l in cm) with the following relation:

$$A = \varepsilon c l \tag{1.1}$$

where the coefficient ε is called molar extinction coefficient.

Due to their peculiar structure, polyynes have recognizable spectra called vibronic spectra, which make UV-Vis a useful method to check their presence and characterize their electronic properties [32]. Vibronic spectra are characterized by the presence of narrow peaks, as shown in Fig. 1.15. Absorption spectra of polyynes depends both on their length and endgroups, for example increasing the length of the chain correspond to a redshift of all the vibronic pattern. Hydrogen- and methyl-capped polyynes feature similar spectra, but methyl-endgroups generate a redshift in the peaks as reported in Fig. 1.15. Cyanopolyynes have further redshifted spectra, however they also show a slightly different shape of the spectra. Hence, UV-Vis spectroscopy is a useful technique to distinguish polyynes with different lengths and terminations.

High-Performance Liquid Chromatography (HPLC)

HPLC is a common technique used in chemistry to detect and separate chemical species contained in a solution, and to check their purity. A fraction of the sample is injected in the apparatus and it is eluted through a porous column, also called stationary phase.
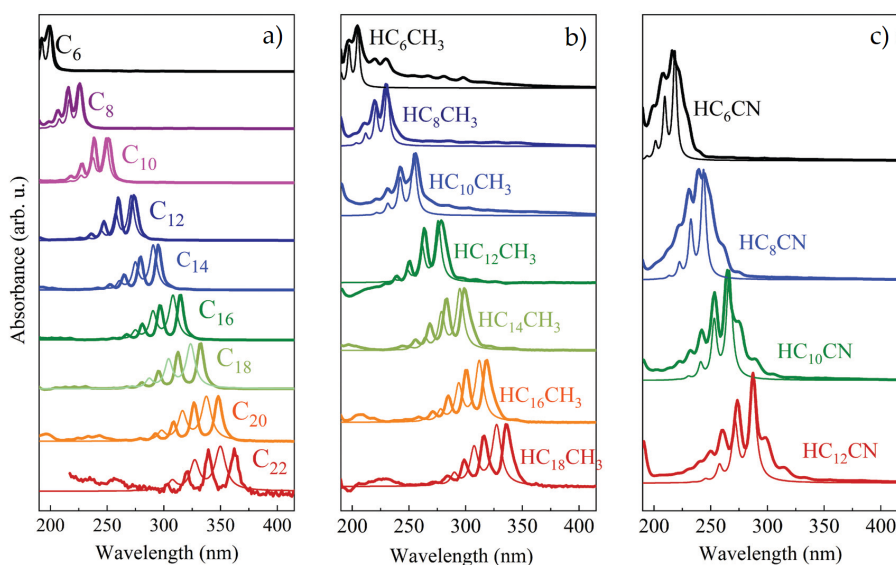
Figure 1.15: UV-Vis spectra of a) hydrogen-capped polyynes, b) methyl-capped polyynes and c) cyano-capped polyynes. The thin lines are simulated spectra [32].

Each species inside the solution interacts with the column in a different way, depending on both the analyte and the stationary phase structure, hence the retention time of each compound is different leading to their detection and separation. Moreover, the separation is also influenced by the interaction with the liquid phase, also called mobile phase, which pushes the solution through the column. Columns are tube usually filled with small particles of certain materials, e.g. commonly porous silica, but also zirconia, alumina, polystyrene or titania. The particles are further functionalized to ensure specific chemical behaviours and interactions, for example giving polar or apolar character, or allowing a better separation of aromatic compound through π-stacking. Speaking of polarity, a high degree of separation is reached selecting the right functionalization, e.g. a 8 carbon atoms alkyl chain is less a-polar than a 18 one and thus non-polar compounds have stronger interactions and will be eluted at larger times with the second functionalization.

Also the mobile phase plays a big role in the separation process. Indeed, it is usually a mixture of different solvents and the choice of the solvents allows to select the interaction and the compatibility with both the analytes and the column. Conversely to the stationary phase, the composition of the mobile phase can be changed during the analysis by varying the percentage of each solvent in the mobile phase. When the mobile phase is kept constant over the whole analysis time, we are performing the so-called *isocratic mode*, while if the composition is changed during time, the HPLC is running in *gradient mode*. For carbon atomic wires analysis, usually the *reverse-phase* configuration is employed, which is common for apolar compounds, having a non-polar stationary phase and a polar

mobile phase [32, 37, 47]. On the contrary the *normal-phase* configuration features a polar stationary phase and a non-polar mobile phase. Further parameter that can be considered are the flow rate of the mobile phase and the temperature of the column, which induce changes in the viscosity and the pressure of the mobile phase and therefore generate different separation outcomes.

The retention time of each species depends on many parameters, such as the molecular dimension and the interaction both with the stationary and mobile phase. For example small molecules are eluted before larger ones. However, if an analyte is chemically affine to the stationary phase, it will remain longer attached to the column than compounds with less affinity. Conversely, a better interaction with the mobile phase corresponds to a quicker elution.

In carbon atomic wires characterizations, HPLC apparatus are usually equipped with a UV-Vis spectrophotometer to record the absorption spectra of the eluted compounds [32, 36, 37, 47, 50]. This is an effective method of detection of CAWs and allows to record also low concentrations, due to the high optical activity and characteristic spectra of CAWs. As mentioned before, reverse-phase configuration is employed, which needs non-polar columns, in literature often employed non-polar columns are C8 and C18, which are column with particles functionalised with 8 and 18 atoms long alkyl chains [32, 37, 47, 50]. With this configuration, longer and more apolar polyynes have greater retention times than shorter and more polar ones [32, 37, 50]. This is quite challenging when dealing with mixtures of polyynes with different terminations, e.g. a cyano-group is quite polar contrary to polyynes which are rather apolar, therefore the two contributions changes increasing the length of the chain, which makes difficult to predict their retention time [32]. The length and dimension of the chains vary a lot between short and long polyynes. Furthermore, the ablated solutions contains several unknown compounds, which can be eluted at the same time of polyynes. For these reasons, it is difficult to set a method employable in every condition.

2 | Pulsed Laser Ablation in Liquid

In the field of nanotechnology, several different techniques have been employed for the synthesis and the fabrication of nanomaterials (NMs) and nanostructure that can be grouped in two main approaches: *top-down* and *bottom-up* techniques [19]. Top-down techniques produce NMs by removing fragments from a bulk material or by breaking it down to nanoparticles (NPs) (e.g. milling) [19]. Bottom-up techniques, instead, build up nanostructures atom-by-atom, molecule-by-molecule or cluster-by-cluster (e.g. colloidal synthesis) [19]. Pulsed laser ablation in liquid embodies some aspects of both bottom-up and top-down approaches [51]. Due to the action of a laser pulse, fragments are detached from a bulk material and a plasma is generated. In the plasma, however, molecules and nanostructures are built up atom-by-atom or cluster-by-cluster and NPs nucleate and grow. The first experiment that employed a laser ablation in liquid was performed by Patil *et al.* in 1987 for the synthesis of iron NPs in water [52]. Since then, PLAL has been shown to provide an efficient approach for the synthesis of various nanostructures [53]. Hence, PLAL is currently a widely used techniques for the production of nanoparticles and nanostructures [51].

As schematically illustrated in Fig. 2.1, a common PLAL setup involves a pulsed laser, optics, a container for the liquid phase and a solid target. However, the position of each component of the setup may change. In this chapter, I will describe the physical processes and the main parameters that characterize a PLAL experiment. Then, in the last part of the chapter, PLAL for carbon atomic wires synthesis will be described.

2.1. Description of PLAL process

In the PLAL process, an intense pulsed laser ablates a target immersed in a liquid phase. The laser beam has a high energy density and it generates a plasma when hits the target surface. Indeed, very hot fragments and atoms of the target are detached from the surface. Several phenomena are involved in the process and many parameters influence each step of
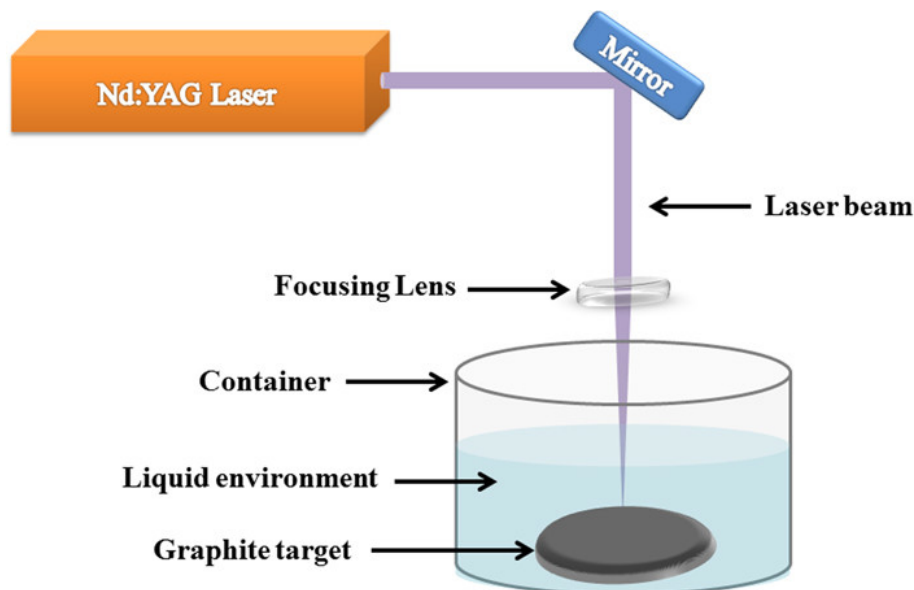
Figure 2.1:   Schematic of a pulsed laser ablation in liquid setup [53].

the overall ablation. Hence, due to the complexity of these phenomena, the comprehension of the process isn't yet complete [54].

In the following, the temporal evolution of the phenomena that take place during the ablation process will be described (see Fig. 2.2). First, the laser beam has to pass through the liquid layer above the target. The liquid environment should be accurately chosen to not interact with the laser and thus deliver the maximum fraction of the laser energy to the target. Therefore, the liquid must not absorb the radiation of the laser, i.e. we should chose a transparent solvent in the range of the selected ablation laser wavelength. However, some exception may be encountered: for example, solute compounds might absorb part of the electromagnetic radiation or synthesized nanomaterials might absorb or scatter part of the laser pulse [51]. Another important phenomenon to be avoided is the plasma breakdown of the liquid phase which can be prevented by using pulses longer than 10^{-12} s and working in defocusing condition [51, 55, 56]. Moreover, high fluences of the laser might induce nonlinear absorption effects in the liquid phase, which may produce strong attenuation of the beam [56]. For example in pure water, nonlinear effects, such as multi-photon absorption, become relevant for fluences larger than 70 J/cm^2 [57]. Also for these nonlinear phenomena, the presence of solutes or suspended nanoparticles (NPs) may affect the process [56]. In any case, for pulses in the order of femtoseconds, the nonlinear effects are already present for fluences usually employed for laser ablation [51].

When the laser pulse hits the target, both linear and nonlinear absorption effects are involved [58], due to the high photon density. As a first approximation, the absorbing
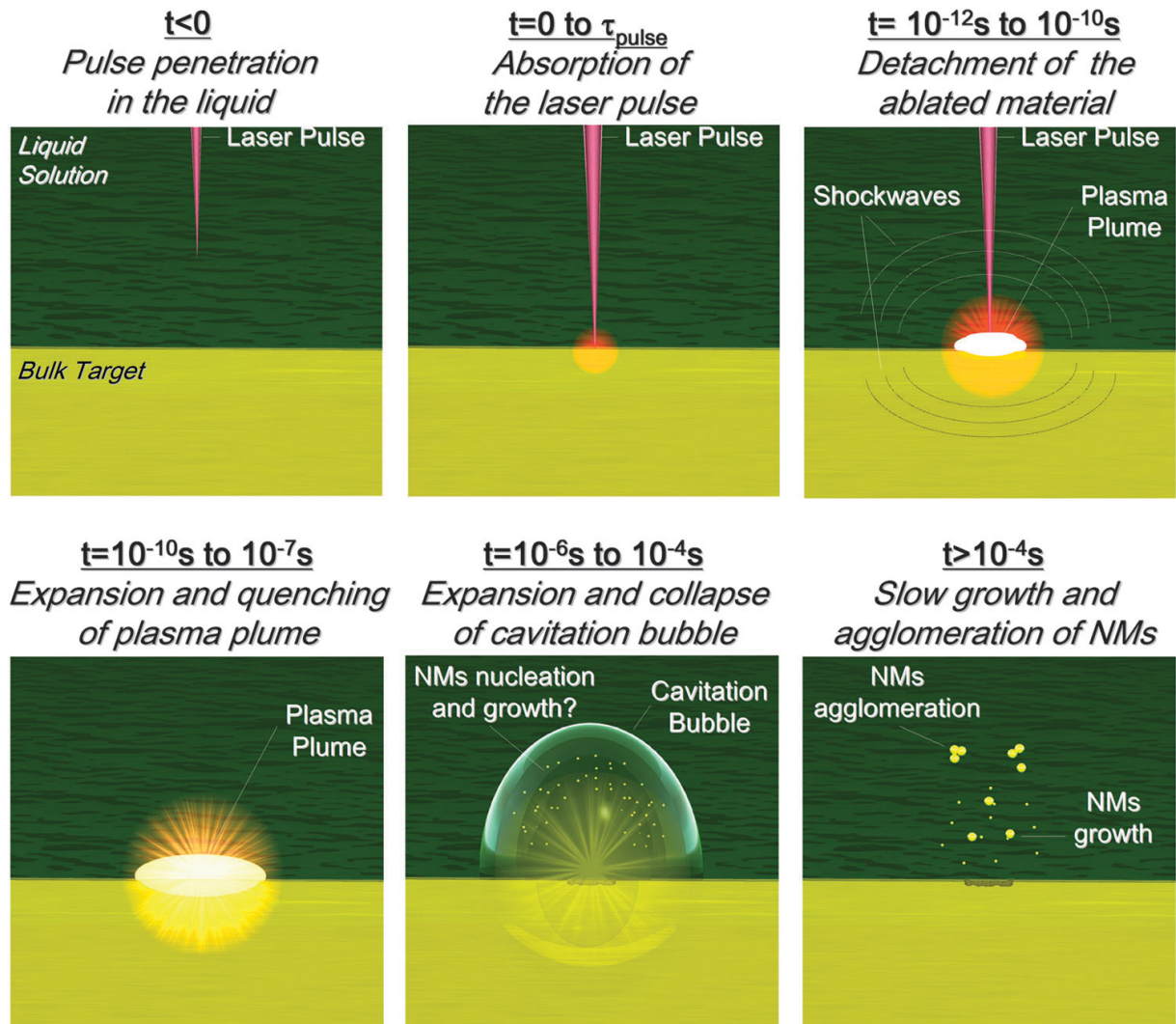
Figure 2.2: Temporal evolution of the various phases in a pulsed laser ablation experiment, occurring before, during and after the laser pulse [51].

material corresponds to the volume underneath the laser-spot area with skin-depth as thickness [51]. The material skin-depth is the thickness of the target which absorbs the light. Several phenomena arise consequently to the absorption, as photoionization due to multi-photon absorption and many thermal processes developed after the absorption [51]. Very short pulses with durations less than picoseconds produce high photoionization effects [59], which becomes possible even if not so probable compared to thermal processes for pulses $< 10^{-8}$s [51]. Direct photoionization has a time scale comparable to short pulse duration ($<$ ps), since laser-matter interaction happens simultaneously to the optical absorption [51]. A strong local charge-field is produced and many ionized species and electrons collide producing the ejection of material from the target [51]. Furthermore, in case of high direct photoionization, as for fs pulses, the emission of many electrons produces highly ionized materials which are divided and ejected with large velocity due to charge repulsion. This phenomenon is called Coulomb explosion [60]. However, for longer pulse ($>$ ps) thermal processes become more probable, indeed 10^{-12}s is the characteristic time for electron-lattice thermalization [51]. Due to the energy transfer to the lattice, a portion of the target, larger than the skin-depth, is affected by the ablation process and phenomena like thermoionic emission, vaporization, boiling and melting induce further material detachment from the target [51, 59]. Moreover, the melted portion around the spot-area is ejected too because of the recoil pressure of vaporization [59].

It is clear that several processes induce material ejection from the target, but it is difficult to describe all the possible paths that lead to the production of nanomaterials. As a first approximation, classical thermodynamic describes three main processes for the detachment of material from a bulk solid: vaporization, boiling and explosive boiling [51]. Explosive boiling, also called phase explosion, occurs when the material is brought above the thermodynamic critical temperature [61]. Then the superheated material undergoes a spinodal decomposition in vapor and liquid phases, i.e. gas bubbles nucleate and grow increasing their pressure which lead to the ejection of the topmost layer [62]. For laser pulse shorter than 10^{-7}s, phase explosion is the principal thermodynamic ablation process. However, fs and ps pulses generate conditions that are too far from the thermodynamic equilibrium to be described as explosive boiling, hence these processes are commonly referred as fragmentation [51].

During the ablation process, the detachment of the ablated material produces a recoil pressure, which generates two supersonic shockwaves: the first one inside the target and the second one towards the liquid. These shockwaves represent abrupt discontinuities in density and temperature profile, heating the surrounding material and leading to further detachment of target fragments [51]. Due to the high temperature and photoionization
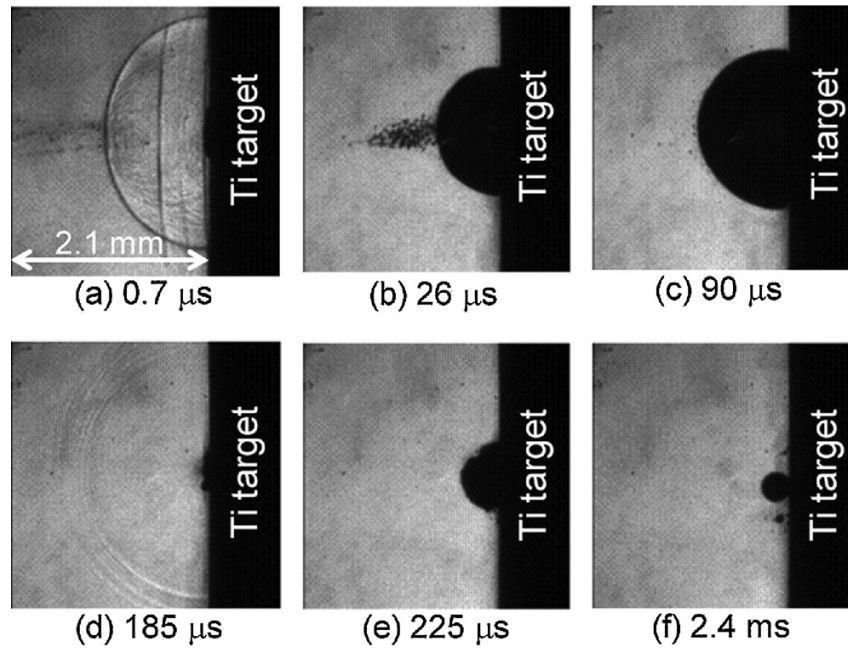
Figure 2.3: Evolution of a cavitation bubble generated by a Nd:YAG laser ablation of a Ti target in water. (a) the shockwave generated by the recoil pressure, (b-c) the expansion of the cavitation bubble, (d) collapse of the cavitation bubble and generation of a second shockwave, (e-f) expansion of a secondary cavitation bubble due to the energy released by the collapse [66].

processes described before, the ejected material is made up by highly ionized species and therefore is considered a non-equilibrium plasma-plume [51]. The plasma is heavily confined by the liquid and reaches temperatures greater than 10^3K and pressures up to 10^9Pa [54, 63]. Hence, further ablation of the target surface is favourite by these temperature and pressure. Indeed, it is reported an enhancement of the ablation efficiency in liquid compared to laser ablation in vacuum or in gas due to the larger confinement of the plasma closer to the target surface [54, 63, 64]. In this situation, the energy transfer between the plasma plume and the target lasts longer than the duration of the laser pulse and the plasma plume is usually quenched after 10^{-7}s [51]. A large fraction of the energy of the plasma which is not absorbed by the target is released in the liquid phase, which is compressed by the fast expansion of the plasma plume and thus generating another shockwave [65]. The solvent between the shock front and the plasma evaporates and, in addition with the expansion of the plume, cools down the plasma creating a cavitation bubble (see Fig. 2.3) [51, 65]. This cavitation bubble expands with supersonic velocity until the internal pressure drops below that of the surrounding liquid [51]. Then, it collapses generating a further shockwave. The role of the cavitation bubble in the formation

of nanomaterials is not completely understood. Indeed, nanomaterials might be formed inside the bubble in the gaseous phase [63] or at the interface between the bubble and the liquid [51]. It was also proposed that the interface between the bubble and the liquid may induce the nucleation and condensation of nanoparticles because of the temperature gradient experienced in that region [67]. Indeed, since the thermal conductivity of the gas is lower than the liquid one, the material inside the bubble remains hot for a longer time than in the liquid [51]. After the collapse of the cavitation bubble and the subsequent shockwave, the system reaches a steady state and a new cycle begins after the laser has fired again.

2.2. PLAL parameters

As outlined in the previous section, the PLAL process consists of several phenomena each one related to many different parameters. The strong interconnection of all the processes that occur during the ablation makes it difficult to correlate a certain parameter to the resulting production of nanostructures. In the following paragraphs, the main PLAL parameters will be presented and their influence on the outcoming products will be critically discussed [51].

2.2.1. Laser parameters

Concerning the ablation laser wavelength, it is typically chosen in the range from the UV to the near IR [51, 56, 68]. As mentioned in section 2.1, a wavelength which is not absorbed by the liquid phase nor by the synthesized nanomaterials should be chosen to maximize the ablation yield [51]. Indeed, nanomaterials in the liquid phase might be excited by the laser wavelength and hence undergo further modifications, for example, due to photofragmentation [68]. Moreover, also the portion of light absorbed by the target is affected by the pulse wavelength, since the absorption coefficient depends on the incident wavelength. Usually, UV radiation is absorbed more uniformly by solid materials than IR, for which the absorption is more related to the presence of impurities [51, 56]. For example, solid platinum reflects IR radiation, while defects can absorb the light and heat up, hence they melt the surrounding material. Liquid platinum has a low reflectivity to IR instead, hence after being heated up by the defects, it can absorb the incident light [56]. Shorter wavelengths also favour multi-photon absorption and non-linear processes, affecting the plasma population and lifetime [64].

The pulse duration (τ_{pulse}) is another fundamental parameter. Indeed, long pulses (for thermal processes long pulses are usually considered greater than ps [51]) reach the char-

acteristic time needed by electrons to transfer the absorbed energy to the lattice, thus making thermal processes more effective than photoionization in the detaching operation [59]. This is clear when observing the craters left by ablation with different τ_{pulse} at fixed fluence. Shorter pulses produce craters with sharper edges than longer pulses due to the absence of thermal processes that involve a larger volume [59]. When the pulse lasts more than 10ps the plasma plume has enough time to experience direct irradiation from the laser. This temporal and spatial overlap between the plasma plume and the laser is called "plasma-shielding" and it is a typical situation when using ns pulses [51, 59]. This overlap ensure a direct transfer of energy from the laser pulse to the plasma, which is heated and becomes more homogeneous leading to a sharper size distribution of nanoparticles [51]. Moreover, for microseconds and milliseconds pulses, photoionization processes are no longer considered and thermal processes prevail, indeed also the plasma plume is no longer generated [51].

The energy delivered by the pulse is another important parameter that can influence the ablation yield. Indeed, the amount of detached material increases with increasing energy, as multiple ablation processes become available for higher energies [64]. Thus, the amount of synthesized nanoparticles and their average dimension are found to be increased by higher energies [51, 68]. However, the control on the size distribution of nanoparticles is lower for high energy pulses, since the explosive boiling process becomes more relevant and it produces a more broad size distribution of clusters and fragments [57, 68].

By changing the focusing of the laser beam, different portion of the target can be lit, and hence the amount of material affected by the laser. The spot area is the amount of the target surface which is lit by the laser pulse and it is strongly related to fluence. By keeping constant the fluence of the pulse and increasing the spot area, it was observed an increase of the amount of ablated material, which leads to a higher concentration of nanoparticles, a bigger average dimension and a broader size distribution [51].

Another parameter that can be selected is the repetition rate, which is the frequency at which the laser shoots consecutive pulses. Increasing the repetition rate allows to detach more material at fixed times, hence it leads to higher productivities [51]. However, since the lifetime of cavitation bubbles is around $10^{-4} - 10^{-3}$s, above a threshold value of $10^3 - 10^4$Hz the productivity reaches a plateau. This is because each pulse experiences a shielding effect due to the cavitation bubble of the previous pulse [61].

Lastly, the number of pulses determines the duration of the overall ablation process, dividing the total number of pulses by the repetition rate the overall ablation time is obtained.

An increase in the duration of the ablation makes more material to be detached increasing the overall production [69]. However, it also may modify the already synthesized nanoparticle and degrade the target surface, which may lead to reduction in the efficiency of the process [51].

2.2.2. Material parameters

Regarding the materials involved in the ablation, we can distinguish among the target, the solvent and, if any, the solutes. Since the ablated material in the plasma plume comes primarily from the target, the target material represents the basic component of the synthesized nanomaterials. In particular, for the synthesis of nanoparticles, several materials are commonly employed. Metals are the most ablated materials to produce nanoparticles. Noble metals as gold and silver are very common for the synthesis of nanoparticles [63, 68], but also copper and platinum are widely employed [57, 59, 68]. Steel [59], zinc [61], titanium [54] and alloys [70] might also be used, but also semiconductors as silicon [63]. Lastly, graphite is usually used to produce carbon-based nanostructures. The shape of the target also affects the yield of the PLAL process. Messina *et al.* demonstrate an increase of the ablation efficiency up to a factor of 15 using a silver wire instead of a planar target [71]. Furthermore, the roughness of the target affects the amount of absorbed light. Indeed, polished surfaces have an higher reflectivity and a lower ablation yield [51].

The liquid phase that surrounds the target has many roles, since it confines the plasma plume but also has the function of collecting the produced nanomaterials [54]. The physicochemical properties of the liquid affect the overall synthesis process, as, for example, the density and the viscosity highly influence the efficiency of the plasma confinement. Indeed, higher viscosities lead to higher plasma confinement. Moreover, the viscosity determines the lifetime and the expansion speed of the cavitation bubbles, and hence also impacts on the diffusion of the synthesized materials [51]. Another important aspect of the liquid phase is its thickness above target, which was shown to strongly modify the production of nanomaterials [54]. Solvents might also determine the chemical nature of the synthesized material. Water, for example, favours the formation of oxides when metals are ablated, while organic solvents are more prone to favour pure metallic nanoparticles [51, 54]. For the same reason, also the solubility of gases in the solvent has to be considered. Solvents in which oxygen is more soluble tend to produce more oxidized nanoparticles than metallic one. The choice of specific organic solvents may also alter the shape of nanoparticles and, due to the degradation of the solvent, may introduce further chemical modifications [51]. Furthermore, solvent molecules might cap the growing nanoparticles by being adsorbed
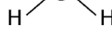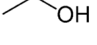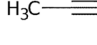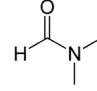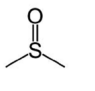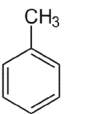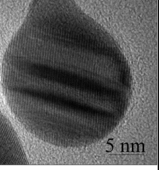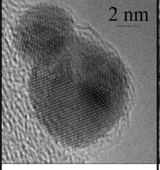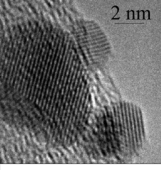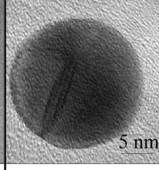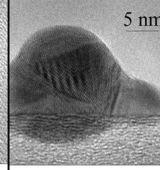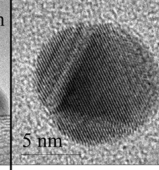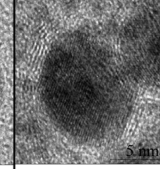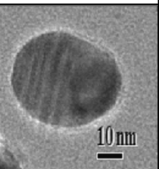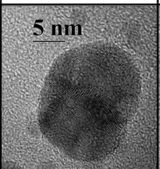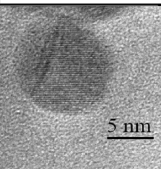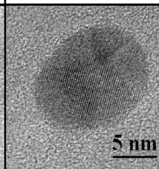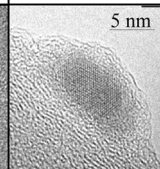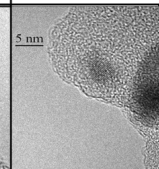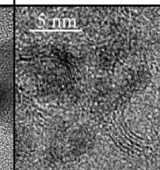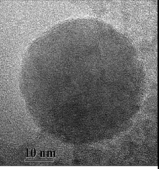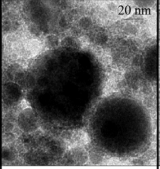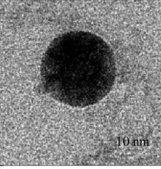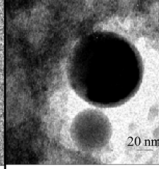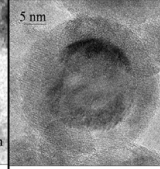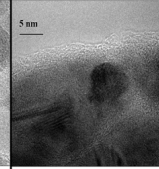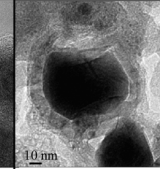
Target → Solvent →	Water H—O—H	Ethanol OH	Acetonitrile H_3C—N	Dimethyl-formamide	Tetra-hydrofuran	Dimethyl-sulfoxide	Toluene CH_3
Au	Metal Au	Metal Au	Metal Au	Metal Au	Metal Au	Metal Au	Metal Au/ Graphite
Ag	Metal Ag/ Oxide AgO	Metal Ag	Metal Ag	Metal Ag	Metal Ag/ Carbon	Metal Ag/ Carbon	Metal Ag/ Graphite
Fe	$Fe_3O_4, Fe_2O_3,$ $Fe(OOH)_2$	$Fe_3O_4,$ FeC_3	$Fe_3O_4,$ Carbon	$Fe_3O_4,$ Carbon	Metal Fe/ Fe_3O_4	Metal Fe/ Carbon	Fe-Carbide/ Graphite

Figure 2.4: Summary of the nanoparticles produced by laser ablation of Au, Ag or Fe bulk targets in different solvents with 9 ns pulses at 1064 nm and $10\,\mathrm{Jcm^{-2}}$ [51].

on the surface, hence determining the average dimension and their chemical properties as their reactivity and polarity [51]. In Fig. 2.4, electron microscopy images of the produced nanoparticles with gold, silver or iron targets in various solvents are reported.

Solutes can be also added to the liquid phase. Solutes may alter the physical properties of the liquid phase, making it, for example, more dense or viscous or acting on its surface tension. Hence, solutes might affect the plasma confinement and the lifetime of the cavitation bubbles. The interactions between the solutes and the growing nanoparticles are another important aspect to be considered. Indeed, solute molecules might be added as capping agents which adsorb on the NPs surface controlling the growth process and hindering coalescence of NPs [69, 72]. Stronger interactions are possible too: indeed, chemical reactions might be promoted by the PLAL process leading to nanoparticles functionalization through ligands chemically attached to the surface [51]. Lastly, chemical modifications of the bulk of nanoparticles are possible leading to a change in the nanoparticle composition [51].

2.3.   PLAL for polyynes synthesis

Pulsed laser ablation in liquid has been recently employed to synthesize polyynes. Indeed, chemical methods for polyynes synthesis were firstly studied and developed and, only during the last decades, physical techniques have been thoroughly studied and improved. The first synthesis of polyynes via laser ablation is reported in the work of Heath *et al.* in 1987, where polyynes were produced by laser ablation in a gaseous environment [73]. In 1993, Wakisaka *et al.* performed ablations of a graphite target both in argon and immersed in liquid benzene to experimentally confirm growth mechanisms of carbon clusters [74]. Indeed, the simplest growth mechanism was proposed as the formation of C_2 clusters via $2\,C \longrightarrow C_2$ [74]. Few years later, Gaumet *et al.* obtained C_1, C_2, C_3 and C_4 carbon clusters and phenyl derived carbon cluster when ablating a graphite target in benzene [75]. For the aromatic clusters, the proposed scheme implies the addition of clusters to phenyl radicals [75]. They also suggested a mechanism of subsequent addition of C_2 or C to explain the growth of the linear clusters [75]. This latter scheme was confirmed by Tsuji *et al.* in 2002 in the case of formation of hydrogen-capped polyynes [76]. As explained by Tsuji, the formation of polyynes proceeds by radical additions of C atoms to a chain previously formed by the ablation process, as shown in Fig. 2.5. Hence, the two main processes that compete for the formation of polyynes are the polymerization and the termination of the growing chains (in this case by means of hydrogen atoms and for this reason it was called hydrogenation) [76].
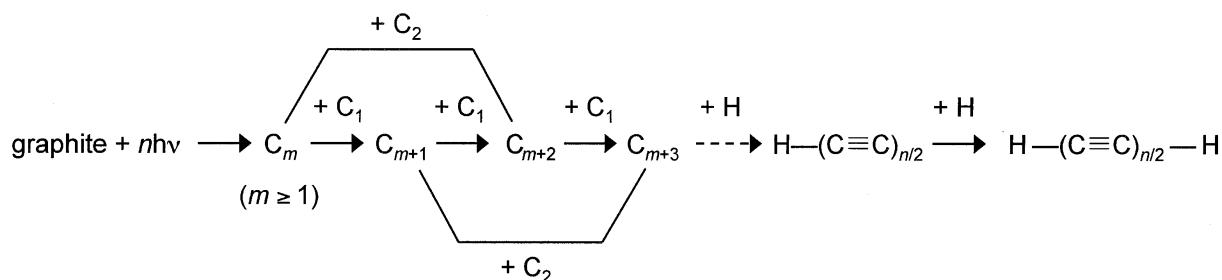
Figure 2.5:   Schematic representation of the proposed mechanism for polyyne growth. The competition between polymerization and hydrogenation is outlined [76].

The mechanism that emerges from these experimental evidences is made up by two main processes. The addition of C and C_2 radicals builds up the chains, which may be terminated by means of combination with monovalent radicals (e.g. $^{\bullet}$H or $^{\bullet}C_2$H). Hence, the concentration of terminating agents in the surrounding of the chain-growth reaction, such as hydrogen atoms, is a key parameter in determining the chain length and the end of the

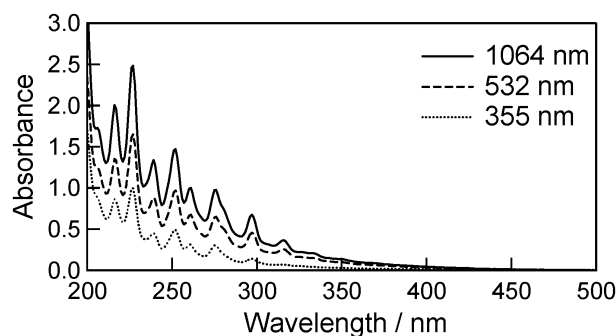**Figure 2.6:** UV-Vis spectra of n-hexane solutions ablated with different wavelength. Stronger absorption peaks are related to longer laser wavelength [80].

polymerization process. Hydrogen is the most common capping for polyynes synthesized by physical methods, since it is inside the majority of liquid solvents. However, because of the complexity of the PLAL process and despite the theoretical efforts, a complete comprehension of the synthesis mechanism has not been yet achieved. Many parameters have shown to strongly affect the production and the size distribution of polyynes, as in the case of NPs. As for the synthesis of NPs, the laser wavelength, pulse energy and duration, as well as the ablation time, the target and the liquid phase strongly affect the yield of polyynes and also the chemical properties of the synthesized sp-carbon chains. In the next paragraphs, the main parameters of polyynes synthesis via PLAL are reported.

2.3.1. Laser parameters

Ns-pulsed lasers are commonly employed in polyynes synthesis via PLAL [32, 74–79]. The most used wavelengths are the fundamental harmonic of Nd:YAG lasers (1064 nm) and its higher harmonics as 532 nm, 355 nm and 266 nm [32, 74–81]. However, ablation with other lasers and thus other wavelengths and pulse durations are also reported in literature [50, 82, 83]. The effect of laser wavelength on polyyne synthesis is still under debate [76, 80]. Indeed, Tsuji *et al.* found an enhancement of the productivity for shorter wavelength (266 and 355 nm) when ablating a solution with suspended graphite particles or fullerenes [76, 81]. Matsutani and co-workers reached a different conclusion, as they found that longer wavelengths lead to higher concentration of polyynes when ablating graphite and fullerene pellets in the same solvents of Tsuji *et al.* [80] (see Fig. 2.6). The same trend was confirmed by Park *et al.* with ablation of a graphite target in water [79, 84]. This disagreement is probably related to the different target configurations. Short wavelengths are more scattered by suspended particles and impurities and more easily absorbed by the liquid phase, thus less energy arrives to a sunk target. Infrared light, instead, passes through the liquid layer more easily and is less scattered by suspended

particles or impurities, thus reaching the target at the bottom of the liquid with a larger fraction of energy. Therefore, when graphite particles or fullerenes are suspended in solution the interaction with shorter wavelengths corresponds to a higher absorption of the carbon particles, while longer wavelengths deliver the energy more effectively in the case of solid targets [80]. Moreover, synthesized polyynes in the solution might also absorb or scatter shorter wavelengths (UV) leading to the degradation of the chains and reducing the energy delivered to the target at the bottom of the vial [80].

Pulse durations different from ns-pulses were studied, especially *fs* pulsed laser. However, the majority of these works are more solvent irradiations than effectively laser ablations [51, 79], since the laser is focused in the solution, and the carbon atoms are provided directly by the solvent degradation [50, 83, 85, 86].

Pulse energy has an effect on the polyyne synthesis similar to the general description made for NMs and NPs. Increasing the energy per pulse corresponds to an increase in the amount of the detached material, hence in a greater amount of synthesized polyynes [84]. However, different results were obtained investigating short and long polyynes at different wavelengths [84], hence the correlation between the synthesis yield of different chains and energy is still under investigation.

Regarding the repetition rate, in the majority of the works [32, 74–79] a repetition rate of 10 Hz is employed with ns-pulsed lasers. However, Santagata *et al.* showed that increasing from 10 Hz to 1 kHz the formation of nanodiamonds was favoured than polyynes, probably due to the high pressure generated which stabilizes nanodiamonds [87]. It is worth noting that in this work a *fs* pulsed laser was employed.

Ablation time strongly affects the size distribution of polyynes, but a clear description is lacking due to contradictory results [79, 88]. When ablating nanodiamonds in suspension, Tabata *et al.* obtained an higher amount of long polyynes for short times (5 min) [88], while Park and co-workers obtained longer chains when increasing the ablation time (up to 60 min) [79]. Moreover, they also found that the overall concentration of polyynes is increased when increasing the time, but the production of polyynes saturates after 30 min [79]. Matsutani and co-workers managed to obtain C_{30} (i.e., the longest polyyne ever produced by physical synthesis methods) after 52.5 min, by optimizing the ablation time for ablation in decalin [78].

2.3.2. Material parameters

Target

A typical source of carbon for nanomaterials synthesis is graphite. Indeed, graphite is the most employed target material also in polyyne synthesis via PLAL. Different configurations of bulk graphite are employed in literature: graphite rods [89], disks [32] or graphite pellets [80]. Other works reported the use of graphite powder suspended in the solution, as for the work of Tsuji et al. [76]. In the paper of Matsutani et al. [80] is highlighted the different behaviour when ablating a suspended powder or a bulk target. Graphite powder produces higher concentration of polyynes while graphite pellets allow to synthesize less concentrated but longer polyynes [80]. When ablating a suspended powder, each particle hit by a laser pulse becomes a nucleation site for polyynes, increasing the overall productivity. However, due to the diffusion of ablated material and the motion of the graphite particles, the polymerization process is less probable than the hydrogenation, resulting in shorter chains. Instead, ablating a pellet produces less polyynes, but longer polyynes are obtained [78]. However, it is important that the diffusion of radicals takes more time then the production rate, keeping a high concentration of carbon radicals in the polymerization region [78]. A further distinction is possible between solid graphite and pellets. Indeed by ablating a solid surface, a reduced amount of powder and impurities is released and dispersed in the solution, which leads to a lower concentration (less nucleation sites) but allows to obtain longer chains [78]. Matsutani et al. [78] obtained the C_{30} ablating a graphite rod, while through the ablation of graphite pellet in the same configuration only C_{28} was detected.

Graphite is not the only material employed for polyyne synthesis but many carbon-based nanostructures were successfully used in the synthesis of polyynes. For example, by using a dispersion of nanodiamonds, polyynes up to C_{16} were obtained [88]. Also fullerenes and nanotubes were used [81, 90]. Carbon-based compounds were also used as targets in some cases, such as solid alkanes. By using fs pulsed laser, solid methane and solid hexane were ablated, however only traces of polyynes and cumulenes were found [82, 91]. Matsutani and co-workers employed a PTCDA (a dye molecule) pellet in the ablation and managed to synthesize polyynes up to C_{18} in liquid hexane [92]. Lastly, naphthalene targets were ablated in various solvents by Benoliel, who demonstrated that naphthalene is a source of polyynes and obtained higher concentrations of long polyynes with naphthalene rather than common graphite target when performing ablations in alcohols [93]. It was suggested that ring-opening phenomena might increase the content of longer chains by providing longer alkyne-radicals [93].

Solvent

As outlined in section 2.2.2, the liquid phase plays a fundamental role in determining the outcome of a PLAL experiment. Several solvents have been used for polyyne synthesis and some of their effects have already been studied. Water is a cheap and easy-to-handle solvent and it was employed in many works [77, 79, 89, 94]. Moreover, it does not contain any carbon atom, which means that does not contribute to the chain growth, but only to the termination through H atoms [32]. Hence, only short polyynes are obtained and the longest polyyne ever detected in water is C_{12} [95].

Better results have been achieved by ablations in organic solvents, which were proven to act as secondary source of carbon atoms for the sp-chain growth. Indeed, laser irradiations in pure organic solvents showed the formation of polyynes without the necessity of a target (by employing fs-pulses) [50]. Furthermore, Wakabayashi *et al.* demonstrated the contribution of the solvent by ablating an ^{13}C-enriched carbon powder (99.9% ^{13}C) in acetonitrile and performing analysis by Nuclear Magnetic Resonance (NMR) [34]. The measurements showed the presence of solvent carbon atoms in the chains [34]. Another parameter to be considered is the hydrogen generation rate, which is a key factor for the termination phenomenon. The higher energy of the O−H (4.8 eV) bond makes water molecules less prone to split than organic solvents containing C−H (4.3 eV), C−C (3.6 eV) and C−O (3.7 eV) bonds, hence the hydrogen generation in water should be reduced making more difficult the synthesis process [32].

Common organic solvents are alcohols (such as methanol, ethanol and isopropyl-alcohol [32, 80, 88, 95–98]), alkanes (as hexane or cyclohexane [76, 80, 86, 95, 96, 99]), acetonitrile [32, 34, 89, 95, 99] and aromatic solvents (such as toluene [50, 76, 81], benzene [76, 100] and decalin [80, 93, 101]). In the field of organic solvents, many parameters affect the polyyne synthesis [63]. For example, an increase in polyyne concentration was found to be related to an increase in the C/H ratio, which is the relative amount of carbon atoms over hydrogen in the solvent molecules [32]. Oxygen is detrimental for polyynes stability and synthesis, leading to oxidation of the chains. Hence, oxygen solubility is another parameter of merit to be considered when selecting a solvent for polyyne synthesis. Peggiani *et al.* reported that acetonitrile leads to a higher concentration of polyynes than alcohols and water when ablated with a 532 nm laser, and indeed it has both a lower oxygen solubility and a higher C/H ratio than the other solvents [32] (see Fig. 2.7). Moreover, acetonitrile undergoes carbonization more easily than alcohols leading to more carbon atoms in the plasma, but also to more byproducts as hydrocarbons (see the inset in Fig. 2.7b) [32]. Another important parameter is the solvent polarity which affects the solubility and the stability of polyynes [32, 96]. Indeed, the productivity of
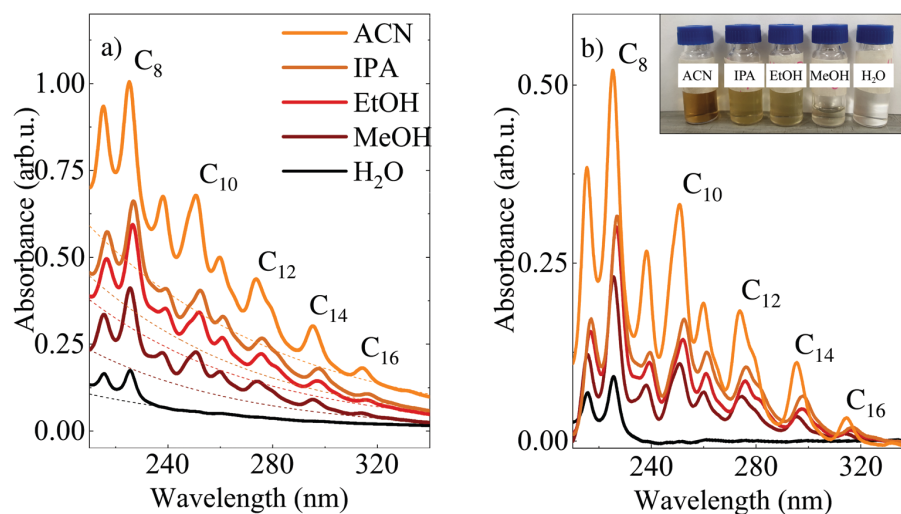
Figure 2.7: UV-Vis spectra of filtered solutions of polyynes synthesized in various solvents before (a) and after (b) the background (dotted-line in pane (a)) removal. In the inset, the different colours of the ablated solutions are thought to be related to the formation of by-products [32].

polyynes was shown to be increased with decreasing solvent polarity [32, 96]. Matsutani and co-workers found a strong correlation between the concentration of polyynes and the solvent polarity, when ablating PTCDA targets [96]. As outlined in section 2.2.2, viscosity seems to play a major role in polyyne synthesis. Indeed, Matsutani *et al.* attributed the achievement of the synthesis of C_{30} to the bigger viscosity of decalin compared to other solvents [78]. Higher viscosities hinder the diffusion mechanisms of ablated species, which may lead to higher concentration of C_2 radicals in the plasma plume and an increase of the polymerization [78]. Moreover, decalin has also a high C/H ratio that probably promote the polymerization due to low hydrogen concentration [78]. In the work of Shin *et al.* , it was shown a dependence between the polyyne synthesis and the pH of the solution [94]. It was shown that an acidic environment favours short chains, while high pH values favour longer ones. The effect was thought to be related to the concentration of H^+ ions which may favour the termination of the chains [94].

Solvents may also contribute with endgroups different from hydrogen ones. Methyl-capped polyynes have been found in ablations of hexane [102], alcohols [32] and acetonitrile [32]. Water was also shown to produce methyl-capped polyynes [32], hence the formation of methyl-endgroups is not strictly related to their presence in the solvent, i.e. carbon coming from the target captures three hydrogen atoms forming a methyl termination also in water. Acetonitrile has been shown to provide cyano-endgroups ($-C{\equiv}N$) [32, 34, 95] which lead to cyano- and dicyano-capped polyynes. Lastly, deuterium-terminated polyynes were

obtained by ablating in heavy water (D_2O) [99].

Regarding the use of solute compounds few works are present in literature. Shin *et al.* employed NaOH to control the pH of the ablated solutions [94]. Benoliel ablated graphite targets in solutions of various solvent with naphthalene, obtaining an increment in the concentration only of shorter polyyne when naphthalene was dissolved in decalin and tetralin [93]. The use of reactive compounds for polyyne synthesis via PLAL are not reported by any authors to the best of my knowledge.

This work aims to investigate the effects and the interactions of a radical initiator, i.e. Benzoyl Peroxide, with the PLAL synthesis process when dissolved in organic solvents. Given the radical nature of the formation and growth mechanism of polyynes, I studied the effect of Benzoyl Peroxide in the synthesis via PLAL. Radicals initiators are compounds capable of producing free radicals upon the application of certain stimuli, such as heat or light. Benzoyl Peroxide is a thermally activated radical initiator, hence it should be activated by the heat produced during the ablation. The dissociation of Benzoyl Peroxide produces reactive free radicals which in the PLAL solution could be quenched by other radicals. Hence, other free atoms or groups, such as hydrogen or methyl-groups, could be captured by Benzoyl Peroxide depleting their concentration. Other radical species could be polyynes chains which are not yet terminated, this could lead to terminations different from hydrogen, methyl- and cyano-endgroups. During this investigation, I performed ablations of a graphite target sunk in solutions of Benzoyl Peroxide with various organic solvents, varying also the concentration. The investigation was also aimed to a better comprehension of the formation process of polyynes and the effects of various ablation parameter, such as ablation time and laser wavelength.

3 | Materials and Experimental Methods

In this chapter experimental details of the synthesis methods, procedures and materials are described. In the first section, fundamental materials needed for the synthesis of polyynes are described in all their aspects. Then, the synthesis and the techniques employed for polyyne characterization are described, starting from the preparation of all the needed solutions. A focus on the employed PLAL setup is given, focusing on the parameters mostly relevant for the synthesis of polyynes. High performance liquid chromatography was used as main characterization method, whose results will be discussed in the next chapter.

3.1. Materials

3.1.1. Solvents

In this work, I employed several different solvents, all of them were organic (Fig. 3.1) with the only exception of water. Deionized water Milli-Q with a conductance of 0.055 μS was used. The organic solvents employed were methanol (**1** - MeOH), ethanol (**2** - EtOH), isopropyl-alcohol (**3** - IPA) and acetonitrile (**4** - ACN), whose chemical formula is reported in Fig. 3.1. All of them were HPLC grade, which means they have a purity ≥99.9% (Sigma-Aldrich). Water was chosen as a reference solvent, but also to perform experiments with solid crystalline Benzoyl Peroxide since it is completely insoluble in water. Teh choice of the organic solvents listed above lies in several reasons. As described in the previous chapter, organic solvents act as secondary source of carbon during the PLAL process increasing the production of polyynes, their stability, solubility and providing other terminations than hydrogen. All these organic solvents have already been used in bibliography as liquid media for PLAL, but they were also chosen since Benzoyl Peroxide is easily soluble, which was fundamental for testing solutions with different concentrations. Furthermore, the choice of the organic solvents is constrained by their compatibility with
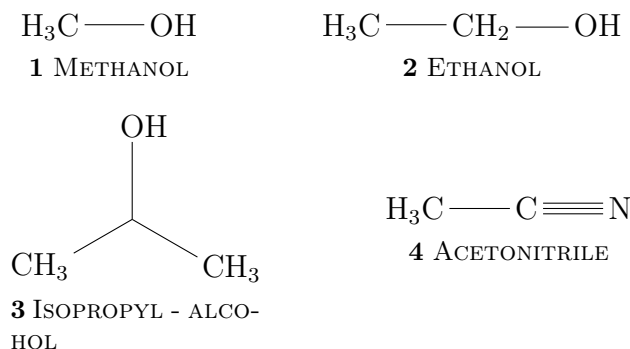
$$H_3C \longrightarrow OH \qquad\qquad H_3C \longrightarrow CH_2 \longrightarrow OH$$

1 METHANOL   **2** ETHANOL

$$OH$$

$$H_3C \longrightarrow C \Equiv N$$

4 ACETONITRILE

$$CH_3 \qquad\qquad CH_3$$

3 ISOPROPYL - ALCO-
HOL

Figure 3.1:   Chemical structures of organic solvents employed in this work.

Solvent	δ (g cm^{-3})	η (cP)	n	ε_r	cut-off λ(nm)
Water	1.000	0.89	1.332	79.7	190
Methanol	0.792	0.54	1.326	32.6	205
Ethanol	0.789	1.08	1,359	22.4	210
Isopropyl-alcohol	0.786	1.90	1.375	18.3	205
Acetonitrile	0.782	0.34	1.342	37.5	190

Table 3.1:   Selected properties of the solvents employed in this work: density δ; viscosity η; refractive index n; dielectric constant ε_r; UV cut-off wavelength.

the columns and with the employed mobile phases of our HPLC apparatus (see section 3.2.4). The configuration of the liquid medium in the laser ablation process consisted of 5 mL put in a cylindrical glass vial of 16 mm of diameter and height around 75 mm. Many properties of the liquid phase had to be taken into account when choosing the liquid medium for ablations. Especially refractive index, viscosity and polarity are important parameters for PLAl and HPLC method. In Tab. 3.1, the most relevant properties of the solvents employed in this work are reported.

3.1.2.   Targets

In the PLAL process, a solid target can be present, which acts as the primary source of ablated material. In this work graphite was chosen as target material, since is a reliable, easy-to-work and non-toxic source of carbon atoms. Moreover, it is also commonly used in bibliography for the synthesis of polyynes. All the employed graphite targets (purity 99.99%, Testbourne Ltd.) were disks with a diameter of 15 mm and a thickness of 3 mm, which fit the inner dimension of the glass vial used for the ablation process.
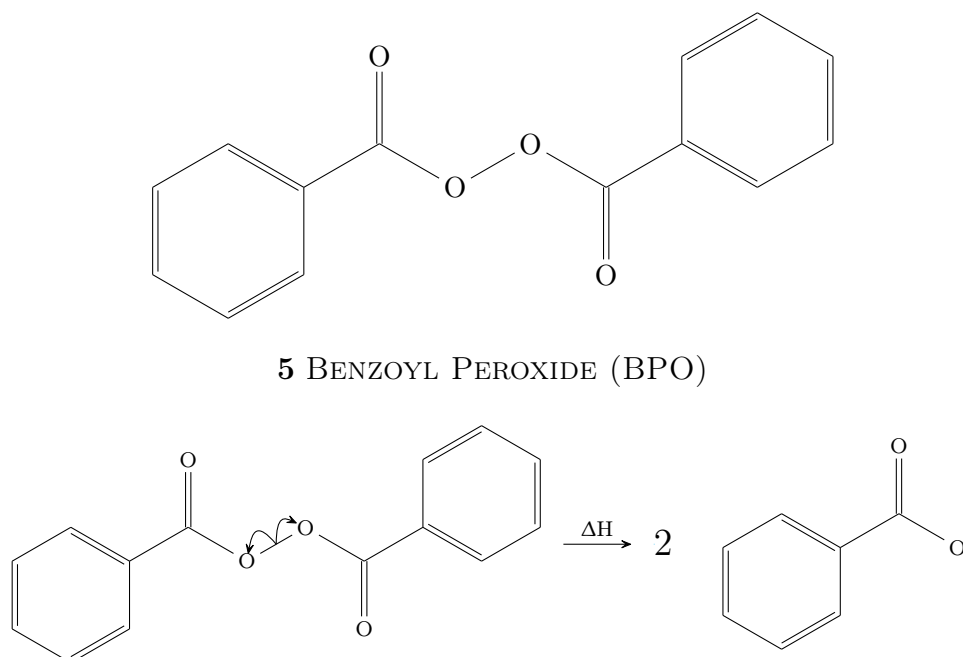
5 Benzoyl Peroxide (BPO)

Figure 3.2: Homolytic dissociation of BPO by breaking of the O−O bond and formation of two benzoate radicals.

3.1.3. Benzoyl Peroxide

In this thesis work the effect on polyynes synthesis via PLAL of Benzoyl Peroxide (**5** - BPO) was studied. Benzoyl Peroxide, also called dibenzoyl peroxide, is a diacyl peroxide often used as free-radical initiator in polymerization reactions [103–106]. As for the majority of diacyl peroxides, the presence of O−O bond makes BPO a very reactive compound. Indeed, the cleavage of this bond can be thermally activated. Indeed, the dissociation energy of O−O bond of BPO is 1.44 eV [107], much lower than those of the C−C or C−H covalent bonds [107]. The homolytic dissociation of the O−O bond leads to the formation of two identical benzoate radicals (see Fig. 3.2) [104]. The decomposition of BPO in solutions occurs already at temperature below 40°C [104, 108], however the stability depends also on the solvent. Experiments conducted at 79.8°C in oxygen-free condition showed a decomposition of BPO of 33% in methanol, 70.6% in ethanol and 86.7% in IPA after 5 min [109]. However, by reducing the temperature to 60°C the decomposition in ethanol decreases at around 70% after 45 min [109]. Thus, the decomposition process of BPO shows a strong dependence on the solvent temperature. In the work of Hongo *et al.* , the stability of BPO in various solvents at 25°C in air was studied [104]. They showed a strong degradation of BPO in methanol, reaching 50% of the initial concentration in less than a day [104]. In ethanol, BPO showed to be more stable, although a reduction in concentration was clearly detected it never reached 50% [104]. In acetone and acetonitrile,
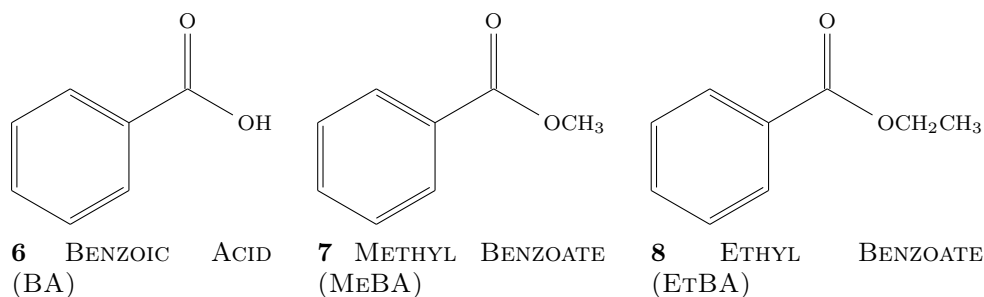
Figure 3.3:   Chemical structures of the main degradation products of BPO

instead, BPO was slightly degraded after one week [104]. The different behaviour of BPO between the work of Hongo *et al.* and the previous works is due to the presence of oxygen [104]. Indeed, oxygen was shown to partially inhibit the degradation of BPO [109, 110], and thus oxygen solubility of solvents is also a parameter of influence in determining the reactivity of BPO.

The decomposition of BPO in solutions follows a free radical mechanism [104, 108]. After the cleavage of the O−O bond the benzoate radicals can react either with other BPO molecules or with solvent molecules [108, 110]. Through this reaction the radical propagates on other fragments. This chain reaction propagates until two radicals couple together [108]. Hence, the kinetic of the overall degradation consists of many different pathways depending also on the solvent-fragment radicals [108], leading to complex orders of reaction [110]. The degradation of BPO is shown to be induced by the presence of free radicals [111], hence an increase in the concentration of free radicals increases the kinetic of the process accelerating the decomposition [108]. If the chain transfer to the solvent produces more stable and less reactive radicals, the solvent has the effect to slow down the chain reaction [111].

The main degradation products of BPO in alcohols are Benzoic Acid (**6** - BA), Methyl Benzoate (**7** - MeBA) and Ethyl Benzoate (**8** - EtBA) [104], whose formula are shown in Fig. 3.3. BA is the main degradation product, obtained from the bond between a benzoate radical and a hydrogen atom.

The UV-Vis absorption spectrum of BPO feature two main peaks around 196 nm and 235 nm and a broad band around 275 nm [112] (see Fig. 3.4). BA, MeBA and EtBA show spectra with the same features, although they are normally blueshifted depending on the solvent. For example, in ethanol the main peak of BA is around 228 nm while in methanol is around 226 nm [113]. However, the similarity between the spectra of the degradation products makes it difficult to identify them only via UV-Vis spectroscopy.
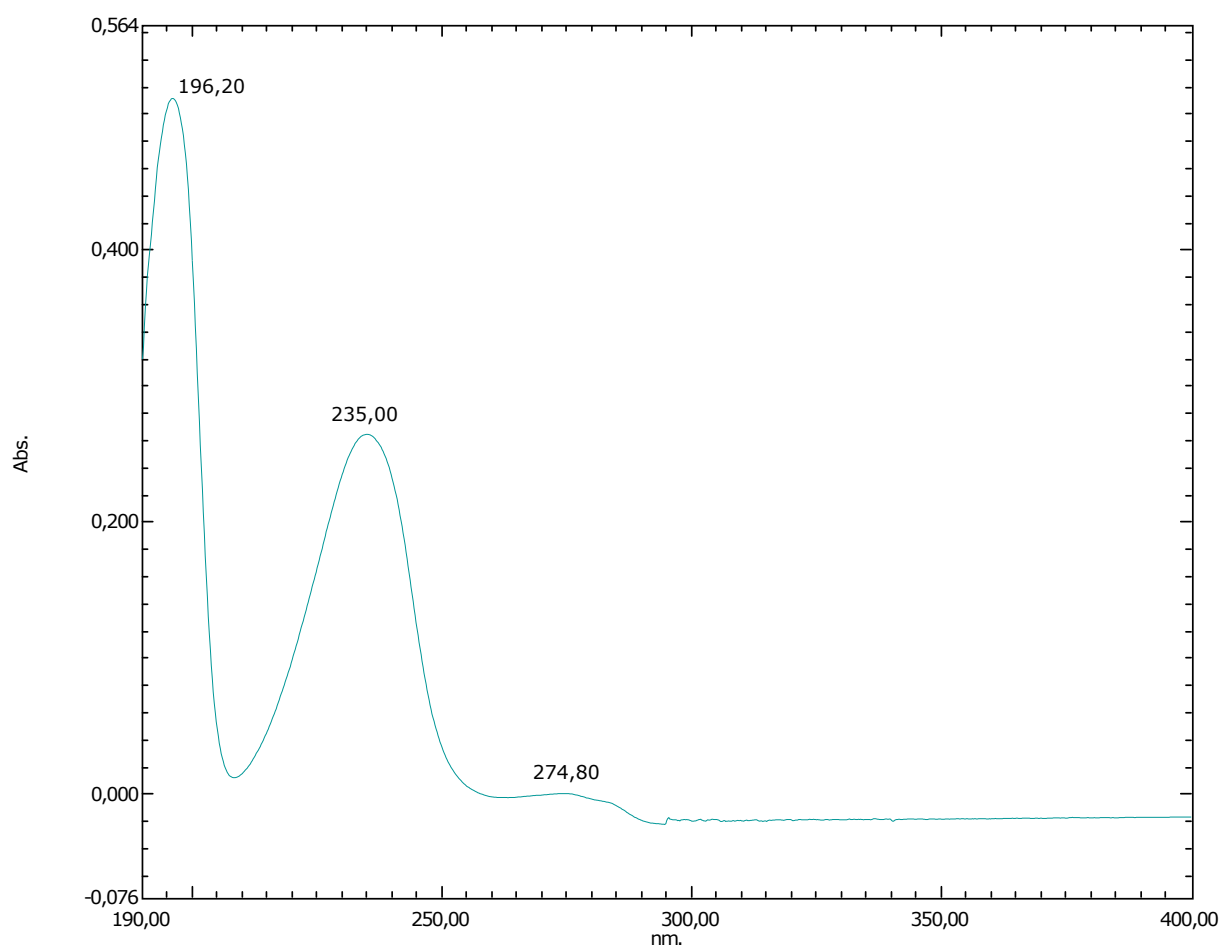
Figure 3.4:   Experimental UV-Vis spectrum of BPO in ACN. Absorbance on the y-axis and wavelength (nm) on the x-axis

Another fundamental parameter is the solubility of BPO in solvents. BPO is an apolar compound, hence is completely insoluble in water [108]. The solubility in organic solvent depends instead on the polarity of the solvent, and hence on the dielectric constant of the solvent. BPO in ethanol shows a solubility around 5.79×10^{-2} mol/l [108]. Less polar solvents as acetone or dichloromethane show higher solubility limits [108]. On the contrary, Benzoic Acid is a polar molecule due to the carboxylic group, hence BA is more soluble in water and more polar solvents [113].

In this thesis work, Luperox®A75 was used, which is 75% crystalline BPO and the remainder water, and comes as a white powder. Several different solutions were made with the already mentioned solvents in various concentrations. The preparation methods will be explained in the following section

3.2. Experimental Methods

3.2.1. Solutions

During this thesis work, different solutions of BPO dissolved in each organic solvents listed before were prepared. The effect of the concentration of BPO in the PLAL synthesis was investigated by employing several solution with different amounts of BPO in IPA. However, there is a limit in the quantity of BPO that can be dissolved in order to not damage the HPLC apparatus as explained later. The chosen concentrations ranged between 10 mM and 0.02 mM, namely: 0.02 mM; 0.05 mM; 0.1 mM; 0.2 mM; 0.5 mM; 0.75 mM; 1 mM; 2 mM; 5 mM; 7.5 mM; 10 mM. Since I was working with volumes of 5 mL a dilution step was required in order to reach very low concentrations. In the following, I report the procedures I followed for the preparation of each solution.

10 mM, 7.5 mM, 5 mM, 2 mM: These concentrations were obtained by weighing the mass of BPO needed to reach the desired value in 5 mL. In order to facilitate the solubilization the solutions were stirred and heated on a hotplate at 50°C until all the powder was gone. For the **10 mM**, the **7.5 mM**, the **5 mM** and **2 mM** solutions, 12.1 mg, 9.1 mg, 6.1 mg and 2.4 mg of BPO were weighed, respectively.

1 mM: First, a 5 mM solution was prepared in 5 mL as already described. Then, 1 mL was extracted from the 5 mM and diluted to a total volume of 5 mL.

0.75 mM: First, a 7.5 mM solution was prepared in 5 mL as already described. Then, 0.5 mL was extracted and diluted to a total volume of 5 mL.

0.5 mM: First, a 2.5 mM solution was prepared by weighing 6.1 mg and dissolving them

Solvent	5 mM	7.5 mM	10 mM
Methanol	1.3262		
Ethanol	1.3592		
Isopropyl-alcohol	1.3752	1.3752	1.3753
Acetonitrile	1.3422		

Table 3.2: Refractive index of highly concentrated BPO solutions

in 10 mL with the same process of the other concentrations. Then, 1 mL was extracted and diluted to a total volume of 5 mL.

0.2 mM: First, a 1 mM solution was prepared by weighing 2.4 mg which were dissolved in 10 mL with the already described method. Then, 1 mL was extracted and diluted to a total volume of 5 mL.

0.1 mM, 0.05 mM: First, a 0.5 mM solution was prepared with the already described method. Then, 1 mL and 0.5 mL were extracted and diluted to a total volume of 5 mL in order to obtain the **0.1 mM** and **0.05 mM** respectively.

0.02 mM: First, a 0.1 mM solution was prepared as described before. Then, 1 mL was extracted and diluted to a total volume of 5 mL.

It is worth noting that these procedures are general and not related to a specific organic solvent, however these concentrations were prepared only in IPA, while with the other organic solvents only the 5 mM solution was prepared.

Another important aspect that must be considered is the change of refractive index due to the addition of BPO to pure solvents. However, the effect was completely negligible for concentration smaller than 5 mM, and, although measurable for larger quantities, it is still very small, i.e. the change was at the fourth decimal place. The calculated values of the refractive indices of BPO solutions are reported in Tab. 3.2.

For experiments in water a target was covered with a layer of BPO, in order to evenly coat the surface a solution was prepared using acetone. BPO was dissolved almost to the solubility limit in acetone, then the target was dipped in the solution and the solvent was allowed to evaporate, then the process was repeated until a uniform layer was formed. When completely dry the coated target was easily used in water.
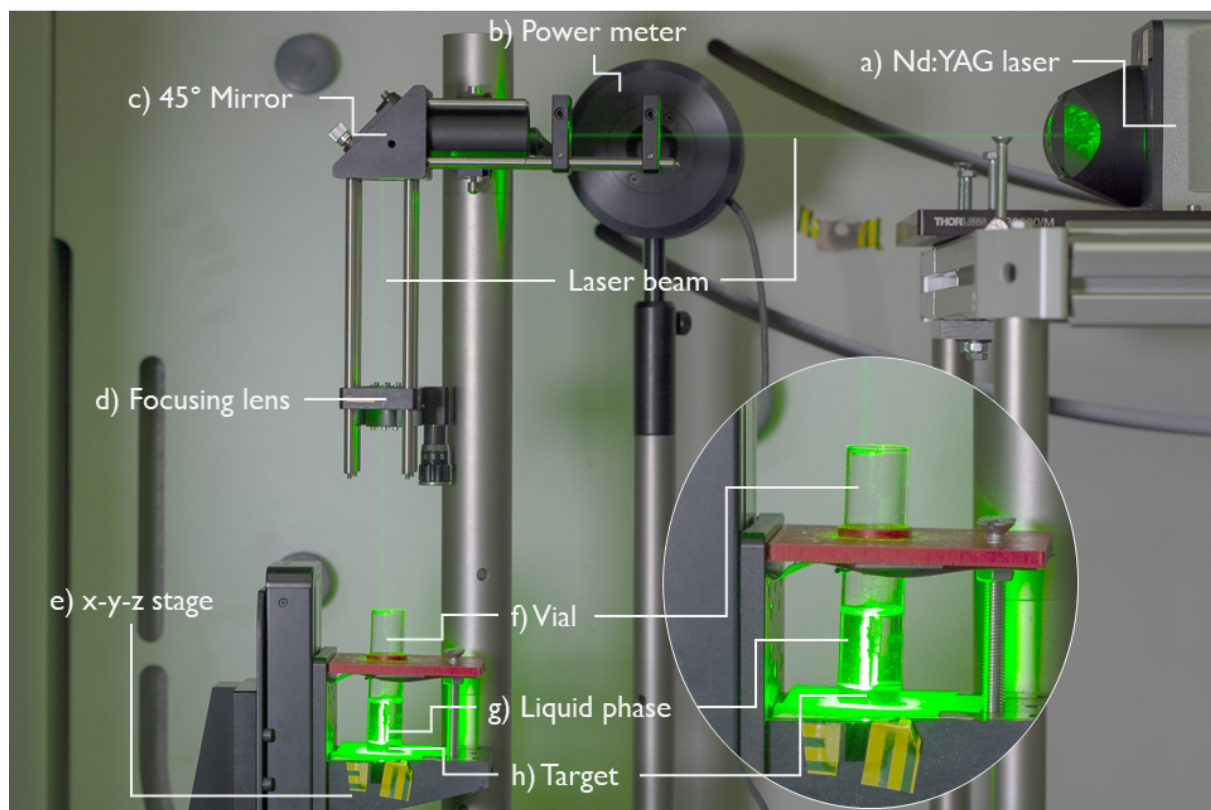
Figure 3.5:   Experimental PLAL setup.

3.2.2.   PLAL

The experimental setup for the PLAL synthesis was made up of several components, as shown in Fig. 3.5. I employed a Nd:YAG pulsed laser (Quantel Q-Smart 850) with a repetition rate of 10 Hz and a pulse duration of 6 ns. Nd:YAG lasers fundamental wavelength fires at 1064 nm, but in this thesis work the first three available harmonics were used, i.e. 1064 nm, 532 nm and 355 nm. The maximum nominal energy per pulse at 1064 nm is 850 mJ, at 532 nm is around 430 mJ and 230 mJ at 355 nm. The apparatus was also equipped with a beam attenuator which allowed to continuously tune the beam energy. For all the experiments the energy was set at 50 mJ using the beam attenuator module with the aid of a power meter (part (b), see Fig. 3.5). During the ablation, the beam leaves the laser head horizontally (part (a), see Fig. 3.5), then hits a 45° angled mirror (part (c), see Fig. 3.5) which deviates the light down toward the focal lens and then to the target. A lens with 20 cm focal length (part (d), see Fig. 3.5) was used to focus the light on the target, however I always worked under defocusing conditions in order to avoid splashes of solvent and damage to the target. I chose to keep a constant

Solvent	Distance - mm
Methanol	179.36
Ethanol	179.98
Isopropyl-alcohol	180.26
Acetonitrile	179.67

Table 3.3: Lens-target distance for each solvent as calculated by the software.

fluence of 2.71 J cm^{-2} in all experiments in order to deliver the same amount of energy per unit surface on the target. To set this fluence, I impose a spot radius of 0.766 mm, indeed fluence is easily calculated taking the energy per pulse (i.e. 50 mJ) divided the spot area. The spot radius depends on the focusing of the laser beam on the target. The focusing is related in turn to the focal length of the lens and to the optical path inside the solvent. Hence, it is important to consider the refractive index of the solvent, indeed the change in refractive index modify the optical path. Therefore, the dimension of the spot can be changed varying the distance between the lens and the target, which takes into account the total optical path of the focused laser beam. Since solvent volume was always the same (i.e. 5 ml), by knowing the height of the target and the dimensions of the vial, the optical path can be calculated. The lens-target distance was calculated each time automatically through a custom Python code, exploiting geometrical optic formulas [114]. The lens-target distances for all the configurations are reported in Tab. 3.3. The solvent and the target were held in a glass vial (part (f), see Fig. 3.5), which was secured on a stage free to move in three directions (part (e), see Fig. 3.5). In order to ablate uniformly the target surface, the stage was kept in a uniform spiral motion, thanks to three translators and the Python code.

To study also the effect of ablation time on the polyynes production and on the effect of BPO, I investigate different ablation times for ablations performed in IPA. Thus, I performed ablations for 15 min, 30 min and 120 min in various IPA solutions. As described in section 3.2.1, I prepared several solutions of BPO in IPA. Hence, I performed ablations in IPA solutions with increasing BPO concentration both at 1064 nm and 532 nm for 15 min. Pure IPA and 5 mM BPO solutions in IPA were ablated also at 30 min and 120 min both at 1064 nm and 532 nm. Regarding also the other solvents, pure solvent and 5 mM BPO solutions were ablated at 1064 nm, 532 nm and 355 nm for 15 min for each solvent. For each configuration at least two ablations were performed.

3.2.3. UV-Vis spectroscopy

Since polyynes have a strong optical absorption with a characteristic absorption spectrum, one of the easiest way to check their presence after the synthesis process is through UV-Vis absorption spectroscopy. Therefore, as a first characterization method, UV-Vis absorption of mixtures of polyynes were performed with a Shimadzu UV-1800 spectrophotometer, which is equipped with two lamps: a deuterium arc lamp, which covers the UV-region (ranging from about 190 nm to 400 nm), and a tungsten lamp, which covers the visible region (ranging from 300 nm to 1100 nm). Although the maximum range of the instrument is from 190 nm to 1100 nm, in this thesis work all measurements were performed between 190 nm and 400 nm, since the signals related to polyynes are in the UV region, especially those of shorter ones. Each ablated solution was diluted 37 times with the respective pure solvent in order not to saturate the detector: 20 µL of the ablated solution were diluted with 720 µL of pure solvent. To perform the analysis, the solution was put in a quartz cuvette with an optical path of 10 mm. A second cuvette containing pure solvent was measured at the same time to perform background removal of the solvent absorption spectra. Solvents should be more transparent as possible in the absorption range of the analysed species, however this is not always possible. Since in the solution the majority of the molecules are solvent molecules, in the range of the absorption spectrum of the solvent the solutes are usually not detectable. The so-called solvent cut-off represents the wavelength below which the solvent absorption is too high to give a reliable signal. However, as the Tab. 3.1 shows, the chosen solvents have quite low UV cut-off wavelengths, which don't bother the signal of polyynes longer than 8 carbon atoms. BPO too has its absorption spectrum right between 200 nm and 270 nm (see Fig. 3.4), therefore in all the experiment with BPO, polyynes signals were covered, and only the most concentrated ones are visible in spectra of solutions with low BPO concentrations.

3.2.4. High Performance Liquid Chromatography

In order to understand how the polyynes production is influenced by the various ablation parameters and the BPO action, *High Perfomance Liquid Chromatography* was extensively employed. In particular, I used reverse-phase liquid chromatography (RP-HPLC) since polyynes better interacts and are more retained by nonpolar stationary phases. A Shimadzu Prominence UFLC was employed (see Fig. 3.6), which is equipped with a photodiode array detector (DAD) UV-Vis spectrometer and a FRC-10A fraction collector. The UV-Vis spectrometer is equipped with a deuterium arc lamp and a tungsten lamp which guarantee a range from 190 nm to 800 nm. Moreover the DAD allows to

Figure 3.6: HPLC apparatus used in this work: the autosampler (a); oven and columns (b); the fraction collector (c); the pump system (d); the photodiode array spectrometer (e); the controller (f); solvent tray (g)

acquire the entire available spectral range simultaneously. In this thesis work, I mainly employed a C18 column (Phenomenex Luna® C18, 150 mm × 4.6 mm, 3 µm particle size), but some analysis were performed also with a C8 column (Shimadzu Shim-pack HPLC packed column GIST, 250 mm × 4.6 mm, 5 µm particle size). These are two chromatographic columns made up by packed silica particle (with a diameter of 3 µm and 5 µm respectively) functionalized with alkyl chains made of 18 and 8 carbon atoms, respectively. Alkyl chains lend an apolar character to the stationary phase, as expected in the reverse-phase configuration.

Each ablated solution was filtered using Phenomenex Phenex RC membrane syringe filters having a pore size of 0.45 µm in order to remove any carbon particulate and other impurities generated during the ablation that might obstruct or damage the columns. The majority of the ablations were analysed using a gradient method on the Luna® C18: this method involved a mobile phase of acetonitrile and water with an initial ACN percentage

equal to 65% which gradually increased during the analysis to 95%. Specifically, after 4 minutes of constant ACN concentration, the percentage of ACN was increased linearly from 65% to 95%, reaching the final value at 20 min, after which the concentration was kept constant until the end of the analysis at 45 min. The flow rate of the mobile phase was set to 0.8 mL/min. A volume of 15 μL was taken from each ablation and injected in the HPLC to be analysed. However, the injection volume was reduced when dealing with solutions with BPO concentration of 7.5 mM and 10 mM. In these two cases, the injection volume was reduced to 10 μL and 7 μL, respectively. Indeed, BPO concentration was a major issue since was orders of magnitude greater than polyynes, therefore we could not inject larger volumes for two main reasons: first, to not clog and damage the column, secondly to avoid enlarging too much the chromatographic peak of BPO. If the concentration of BPO was too high, it would have overloaded the column, increasing the pressure and leading to the automatic interruption of the analysis. This method was chosen since it allows me to achieved a good separation of the chromatographic peaks of hydrogen-, methyl- and cyano-capped polyynes, with chains length up to 22 carbon atoms in reasonable times (i.e 45 min). A good separation of chromatographic peaks is required to precisely calculate their area and therefore the concentrations of each species, which was fundamental in order to understand possible changes in their production. However, it does not manage to separate $HC_{12}CH_3$ from $HC_{12}CN$, which is the only case of superposition of two chromatographic peaks of polyynes. Another problem arose when dealing with BPO, whose chromatographic peak covers (completely or partially depending on the solvent) that of HC_8CH_3. When searching for chains longer than 22 carbon atoms, the Shim-pack C8 column was employed due to its lower retention power of polyynes that allows a quicker elution of long polyynes. Also in this case, a gradient method was employed. The ACN percentage was increased from 50% at 3 min to 90% at 20 min, then the concentration was kept constant till the end at 70 min and the flow rate was set at 1.000 mL/min.

The results of the HPLC analysis are gathered in the so called chromatogram. In the chromatogram the absorption of each species is recorded as a function of the elution time and the wavelength at which the absorption is occurred. Hence, by fixing the wavelength, the chromatogram presents a series of peaks (i.e. chromatographic bands) related to the species which absorb that specific wavelength, as shown in Fig. 3.7. Since the absorption is related to the concentration of the species, as explained in section 1.3.4, by measuring the area of each peak the concentration of each species is retrieved. Chromatographic areas of each polyyne were always considered only at certain specific wavelength, indeed, each polyyne has its own wavelength at which the most intense transition (MIT) occurs.
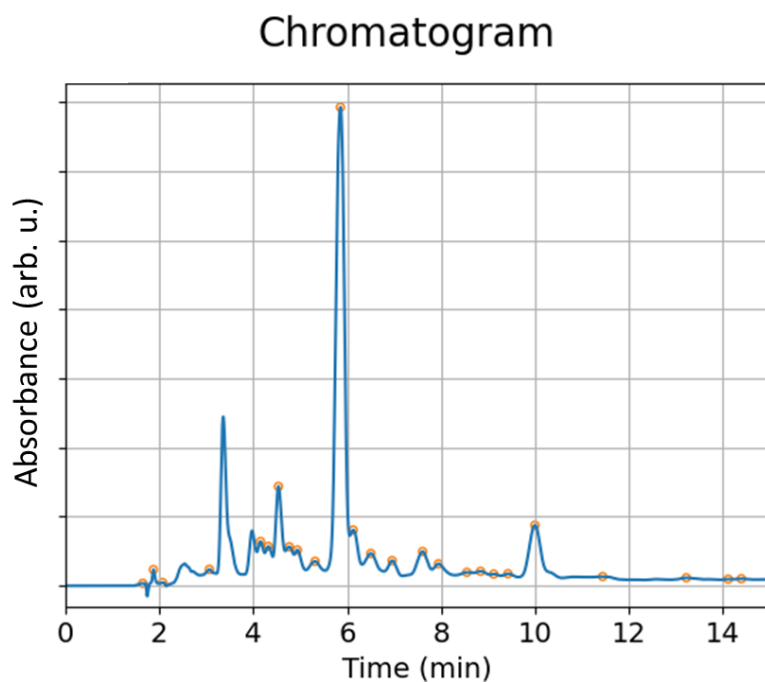
Figure 3.7:   The chromatogram at a fixed wavelength of 226 nm of an ablation in pure IPA. The main peak is related to the 8 atoms long hydrogen-capped polyyne.

Therefore, a channel for each MIT wavelength was created in the HPLC program and the chromatographic area of each band related to polyynes was measured at its own MIT wavelength. The conversion between chromatographic areas and concentrations is obtained through a constant factor, which was derived from a calibration curve. Hence, by multiplying the chromatographic area by 1.349×10^{-12} mol/l the concentration in mol/l were obtained.

4 | Experimental results

In this chapter I will present the results obtained from the experimental work. To the best of my knowledge, no previous work reported the use of a radical initiator in pulsed laser ablation in liquid for polyyne synthesis, thus I decided to investigate the effect of several PLAL parameters, such as ablation wavelength, solvent and ablation time. Benzoyl peroxide stability and reactivity depends on the solvents in which it is dissolved, the free radical concentration and the temperature of the solution. Hence, I decided to study the effect of BPO by ablating a graphite target in isopropyl alcohol at two laser wavelengths (1064 nm and 532 nm) with a fixed fluence of $2.7 \, \text{J/cm}^2$. Moreover, I expanded my analysis to three further solvents (methanol, ethanol and acetonitrile) and an additional laser wavelength (355 nm) to study the effect of each parameter. Since the ablation time affected also the synthesis yield of polyynes, different ablation times were also employed. In all the ablated solutions, I detected hydrogen-capped (HC_nH) and methyl-capped polyynes (HC_nCH_3), and when dealing with acetonitrile also cyano-capped polyynes (HC_nCN). For simplicity sake, from now on I will not explicitly write hydrogen terminations. Hence, I will refer to hydrogen-capped polyynes as C_n, to methyl-capped polyynes as C_nCH_3 and to cyano-capped polyynes as C_nCN. Although the principal investigation was on BPO effects, several considerations were also possible for ablation in pure solvents. Therefore, the effect of the pure solvents, the laser wavelength and the ablation time on the synthesis of polyynes via PLAL were also investigated. In the first section, the ablations in solutions of BPO and IPA are presented. In particular, I investigated the effect of concentration, laser wavelength and ablation time. Then, I provide some hypothesis of BPO-related effects on the synthesis of polyynes, based on the experimental evidences. In the second section, the results from the ablations in solutions of BPO in methanol and ethanol are presented. Lastly, the effects of BPO in ablations in acetonitrile are reported in the last section.
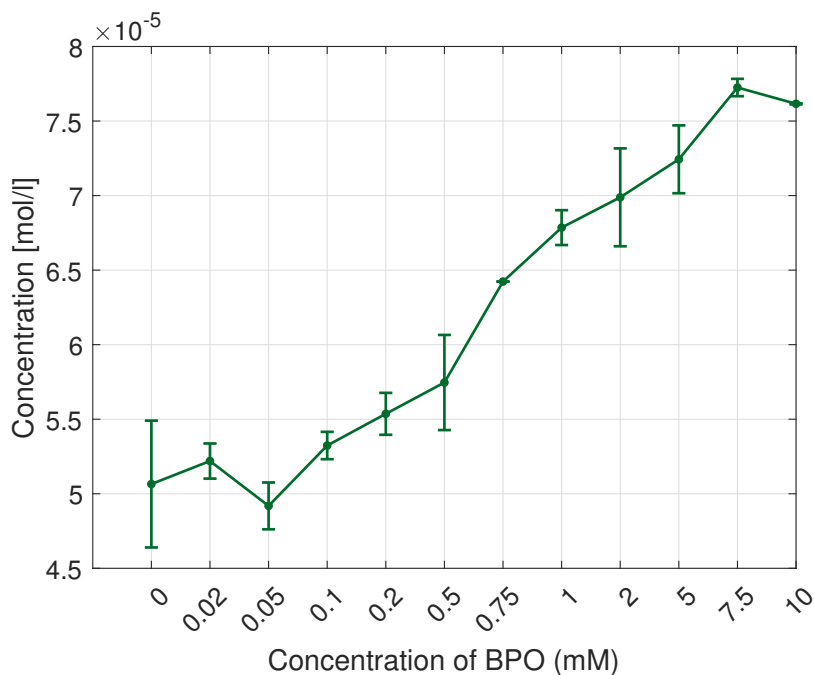
Figure 4.1:   Overall concentration of hydrogen-capped polyynes produced by ablations (532 nm,15 min) in IPA with increasing concentration of BPO. The 0 value of the x axis refers to ablation in pure IPA.

4.1.   Effects of the addition of BPO to ablations in isopropyl-alcohol

The first set of ablations concerns PLAL experiments performed in isopropyl-alcohol. Hence, solutions with increasing concentration of BPO were ablated both at 532 nm and 1064 nm for 15 min. The concentration of each polyynes were then measured through the HPLC method discussed in section 3.2.4. First, the data of the overall concentration will be presented to evaluate the effect of BPO in the synthesis yield. Different laser wavelengths have been shown to lead to different concentrations of polyynes (see section 2.3.1). Therefore, for each ablated solution, I considered the ratio between the productions in the BPO solution over the production in pure IPA, when comparing the effect of BPO at both wavelength. This was done to exclude the contribution of the laser wavelength to the polyyne concentrations.

4.1.1.   Effect of BPO on the synthesis yield of polyynes

The total concentration of synthesized polyynes from the ablations at 532 nm in solutions of IPA with and without BPO are reported in Fig. 4.1. Just as a reminder, I ablated
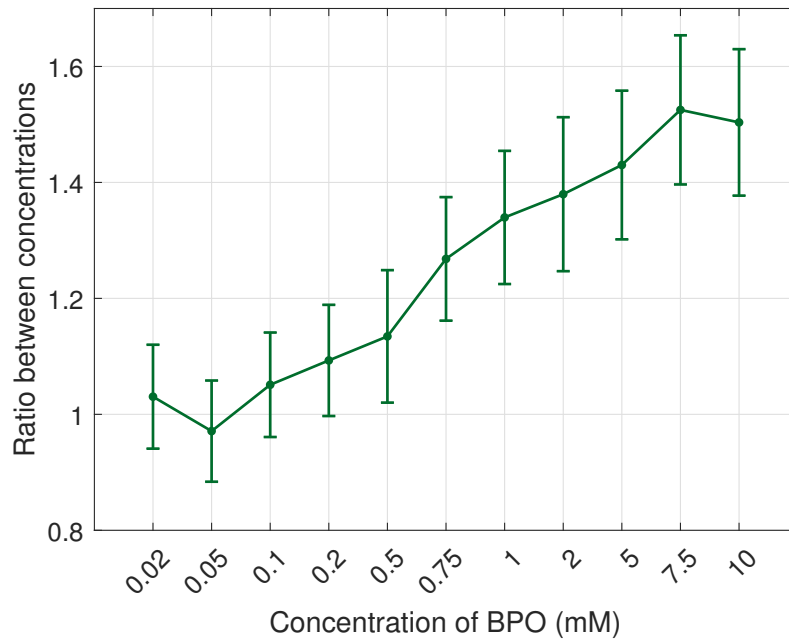
Figure 4.2: Ratio between the mean total concentration of polyynes in solutions of IPA with different concentrations of BPO over the mean total concentration of polyynes produced in pure IPA. Ablations were performed at $532\,\text{nm}$ for $15\,\text{min}$.

in each configuration presented in this thesis at least two times, and thus all the data are averages. The error bar takes also into account the standard deviation from the average. In pure IPA, the average concentration of polyynes is shown to be $(5.1 \pm 0.4) \times 10^{-5}\,\text{mol/l}$. The addiction of small quantities of BPO up to $0.1\,\text{mM}$ does not provide any significant effect on the total concentration of polyynes. However, an increase in the total concentration of polyynes is observed when the ablations were performed in solution with higher quantities of BPO. As shown in Fig. 4.1, increasing the BPO concentration corresponds to an increase in the mean polyynes concentration. It also seems that the concentration of polyynes saturates for BPO concentration higher than $7.5\,\text{mM}$, since no further increase is shown for $10\,\text{mM}$ BPO solution. By considering the ratio between the polyyne concentration in each solution with BPO over the polyyne concentration in pure IPA (see Fig. 4.2), we can easily evaluate the increase in polyyne synthesis due to the action of BPO. In this case, ratios greater than one represent the increase in the synthesis yield, i.e. the total concentration of polyynes is increased with respect to the case of ablations in pure IPA. As shown in Fig. 4.2, the synthesis yield of polyynes was increased by increasing the concentration of BPO. Higher BPO concentrations correspond to higher synthesis yield for PLAL in IPA. A ratio of 1.3 ± 0.1 was obtained for concentration of BPO at about $1\,\text{mM}$, which corresponds to an increase of 30% in the synthesis yield.
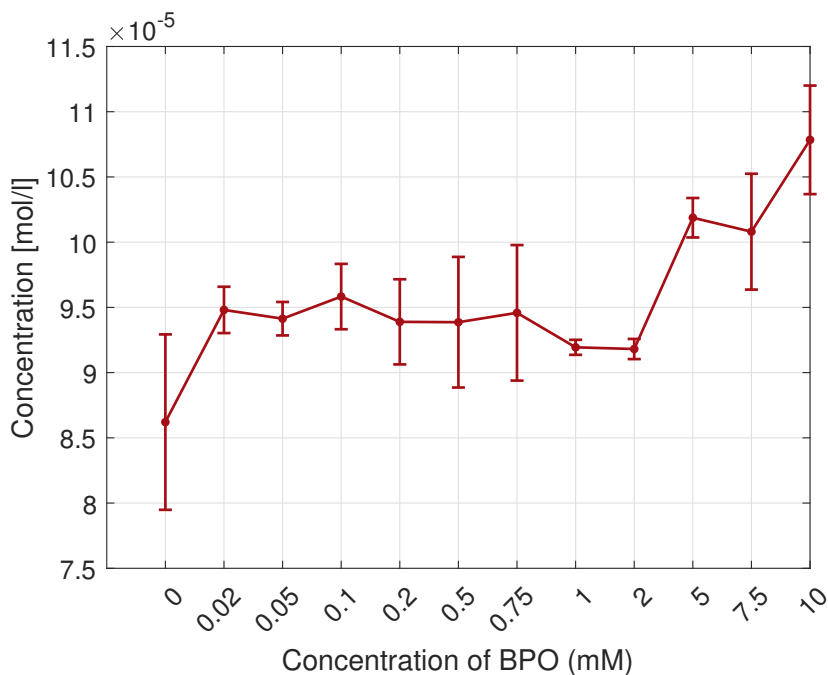
Figure 4.3:   Overall concentration of hydrogen-capped polyynes produced by ablations (1064 nm,15 min) in IPA with increasing concentration of BPO. The 0 value of the x axis refers to ablation in pure IPA.

In the solutions with 5 mM of BPO a ratio of 1.4 ± 0.1 was obtained, corresponding to a mean total concentration of $(7.2 \pm 0.2) \times 10^{-5}$ mol/l. The maximum concentration of polyynes was obtained by ablating the 7.5 mM solution, reaching an average value of $(7.72 \pm 0.06) \times 10^{-5}$ mol/l (see Fig. 4.1), which corresponds to a ratio of 1.5 ± 0.1 (see Fig. 4.2). The 10 mM produced slightly less than the 7.5 mM, hence it seems that the synthesis yield saturates for concentrations of BPO higher than 7.5 mM, still the synthesis yield was increased by roughly 50%.

The same set of experiments was performed also employing 1064 nm as ablation wavelength. In Fig. 4.3 the total concentration of synthesized polyynes from the ablation at 1064 nm in solutions with and without BPO are reported. Also in this case, a general increase in the polyyne concentration is detected. Ablations performed in solutions containing BPO showed to produce more polyynes, and also in this case higher concentration of polyynes were obtained by ablating in 5 mM, 7.5 mM and 10 mM BPO solutions (see Fig. 4.3). However, some differences between the two ablation wavelength employed (i.e. 532 nm and 1064 nm) can be highlighted. The increase in the synthesis yield is detected for all BPO concentrations, whereas for 532 nm ablations 0.02 mM, 0.05 mM and 0.1 mM no increase was visible. Contrary to 532 nm, for 1064 nm ablations there was not any saturation, and the concentration of polyynes reached the maximum value for 10 mM BPO
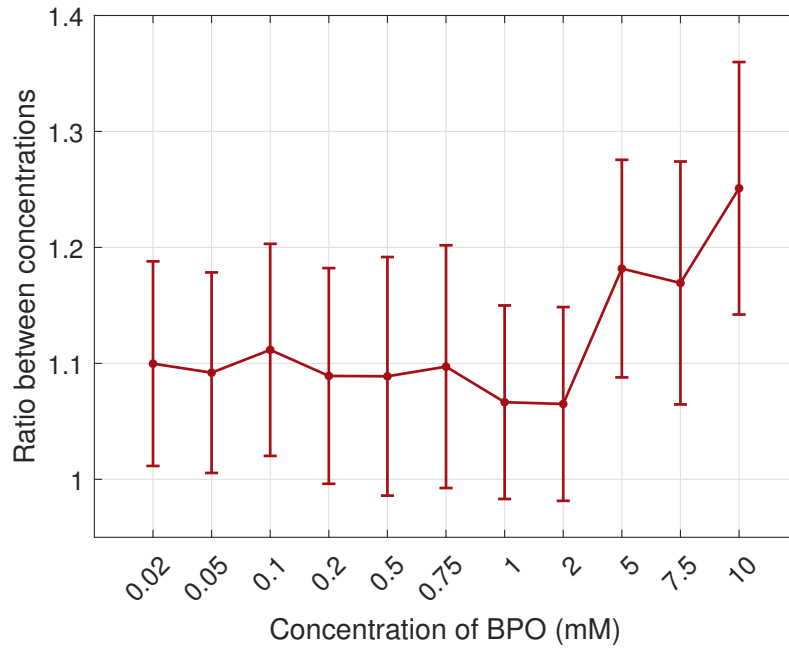
Figure 4.4: Ratio between the mean total concentration of polyynes in solutions with BPO over the mean total concentration of polyynes in pure IPA. Ablations performed at 1064 nm for 15 min.

solution. A further difference between the two ablation wavelength employed is the increase in the synthesis yield for BPO solution. As for 532 nm, in Fig. 4.4 the ratio between polyyne concentration in BPO solution and pure IPA is reported. The mean increase in polyyne production for ablations performed with 1064 nm is around 1.1 for BPO concentration from 0.02 mM to 2 mM. The increase was more relevant for BPO concentration of above 5 mM, and indeed the maximum increase was reached for the 10 mM solution, with a ratio of 1.3 ± 0.1. Hence, the solutions with BPO, despite its concentration, have a higher synthesis yield of polyynes compared to ablations in pure IPA for both wavelength at 15 min. However, the highest increase in the synthesis yield of polyynes was obtained by ablating 7.5 mM solutions at 532 nm. Moreover, the efficiency of polyynes production seems to depend on the concentration of BPO in solution. Indeed, for 532 nm, a clear increasing trend is shown by increasing the concentration of BPO (see Fig. 4.1). It is worth noting, that the concentration of BPO in the less concentrated solutions (0.02 mM and 0.05 mM) approaches that of polyynes in pure IPA (i.e. 5×10^{-5} mol/l, see Fig. 4.1).
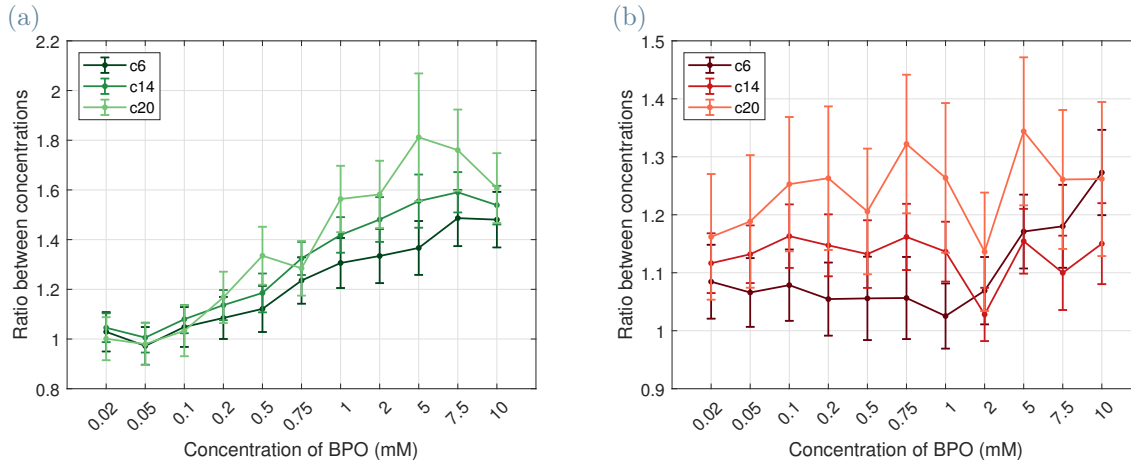
Figure 4.5: Ratios between the concentrations of size-selected hydrogen-capped polyynes produced in BPO solutions over those in pure IPA, for ablations performed for 15 min at (a) 532 nm and (b) 1064 nm. Three size-selected polyynes are displayed, namely C_6, C_{14} and C_{20}.

4.1.2.   Effect of BPO on size-selected hydrogen-capped polyynes

To further investigate the action of BPO in the ablation process, I considered the concentrations of size-selected hydrogen-capped polyynes produced in the previous solutions. Then, I calculated the ratio of the concentration of each polyyne in the ablations with BPO over the concentration of the same polyyne in pure IPA. The ratio of C_6, C_{14} and C_{20} at the two different ablation wavelengths are reported in Fig. 4.5. As shown by Fig. 4.5a, for 532 nm ablations the presence of BPO leads to different increases depending on the chain length. Moreover, I observed a larger increase in the concentration of longer polyynes compared to that of shorter one. Indeed, already for 1 mM solutions the ratio went from $1.3\pm0.1 \rightarrow 1.42\pm0.07 \rightarrow 1.6\pm0.1$ for increasing chain length $C_6 \longrightarrow C_{14} \longrightarrow C_{20}$, respectively. C_{20} reached its maximum increase for the 5 mM solution, with a ratio of 1.8 ± 0.3, while the maximum increase for C_{14} and C_6 can be found at 7.5 mM with a ratio of 1.59 ± 0.08 and 1.5 ± 0.1, respectively. Hence, in agreement with the results on total polyyne concentrations, an increase in BPO concentration corresponded to an increase in the concentration of each size-selected hydrogen-capped polyyne. The growth of the synthesis yield seems to slightly depend pn the chain length. Indeed, for hydrogen-capped polyynes longer than C_{16}, the maximum increase is found at 5 mM concentration of BPO, while for shorter chains is observed at 7.5 mM. The ratio for C_{16} were almost the same for both BPO concentrations.

Regarding the ablations performed at 1064 nm, also in this case the concentration of

longer chains features a larger increase compared to that of shorter ones, as shown in Fig. 4.5b. However, the increase was less significant compared to the ablations at 532 nm, as already observed in the total concentration (see Fig. 4.4). Shorter chains as C_6 have ratios between 1 and 1.1, and only for the most concentrated BPO solutions a higher increase was recorded. Longer chains have slightly higher ratios. The increase ratio of C_{14} oscillates around 1.1. C_{20} had a bigger increase around 20%, irrespective of the concentration of BPO. Indeed, the highest increase of C_{20} concentration was recorded for 5 mM solutions, but a close value was also obtained for 0.75 mM solutions. Despite what described before, an increase is always present also for very low BPO concentrations in 1064 nm ablations. Thus, the ablations at 1064 nm and 15 min appear to show a weaker dependence on the BPO concentration.

To further investigate the effect of BPO on the production of polyynes with different chain lengths, I chose to consider solutions with a fixed concentration, i.e. 5 mM. This BPO concentration was chosen for several reasons. 5 mM solutions showed a clear gain in polyynes production at both wavelength, and they were easier to prepare than less concentrated solutions. Moreover, 5 mM was also the highest concentration of BPO that fits the constraints for the HPLC analysis in terms of column overloading.

A comparison between the gains of each chain is reported in Fig. 4.6 for both the ablation wavelengths, keeping fixed the BPO concentration at 5 mM. As explained before, the 532 nm ablations show larger increases in production efficiency than 1064 nm. This effect is true for every chain length as shown in Fig. 4.6. Moreover, the gain in concentration grows with the chain length at 532 nm. For 1064 nm the gain is almost constant around 1.2 with the exception of long polyynes, namely C_{18}, C_{20} and C_{22}. The chromatographic peak and, as a consequence, the concentration of C_{22} was too low to be detected and calculated without large errors with ablation at 532 nm. Indeed, as reported in Fig. 4.3, the overall production of polyynes and, in particular, of C_{22} by the 1064 nm ablation laser is larger than those by 532 nm. I will discuss the effect of the ablation wavelength on the concentration of polyyne in section 4.1.4.

4.1.3. Effect of BPO on size-selected methyl-capped polyynes

As already described in the previous chapters, organic solvents may provide also other endgroups, and in particular it was shown in literature that ablations in IPA are able to produce methyl-capped polyynes [32]. Indeed, also in this work, I observed the formation of methyl-polyynes by ablations in IPA. As in the case of hydrogen-capped polyynes, I investigated the effect of BPO on the synthesis yield of methyl-capped polyynes. Unfor-
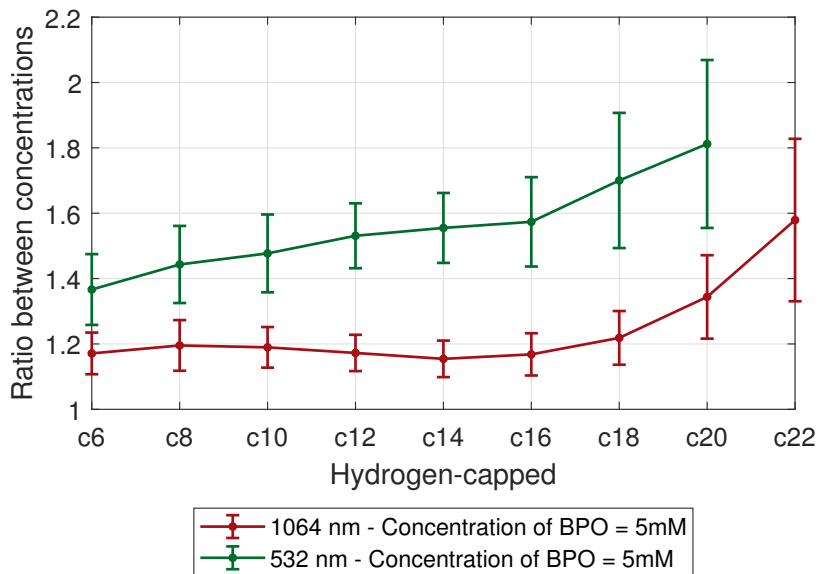
Figure 4.6:   Ratio between concentrations of hydrogen-capped polyynes in $5\,\text{mM}$ solutions over those in pure IPA, for both wavelengths ($532\,\text{nm}$ - green line, $1064\,\text{nm}$ - red line).

tunately, the chromatographic peak of C_8CH_3 was covered by the peak of BPO, since they both absorb around $230\,\text{nm}$ and are eluted at the same time. Therefore, no data regarding this polyyne was recorded in BPO solutions. As for the hydrogen-capped polyynes, the ratios between concentration of size-selected methyl-capped polyynes in BPO solutions over those in pure IPA were calculated. The results for three size-selected methyl-polyynes ($C_{10}CH_3$, $C_{12}CH_3$ and $C_{16}CH_3$) at the two different ablation wavelengths are shown in Fig. 4.7. As it is shown in Fig. 4.7a, the same trend of hydrogen-capped polyynes is also observed for methyl-capped polyynes, when ablating at $532\,\text{nm}$. An increase in the BPO concentration corresponded to a growth of the concentration of each methyl-capped polyyne. As for hydrogen-capped, small amounts of BPO do not seem to provide any relevant effect. A clear gain in the concentration of methyl-capped polyynes is found above $1\,\text{mM}$. The maximum concentrations at all chain lengths of methyl-capped polyynes were achieved for ablations in $7.5\,\text{mM}$ solutions, as shown in Fig. 4.7a.

Regarding the ablations at $1064\,\text{nm}$, the effect of BPO does not show a clear trend. For shorter methyl-capped chains, an increase in their concentrations was recorded at all BPO concentrations, though small and relevant only above $5\,\text{mM}$ (see Fig. 4.7b). However, longer chains showed a decrease in their synthesis efficiency at high BPO concentrations, with concentrations smaller than that of pure IPA (i.e. ratios smaller than 1).
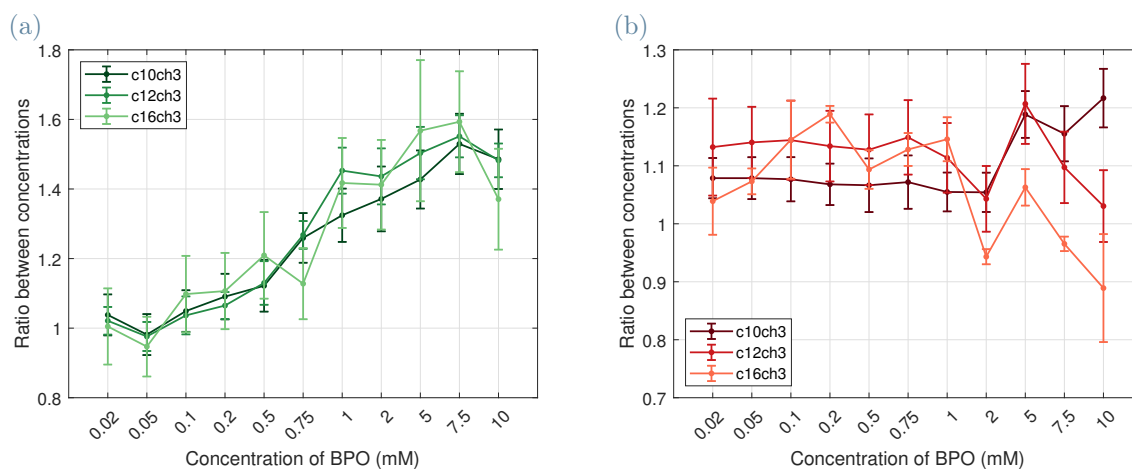
Figure 4.7: Ratios between the concentrations of size-selected methyl-capped polyynes produced in BPO solutions over the respective concentrations in pure IPA for ablations performed for 15 min at (a) 532 nm and (b) 1064 nm. Three methyl-polyynes are displayed $C_{10}CH_3$, $C_{12}CH_3$ and $C_{16}CH_3$.

Considering the ratio of each size-selected methyl-capped polyyne by keeping fixed the BPO concentration at 5 mM, reported in Fig. 4.8, there is no clear trend related to the chain length. However, from the graph in Fig. 4.8 it is clear that the greater gain in BPO solutions was still obtained at 532 nm. The chromatographic peak of $C_{18}CH_3$ was too low and affected by noise to calculate the ratio at 532 nm. On the contrary, the overall production of polyynes by the 1064 nm ablation laser was high enough to detect $C_{18}CH_3$ with a greater precision.

4.1.4. Effect of the ablation wavelength on polyyne production

In the previous paragraphs, I showed the effect of the presence of BPO in ablations performed with two different wavelengths (1064 nm and 532 nm). However, as described in section 2.3.1, laser wavelength affects the concentration and the length distribution of polyynes [80]. In this work, I also observed this phenomenon, as shown in Fig. 4.1 and 4.3. By considering only the effect of the laser wavelength in ablations in IPA, I ablated pure IPA with all the available wavelengths of our ablation setup, namely 1064 nm, 532 nm and 355 nm. The concentration of each size-selected polyyne detected by HPLC for the three different wavelengths is reported in Fig. 4.9. The overall concentration of polyynes decrease going from 1064 nm to 355 nm ablations (see Fig. 4.9). For example, C_6 was produced in concentration of $(2.8 \pm 0.1) \times 10^{-5}$ mol/l via ablations at 1064 nm, while the concentration was $(2.3 \pm 0.2) \times 10^{-5}$ mol/l at 532 nm and $(1.28 \pm 0.05) \times 10^{-5}$ mol/l
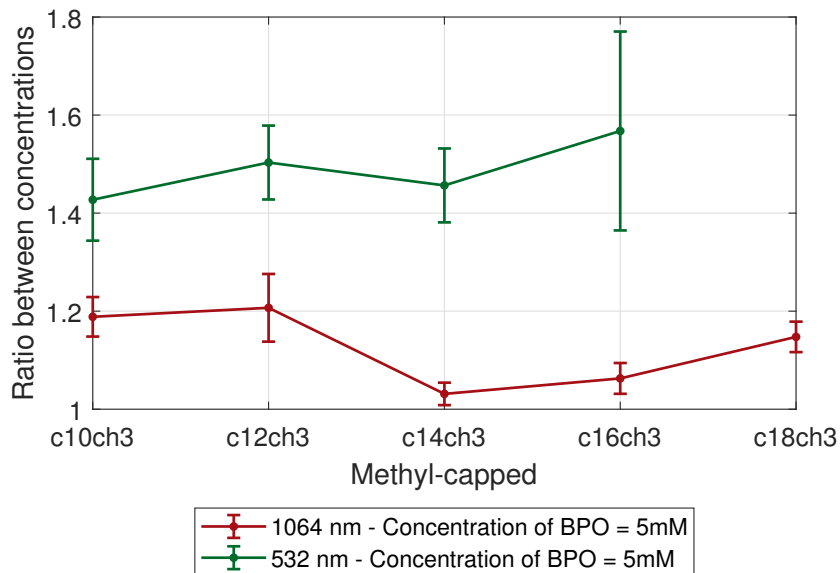
Figure 4.8: Ratio between the concentrations of size-selected methyl-capped polyynes in 5 mM solutions over those in pure IPA, for both ablation wavelengths.
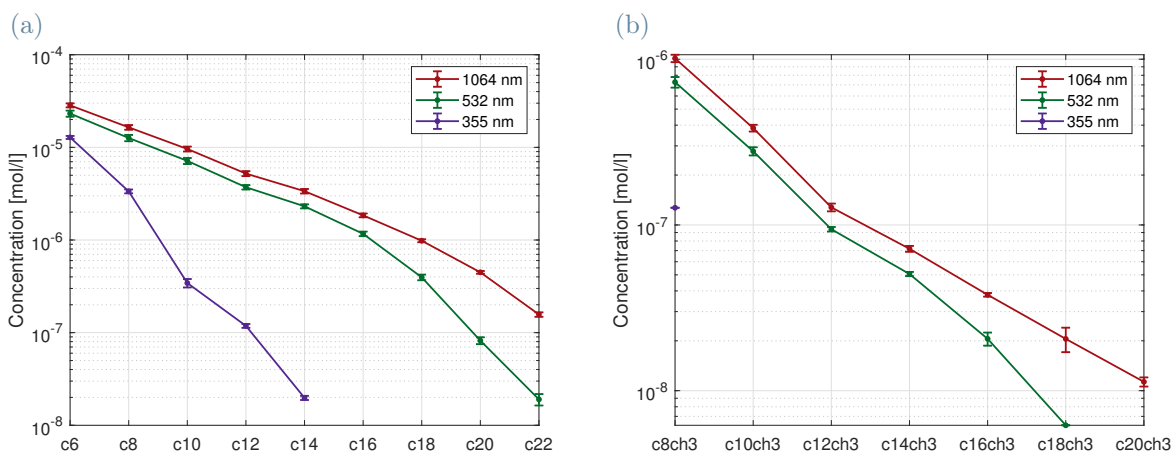
Figure 4.9: Concentrations of size-selected (a) hydrogen- and (b) methyl-capped polyynes after ablations in pure IPA at 1064 nm (red line), 532 nm (green line) and 355 nm (purple line) for 15 min.

at 355 nm. Hence, I found that longer laser ablation wavelengths correspond to higher production of polyynes, when ablating a solid graphite target in pure IPA. As shown by Fig. 4.9, longer chains were produced in lower concentrations with respect to shorter ones, while keeping fixed the employed laser wavelength. However, longer chains were also favoured by ablations with longer laser wavelength. Indeed, ablations at 1064 nm produced significant concentrations of C_{20} and C_{22} with concentration of $(4.5 \pm 0.2) \times 10^{-7}$ mol/l and $(1.57 \pm 0.09) \times 10^{-7}$ mol/l respectively, while at 532 nm the concentration of C_{20} was $(8.2 \pm 0.7) \times 10^{-8}$ mol/l and C_{22} was an order of magnitude less than 1064 nm with concentration of $(1.9 \pm 0.3) \times 10^{-8}$ mol/l, while there was not any trace of hydrogen-capped polyynes longer than C_{14} in ablations with 355 nm. This result is in agreement with those of Matsutani *et al.* and Park *et al.* , which showed that longer ablation wavelengths produce more polyynes than shorter ones in ablations with solid targets [79, 80]. In this thesis work, I obtained this result both for hydrogen-capped (Fig. 4.9a) and methyl-capped polyynes (Fig. 4.9b). Indeed, regarding methyl-capped polyynes, in 1064 nm ablations, it was possible to detect chains with length up to $C_{20}CH_3$ with a concentration of $(1.13 \pm 0.07) \times 10^{-8}$ mol/l, while in 532 nm $C_{18}CH_3$ was barely detectable with a concentration at around 6×10^{-9} mol/l. In 355 nm ablations, I managed to detect hydrogen-capped chains up to C_{14} with a concentration of $(1.9 \pm 0.1) \times 10^{-8}$ mol/l (two orders of magnitude less than the other two wavelengths), while the only methyl-capped polyyne detected was C_8CH_3 with a concentration around 1.2×10^{-7} mol/l. The different behaviour of shorter wavelengths is probably related to photofragmentation phenomena as described in section 2.3 [80]. Indeed, shorter wavelengths are more scattered than longer ones, hence they are more easily absorbed by the liquid phase containing the synthesized polyynes. This effect, in conjunction with non-linear optical processes as multi-photon absorption, can lead to a higher fragmentation of the chains for shorter ablation wavelengths, reducing the production as occurs in Fig. 4.9. Moreover, longer chains have a higher probability to absorb incident photons, due to their lower HOMO-LUMO gap. Therefore, long chains are more prone to be fragmented than shorter one. Indeed, ablations with 355 nm did not manage to produce long chains (see Fig. 4.9).

From this comparison, it is possible to conclude that 1064 nm produces the highest concentration of polyynes and favours the synthesis of longer ones. C_{22} and $C_{18}CH_3$ were also detected in 532 nm, however their concentration were closer to the sensitivity of the instruments and hence are more affected by experimental error. For this reason, when considering ablations performed in BPO solutions, the ratios of C_{22} and $C_{18}CH_3$ in 532 nm are not reported, as well as the ratio of $C_{20}CH_3$ for 1064 nm ablations, since their errors were too great to be compared with the other results.

4.1.5.   Effect of the ablation time on polyyne synthesis yield in BPO solutions

The results described in the previous paragraphs were obtained through ablations with an ablation time of 15 min. Since ablation time was shown to affect the polyyne productivity [78, 79, 88], I decided to investigate the effects of BPO also for longer times. Hence, ablations with 1064 nm and 532 nm were performed for 30 min and 120 min in 5 mM BPO solutions. In order to study only the effect of BPO, ablations in pure IPA are performed as well and taken as reference. Since the 355 nm productivity was way lower than the other two wavelengths, I did not performed any 355 nm ablations at longer times. Contrary to the ablations presented before, only a single experiment per each of these configurations was performed due to the long ablation time. Hence, the data presented in this section are single data point. By ablating pure IPA, an overall increase in the concentration of polyynes was recorded for growing ablation times compared to 15 min and the highest concentration was reached after 120 min. This result was true for both wavelengths, i.e. the concentration in ablations for 120 nm was higher than that at 30 min by keeping fixed the ablation wavelength. Hence, the total concentration of polyynes increases as the ablation time increases in pure solvent ablations, irrespective of the wavelength employed. When increasing the time from 30 min to 120 min, the total concentration of synthesized polyynes seemed not to reach a saturation value. However, the change in the synthesis yield was not the same for each chain length: indeed, for ablation at 532 nm and 120 min, shorter chains were favoured, while longer chains, as C_{20} and C_{22}, were less concentrated than at 15 min. This effect could be related to photofragmentation phenomena induced in longer chains by the 532 nm laser. Therefore, though the increase in the ablation time, ablations with the 532 nm laser does not allow to synthesize a significant amount of polyynes longer than C_{22}. On the contrary, I did not record this effect for 1064 nm, for which the concentration of each polyyne was increased at longer ablation times compared to 15 min. To further study the effect of ablation time on the length of the chains, I analysed the ablations at 1064 nm with another chromatographic method (Shimpack C8 - gradient). From this analysis I found chains up to C_{26} in 30 min and 120 min ablations. As for the shorter polyynes, by increasing the ablation time also the concentrations of C_{24} and C_{26} were increased in ablations at 1064 nm. The experimental spectrum of C_{26} is reported in Fig. 4.10, showing the main peak of the vibronic spectrum at 385 nm.

Regarding the effect of BPO, Fig. 4.11 shows the ratio of the concentration of size-selected hydrogen-capped polyynes between 5 mM and pure IPA solutions for both wavelength for 30 min (Fig. 4.11a) and 120 min (Fig. 4.11b) of ablation times. It is worth noting that the concentrations of C_6 and C_8 were so high to overcome the detection limit of the UV-Vis
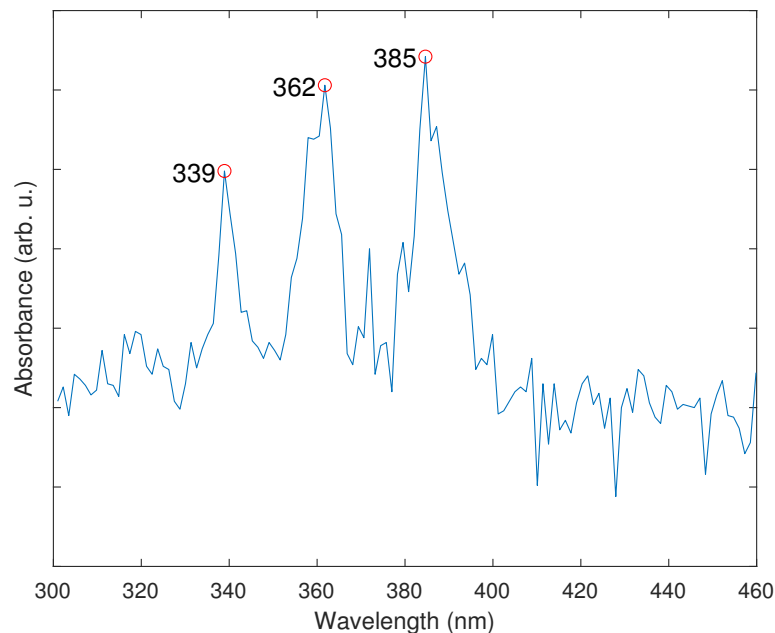
Figure 4.10: UV-Vis absorption spectrum of C_{26} obtained by ablating pure IPA for 30 min with 1064 nm laser light.
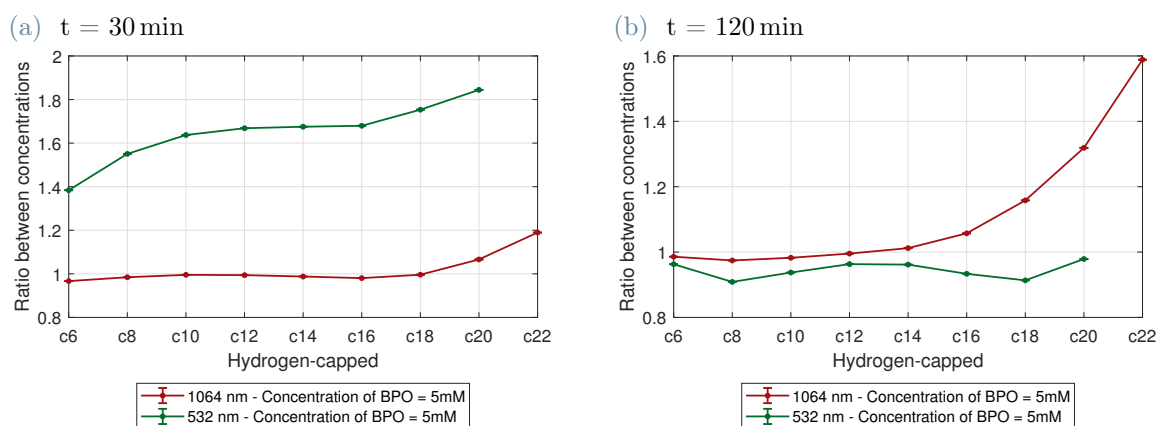
Figure 4.11: Ratio between the concentrations of size-selected hydrogen-capped polyynes in 5 mM BPO solutions and pure IPA for ablations performed at 1064 nm (red line) and 532 nm (green line) for (a) 30 min and (b) 120 min.

(a) t = 30 min
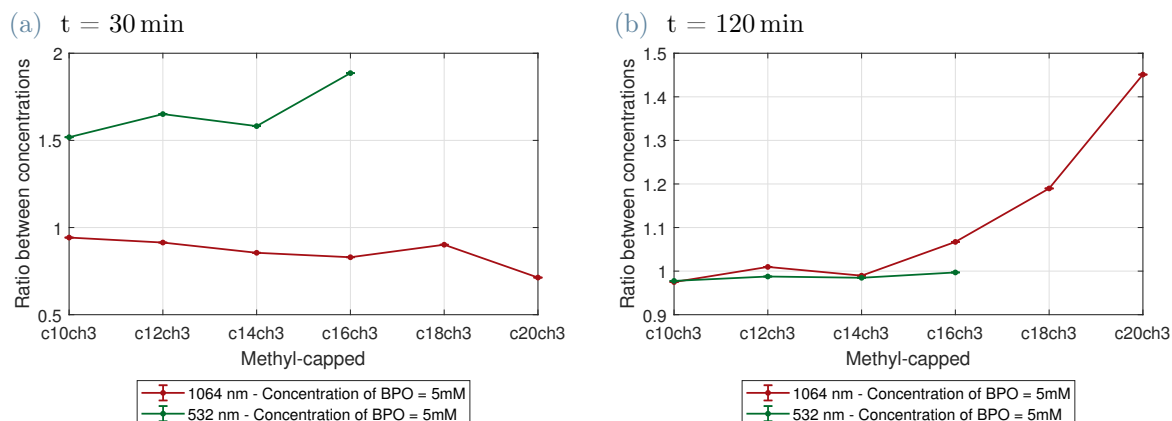
(b) t = 120 min

Figure 4.12:   Ratio between the concentrations of size-selected methyl-capped polyynes in 5 mM BPO solutions and pure IPA for ablations performed at 1064 nm (red line) and 532 nm (green line) for (a) 30 min and (b) 120 min.

detector of the HPLC apparatus. As shown in Fig. 4.11a, the effect of BPO in ablations of 30 min seems to be similar to the results at 15 min (see Fig. 4.6), with a bigger gain for ablations performed with the 532 nm laser. However, by further increasing the ablation time to 120 min a larger increase was obtained for 1064 nm, while for 532 nm the ablations in 5 mM BPO solutions showed a lower production than in pure IPA (see Fig. 4.11b). This result suggest the presence of different processes occurring during the ablations with different laser wavelength. However, this effect is still under investigation. Regarding the production of long polyynes, by ablating a 5 mM BPO solution for 120 min at 1064 nm, I recorded the highest concentrations of longer polyynes. Indeed, the C_{20} concentration reached a value of 2.25×10^{-6} mol/l and C_{22} a value of 6.58×10^{-7} mol/l. By analysing these solutions with the column Shimpack C8, I observed an improved synthesis yield also for C_{24} and C_{26}.

Regarding methyl-capped polyynes, in pure IPA an increase in the concentration of methyl-capped polyynes was found for both times, i.e. 30 min and 120 min, and wavelengths, i.e. 532 nm and 1064 nm, compared to the 15 min cases. However, as for hydrogen-capped chains, 532 nm did not favour longer chains. Instead, 1064 nm favoured the concentration of each polyyne up to $C_{20}CH_3$. The effect of BPO was the same as for hydrogen-capped polyynes, Fig. 4.12 shows the ratio of the concentration of size-selected methyl-capped polyynes between 5 mM and pure IPA solutions for both wavelength for 30 min (Fig. 4.12a) and 120 min (Fig. 4.12b) of ablation times. For times up to 30 min 532 nm ablations in BPO solutions had ratios oscillating around 1.6 (see Fig. 4.12a).
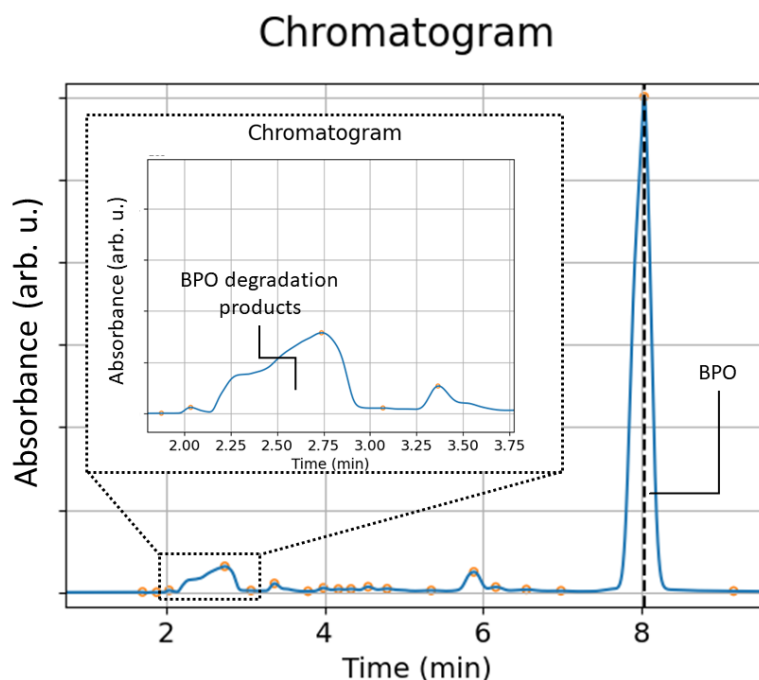
Figure 4.13: Part of the chromatogram at 230 nm of an ablation in 2 mM BPO solution at 1064 nm for 15 min, showing the peak of BPO at 8 min and a broad band belonging to degradation product od BPO.

Instead, for 120 min the highest ratios were for 1064 nm ablations, which showed also a greater increase in the synthesis yield of longer polyynes (see Fig. 4.12b).

4.1.6. Reaction mechanism of BPO during PLAL

Ablations in solutions with Benzoyl Peroxide were shown to produce more polyynes, but a clear mechanism does not emerge from the presented results. By considering the HPLC analysis, BPO was eluted after 8 min when using the gradient method on the Luna® C18 column, as shown in Fig. 4.13. Moreover, I recorded the presence of many compounds in a broad chromatographic band (see Fig. 4.13) with UV-Vis spectra similar to the spectrum of Benzoic Acid (BA). Hence, I suppose they were degradation products of BPO and the most concentrated one can be BA, followed by MeBA and EtBA. Indeed, these compounds were eluted in the first minutes, since they are smaller, more polar than BPO and more soluble in water. The presence of degradation products was also recorded through UV-Vis analysis in ablations with water and a graphite target covered by crystalline BPO. Indeed, in contrast to BPO, benzoic acid is soluble in water due to its higher polarity. As described in section 3.1.3, these compounds are the result of the radical degradation of BPO in alcohols [104]. This implies that some percentage of BPO reacted

through the cleavage of the O−O bond, by thermal or photo-induced activation. In 15 min ablations, the chromatographic area of the band related to the degradation products was very similar between ablations with the same BPO concentration, irrespective of the employed laser wavelength. Hence, I measured the temperature variation of the solvent throughout ablations at 15 min and 30 min for both wavelengths (1064 nm and 532 nm). I fixed a thermocouple in the solvent as close as possible to the target but avoiding that the laser beam could hit it and I recorded the temperature evolution. The results showed that the temperature of the solvent increased up to a plateau around 30°C in about 12 min. Longer ablations did not show any significant further increase. By ablating both at 1064 nm and 532 nm, I did not detect any temperature evolution difference. However, these measurements represent the average temperature of the solvent during the ablation, but much higher temperatures are expected to be reached closer to the plasma plume. Hence, the dissociation of BPO should be more probable closer to the plasma plume.

Benzoate radicals, i.e. the products of the cleavage of the O−O bond, need hydrogen atoms to form benzoic acid and in PLAL experiments the only source of hydrogen atoms was the solvent. In the PLAL process, the plasma generated by the laser atomizes the solvent molecules, thus a source of free hydrogen atoms is the plasma plume and the interface between the plume and the solvent. Hence, BPO molecules close to the plasma should have a higher probability to react and capture H-atoms or other fragments, thus forming degradation products. This process may induce a depletion region of endgroups around the plasma favouring the polymerization of polyynes at the expense of hydrogenation and termination processes. For these reasons, I observed experimentally an increase in the overall polyyne concentration and, in particular, this mechanism can favour the formation of longer polyynes. Indeed, since the termination reactions are less probable, the polymerization process allow the chains to grow longer.

The effect of BPO was shown to depend both on BPO concentration, laser wavelength and ablation time. Considering the hypothesis on the reaction mechanism, an increase in the BPO concentration corresponds to a higher concentration of benzoate radicals around the plasma plume, and hence to a greater depletion of hydrogen atoms. Therefore, higher concentrations of BPO produce more and longer polyynes as shown by the results presented so far. The different behaviour of BPO solutions with 1064 nm and 532 nm laser wavelength could be related to different phenomena. As said before, the macroscopic temperature of the solutions during the ablations at the two different wavelengths follow the same evolution and thus cannot be the cause under such differences. The local temperature of the plasma plume, instead, may be different when ablating at different wavelengths. However, the plasma temperature (from 2000 K to 5000 K [51, 115]) is or-
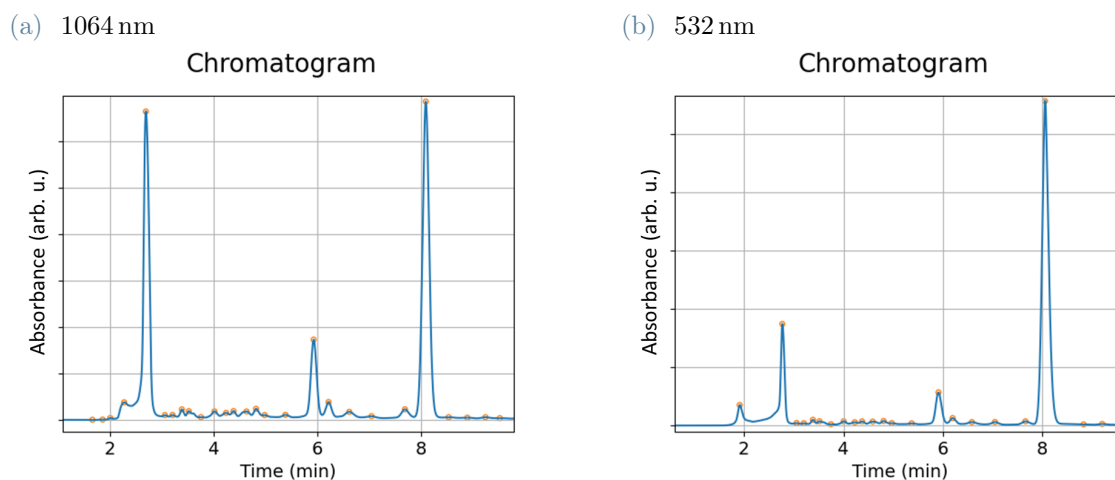
(a) 1064 nm

(b) 532 nm

Figure 4.14: Chromatograms recorded at 230 nm of ablations in 5 mM BPO solutions for 120 min at (a) 1064 nm and (b) 532 nm.

ders of magnitude higher than the thermal activation of BPO (at about 310 K), thus there would not be any significant difference between the two wavelengths. Hence, the majority of the BPO dissolved in solution should behave in the same way. Productivity with 1064 nm showed to be higher than with 532 nm in pure IPA, thus the gain in productivity could be less relevant in ablations at 1064 nm, since the concentrations of polyynes are already higher. However, the effect of the two laser wavelengths at longer times showed to be different from the behaviour at 15 min. In the ablations at 120 min, the 1064 nm laser generate a larger amount of degradation products of BPO compared to the 532 nm laser. Indeed, as shown in Fig. 4.14a, the peak of BPO and BA had almost the same absorbance at 1064 nm, while at 532 nm less BPO seemed to be degraded (see Fig. 4.14b). Therefore, the degradation of BPO seems to be favoured by 1064 nm, and this condition correspond to a gain in the polyyne concentrations with respect to pure IPA. On the contrary, with 532 nm BPO solution produced less than pure IPA at the same wavelength. However, this effect is shown only at longer ablation times above 30 min. The different behaviour at the two wavelengths and increasing ablation times could be related to the presence of more phenomena occurring in parallel. For example, processes of ring-opening of the two phenyl groups in BPO could increase the production providing larger radicals. This phenomenon could be favoured by employing the 532 nm laser due to more energetic photons. However, this process should not form BA as degradation product since the BPO molecules would be destroyed. 1064 nm photons could instead excite vibrational mode of the BPO molecules, hence increasing the probability of the radical activation of BPO.

(a)

(b)

(c)

(d)
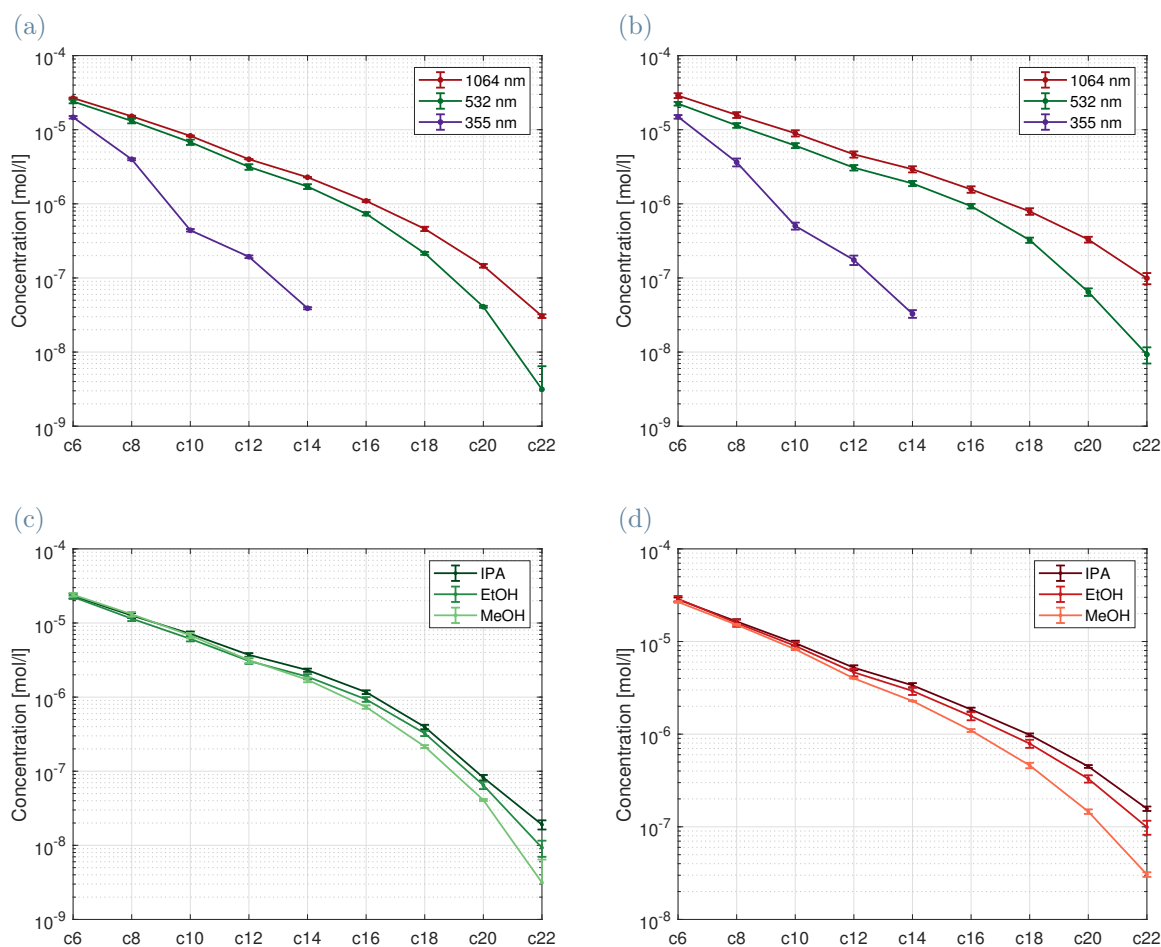
Figure 4.15:   Concentration of hydrogen-capped polyynes at different wavelengths (1064 nm, red line, 532 nm, green line, 355 nm, purple line) for (a) pure MeOH and (b) pure EtOH. Comparison between the production of hydrogen-capped polyynes in pure MeOH, pure EtOH and pure IPA for (c) 532 nm and (d) 1064 nm.

4.2.   Effect of BPO in pulsed laser ablation in alcohols

The ablation solvent has been proved to be a fundamental parameter for synthesis of polyynes via PLAL, hence I decided to test the effect of BPO also in other organic solvents. For this reason, I performed ablations with 5 mM BPO solutions and pure solvents in other two alcohols, i.e. methanol and ethanol. Both 1064 nm and 532 nm were employed in the ablations and I fixed 15 min as ablation time. Ablations in pure solvents were performed also with 355 nm light. The concentrations of synthesized hydrogen-capped polyynes in pure MeOH and EtOH were higher for the 1064 nm laser, as shown in Fig. 4.15a and 4.15b, respectively. Hydrogen-capped polyynes up to C_{22} were detected in both solvents, but a smaller amount of C_{22} was detected in 532 nm ablations as for IPA. Methyl-
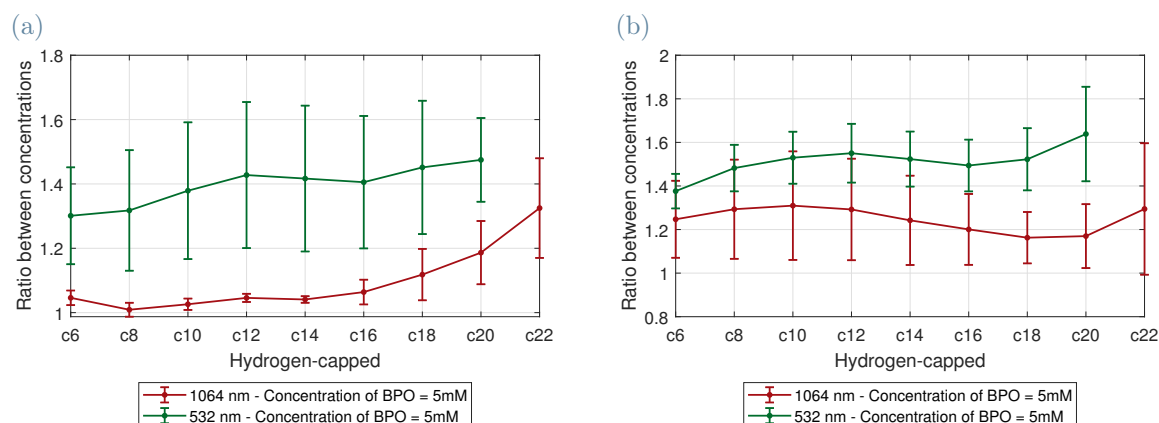
Figure 4.16: Ratio between concentrations of size-selected hydrogen-capped polyynes in 5 mM solutions over areas of the same polyyne in pure (a) MeOH and (b) EtOH, for both wavelengths, i.e. 532 nm (green line) and 1064 nm (red line).

capped polyynes were also detected with length up to $C_{18}CH_3$. Ablations with the 355 nm laser produced the lowest concentration of both hydrogen- and methyl-capped polyynes and chains longer than C_{14} were not detected. In Fig. 4.15c and 4.15d a comparison between the concentration of each hydrogen-capped polyyne in each alcohol is reported for 532 nm and 1064 nm ablations, respectively. As it is shown, the concentration of shorter polyynes is comparable for the three solvents, while longer chains, instead, were more concentrated in IPA followed by EtOH and lastly MeOH, for both wavelengths. Indeed, the concentration of C_{20} in ablations at 532 nm in IPA was twice that obtained in MeOH, while regarding ablations at 1064 nm the concentration of C_{20} in IPA was three times that in MeOH. This difference could be related primarily on two factors: viscosity and C/H ratio. Indeed, IPA has the highest viscosity and C/H ratio among the three alcohols tested, while MeOH has the lowest viscosity and C/H ratio. Higher viscosity should increase the production of longer chains due to the lower diffusion rate of growing polyynes in the solvent and better confinement of the plasma plume. Higher C/H ratio should also enhance the production by favouring the polymerization at the expense of hydrogenation.

To evaluate the effect of BPO at different wavelength and with different solvents, the ratio between the concentrations of size-selected polyynes in BPO solutions and in pure solvent was calculated. The result for hydrogen-capped polyynes is shown in Fig. 4.16. The main effect that emerges is that ablations in BPO solutions produced more polyynes than in pure solvents. As for IPA, 532 nm led to a higher gain in the polyyne concentrations

(a)

(b)
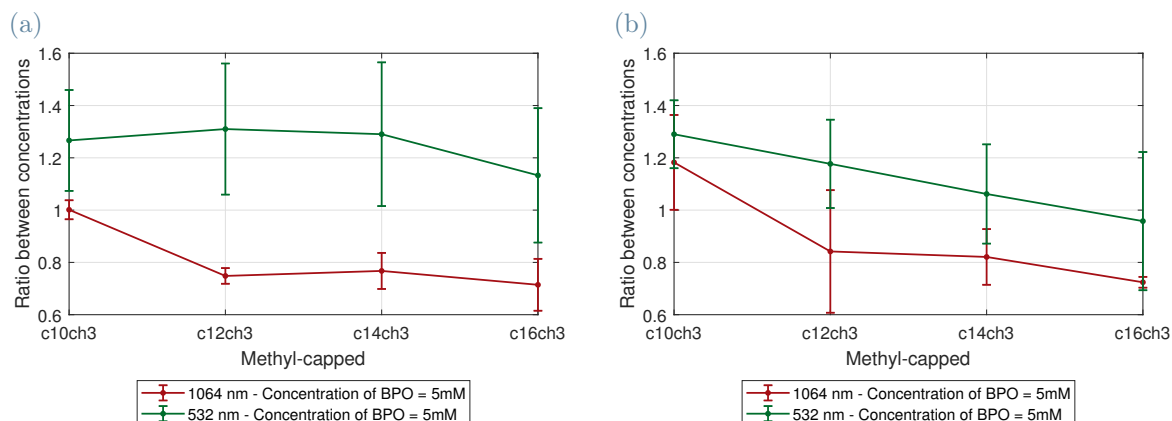
Figure 4.17: Ratio between concentrations of size-selected methyl-capped polyynes in 5 mM solutions over areas of the same polyyne in pure (a) MeOH and (b) EtOH, for both wavelengths, i.e. 532 nm (green line) and 1064 nm (red line).

than 1064 nm for both MeOH and EtOH. However, by comparing Fig. 4.16a, 4.16b and Fig. 4.6 the gain is shown to be dependent also on the employed solvent. Considering only the ablations with 532 nm, ablations of BPO solutions in IPA showed the highest ratios followed by EtOH and then MeOH. Considering ablations with the 1064 nm laser, they showed smaller gains in the polyyne concentrations compared to 532 nm as already observed in IPA (see Fig. 4.6). The effect of BPO, also in these cases, seems to be more relevant on longer chains, however the gains for both MeOH and EtOH are smaller compared to IPA. Indeed, the average ratio of C_{20} with 532 nm for MeOH is 1.5 ± 0.1, for EtOH is 1.6 ± 0.2 compared with 1.8 ± 0.3 of IPA. Considering ablations with the 1064 nm laser, the ratios of shorter chains in MeOH are close to the unity with small increase in the synthesis yield, but they increase significantly for chains longer than C_{18}, reaching 1.3 ± 0.2 for C_{22}. On the contrary, for ablation in EtOH with the 1064 nm laser, BPO solutions produced higher gains compared to MeOH and the ratios oscillate around 1.2 for all the chains.

As for hydrogen-capped polyynes, Fig. 4.17 shows the ratio between the concentrations of size-selected methyl-capped polyynes in BPO solutions and in pure solvent. The effect of BPO on methyl-capped polyynes was favoured by 532 nm ablations in both solvents, as for IPA (see Fig. 4.8). In ablations in MeOH, ratios of methyl-capped polyyne were above 1.2 (see Fig. 4.17a), while in ablations in EtOH the ratios decrease for longer chains and $C_{16}CH_3$ ratio was under 1 (see Fig. 4.17b). On the contrary, ablations with 1064 nm laser in BPO solutions reported a decrease in the concentration of polyynes for

both solvents. This result is opposite to the result obtained in ablations in IPA, which showed an increase, though small, in the synthesis yield of methyl-capped polyynes with the 1064 nm laser (see Fig. 4.8).

From these experimental observations, the effect of BPO on the synthesis yield of polyynes seems to be related also on the employed solvent. When using alcohols, the effect of BPO was improved from MeOH to EtOH and IPA. This effect could be related to the different C/H ratio of alcohols. Indeed, if we assume that the same percentage of BPO reacts in each solvent, the same amount of hydrogen is captured. Nevertheless, since IPA has a lower relative content of hydrogen compared to carbon atoms, ablations in solutions with BPO and IPA should be characterized by the lowest hydrogenation rate among the tested alcohols. Hence, higher gain in the production should be achieved. Another parameter could be the stability of BPO in each solvent. Indeed, BPO in MeOH was shown to be more unstable [104], which could correspond to a higher fraction of BPO degraded before the ablation, hence to less BPO reacting during the ablation.

4.3. Effect of BPO in pulsed laser ablation in acetonitrile

To further study the mixed effect of the solvent and BPO, I decided to employ also acetonitrile. Indeed, ablations in ACN with 532 nm reported in literature were shown to produce higher concentrations of polyynes compared to the previous alcohols [32]. Moreover, acetonitrile provides also cyano-endgroups to synthesized cyano-capped polyynes. As for the previous solvents, I performed ablations in pure ACN with the three wavelengths and in 5 mM BPO solutions with 1064 nm and 532 nm.

4.3.1. Synthesis of polyynes in pure ACN

Regarding the ablations in pure ACN, I observed that the productivity of polyynes in ACN is different from alcohols. As shown in Fig. 4.18, shorter chains up to C_{10} were favoured by 1064 nm, while longer chains above C_{12} were favoured by 532 nm instead. Indeed, ablations with the 532 nm laser provided higher concentrations of longer chains and I was able to detect chains up to C_{22}, which was not visible by employing the 1064 nm laser. For example, the concentration of C_6 was $(2.63 \pm 0.06) \times 10^{-5}$ mol/l for 1064 nm, $(1.95 \pm 0.05) \times 10^{-5}$ mol/l for 532 nm and $(1.4 \pm 0.6) \times 10^{-5}$ mol/l for 355 nm. On the contrary, the concentration of C_{20} was $(1.36 \pm 0.09) \times 10^{-7}$ mol/l for 532 nm, $(3 \pm 1) \times 10^{-8}$ mol/l for 1064 nm and no traces were found for 355 nm. Ablations with the 355 nm
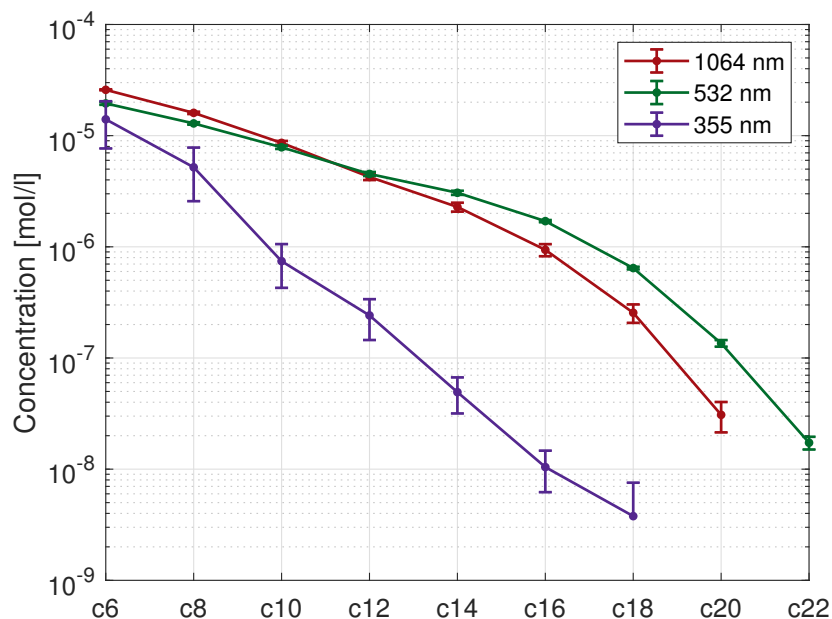
Figure 4.18:   Concentration of size-selected hydrogen-capped polyynes in pure ACN by ablations of 15 min with three different wavelengths (1064 nm, red line, 532 nm, green line, 355 nm, purple line).

laser produced the lowest concentration of polyynes as for alcohols, however, chains up to C_{18} were detected, although only small traces of C_{18} were recorded. The production of shorter polyynes, i.e. up to C_{10}, with both 532 nm and 1064 nm lasers is comparable to that of employed alcohols, as shown by Fig. 4.19. Instead, for longer chains ACN showed to produce more polyynes than the other solvents when ablating with the 532 nm laser (Fig. 4.19a). Indeed, the concentrations of C_{14} and C_{16} at 532 nm ($(3.1 \pm 0.1) \times 10^{-6}$ mol/l and $(1.70 \pm 0.04) \times 10^{-6}$ mol/l respectively) were comparable with the concentrations of the same chains in ablations at 1064 nm in pure IPA ($(3.4 \pm 0.2) \times 10^{-6}$ mol/l and $(1.85 \pm 0.09) \times 10^{-6}$ mol/l). On the contrary, when ablated with 1064 nm laser ACN produced less longer chains than the other three alcohols (Fig. 4.19b). For ablations with 1064 nm, C_{16}, C_{18} and C_{20} were significantly less concentrated in ablations in pure ACN, and C_{20} was an order of magnitude less concentrated than in the other solvents.

In all ACN ablations, I also detected methyl-capped and cyano-capped polyynes with chains of various lengths. The employed HPLC gradient method managed to separate well all the different chain lengths and terminations, with the only exception of $C_{12}CH_3$ and $C_{12}CN$ which were eluted at the same time. Regarding methyl-capped polyynes (see Fig. 4.20a), chains up to $C_{18}CH_3$ were detected both with 1064 nm and 532 nm. The production of methyl-capped polyynes was higher with 532 nm than 1064 nm in pure ACN,

(a)

(b)
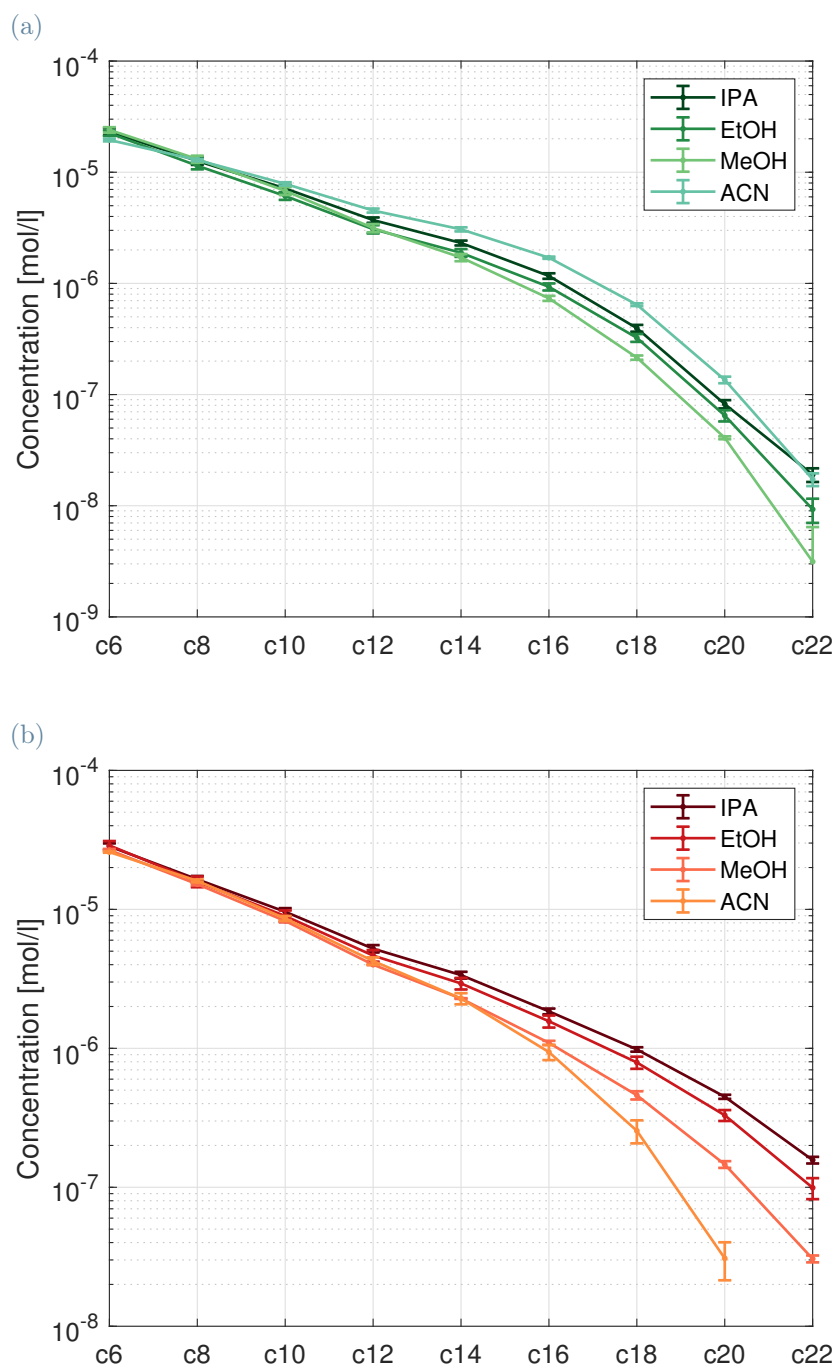
Figure 4.19:   Concentrations of size-selected hydrogen-capped polyynes in pure solvents (IPA, EtOH, MeOH and ACN) for 15 min of ablation for (a) 532 nm and (b) 1064 nm lasers.
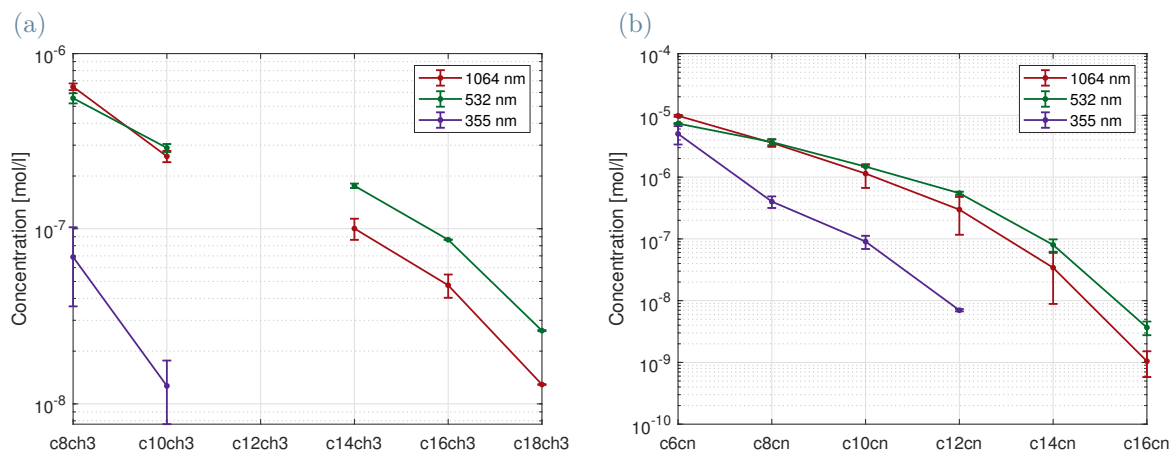
Figure 4.20: Concentrations of size-selected (a) methyl- and (b) cyano-capped polyyne for ablations with three different wavelength (1064 nm, red line, 532 nm, green line, 355 nm, purple line) in pure ACN for 15 min.

with the only exception of C_8CH_3, whose concentration was higher in 1064 nm ablations (see Fig. 4.20a). C_8CH_3 and $C_{10}CH_3$ were also detected for 355 nm ablations. In Fig. 4.21 the comparison between the production of methyl-capped polyynes in pure solvents (IPA, EtOH, MeOH and ACN) is shown. Compared with the alcohols, the concentration of methyl-capped polyynes were similar to the one of EtOH and IPA by comparing 1064 nm ablations (see Fig. 4.21b), while in 532 nm the production of longer methyl polyynes as $C_{14}CH_3$, $C_{16}CH_3$ and $C_{18}CH_3$ was higher than that of the alcohols (see Fig. 4.21a). Indeed, in this last configuration (i.e. pure ACN and 532 nm) the highest concentrations of $C_{14}CH_3$, $C_{16}CH_3$ and $C_{18}CH_3$ were reached with values of $(1.76 \pm 0.05) \times 10^{-7}$ mol/l, $(8.66 \pm 0.03) \times 10^{-8}$ mol/l and $(2.62 \pm 0.02) \times 10^{-8}$ mol/l. However, only small traces of $C_{20}CH_3$ were detected, lower than the concentrations founded in pure IPA that seems to be a favourable environment for the growth of long polyynes.

Cyano-capped polyynes were also synthesized and I detected chains with lengths ranging from C_6CN to $C_{16}CN$, reported in Fig. 4.20b. As for hydrogen-capped chains, 532 nm favoured the production of longer chains, while only C_6CN was more concentrated in 1064 nm ablations. Also in this case, ablations performed with the 355 nm laser feature the lowest production and chains only up to $C_{12}CN$ were detected (see Fig. 4.20b). It is worth noting that the concentrations of short cyano-capped polyynes, i.e. C_8CN and $C_{10}CN$, are higher than the concentrations of the methyl-capped polyynes with the same length, i.e. C_8CH_3 and $C_{10}CH_3$ (see Fig. 4.20). On the contrary, the concentration of $C_{14}CN$ ($(8 \pm 2) \times 10^{-8}$ mol/l) is lower than that of $C_{14}CH_3$ ($(1.76 \pm 0.05) \times 10^{-7}$ mol/l), and the concentration of $C_{16}CN$ is $(3.7 \pm 0.9) \times 10^{-9}$ mol/l which is an order of magnitude

(a)

(b)
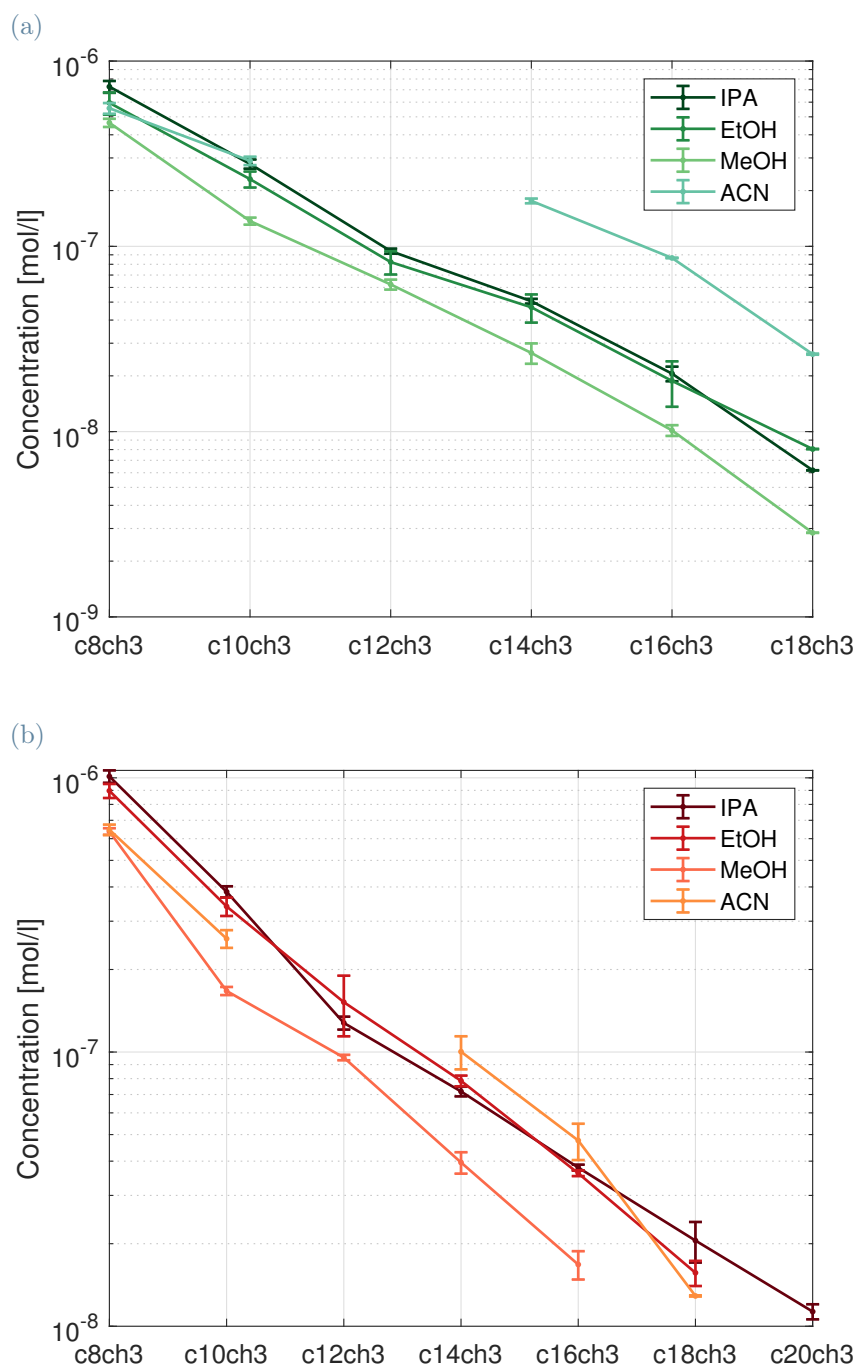
Figure 4.21:   Concentrations of size-selected methyl-capped polyynes in pure solvents (IPA, EtOH, MeOH and ACN) for 15 min of ablation for (a) 532 nm and (b) 1064 nm lasers.
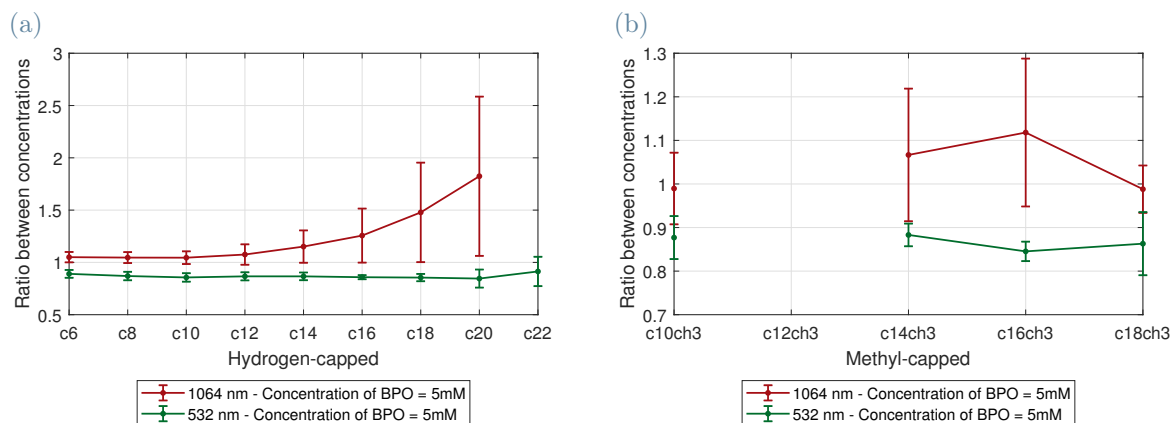
Figure 4.22:   Ratio between the concentrations of size-selected (a) hydrogen- and (b) methyl-capped polyyne in $5\,\mathrm{mM}$ BPO solutions and those of the same polyyne in pure ACN for ablation of $15\,\mathrm{min}$ with $1064\,\mathrm{nm}$ (red line) and $532\,\mathrm{nm}$ (green line) laser.

less than $C_{16}CH_3$ $((8.66 \pm 0.03) \times 10^{-8}\,\mathrm{mol/l})$ (see Fig. 4.20). Hence, the concentration of cyano-capped polyynes decreases more rapidly by increasing the chain length than methyl-capped. The main reason is related to the high reactivity of the cyano-group, which hinders the formation of long chains and affects their stability. On the contrary, the methyl-endgroup is more stable and less reactive since it is formed by sp^3 carbon. As a consequence, longer methyl-capped chains are detected in all configurations.

4.3.2.   Effect of BPO in ACN

To study the effect of BPO on ablations in ACN, I considered the concentrations of size-selected polyyne in $5\,\mathrm{mM}$ BPO solutions in ACN. Hence, I calculated the ratio between the concentrations of each chain in BPO solutions over that of the same chain in pure ACN, as shown in Fig. 4.22. As it is shown by the graph 4.22a, the concentration of hydrogen-capped polyynes in $532\,\mathrm{nm}$ ablations was just below that of pure ACN, while in $1064\,\mathrm{nm}$ ablations a small but not negligible increase was observed. Only longer chains in $1064\,\mathrm{nm}$ ablations had larger gains, although C_{18} and C_{20} ratios are affected by large error bars due to their low concentration in the ablations in pure ACN. Similar results were achieved for methyl-capped polyynes (see Fig. 4.22b). In $532\,\mathrm{nm}$ ablations, the concentrations of each methyl-capped polyyne was lower than those in pure ACN, while in $1064\,\mathrm{nm}$ ablations an increase was detected (see Fig. 4.22b).

As described in section 3.2, the chromatographic peak of BPO covers the peak of C_8CH_3, and, unfortunately, also the peak of C_8CN was covered and hence no data were retrieved.
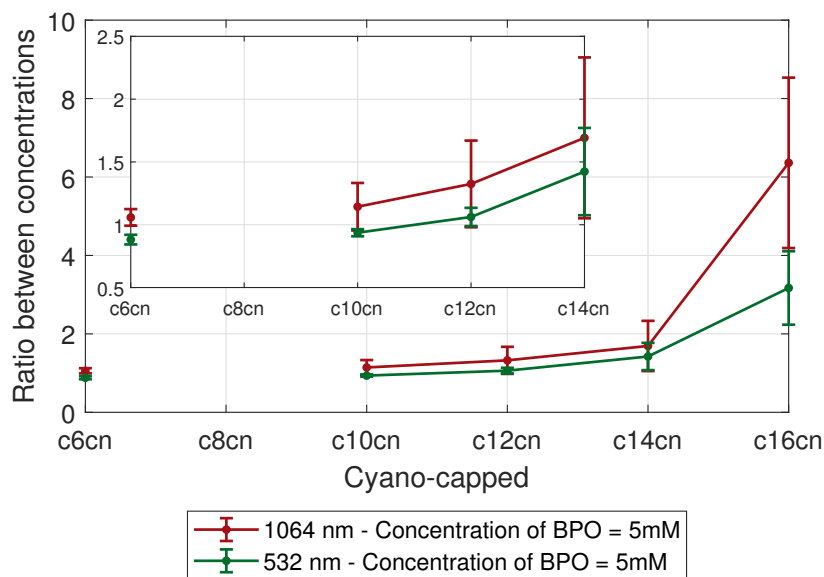
Figure 4.23: Ratio between the concentrations of size-selected cyano-capped polyyne in 5 mM solutions and those of the same polyyne in pure ACN for ablation of 15 min with 1064 nm (red line) and 532 nm (green line). The inset shows the zoomed area between C_6CN and $C_{14}CN$.

For ablation with the 532 nm laser, the C_6CN and $C_{10}CN$ ratios were below the unity, i.e. lower productivity when BPO is present, however the concentration of longer chains in BPO solutions were larger than in pure ACN (see Fig. 4.23). Indeed, as shown in Fig. 4.23, the ratios of $C_{12}CN$ and $C_{14}CN$ in 532 nm ablations were 1.06 ± 0.07 and 1.4 ± 0.3, respectively. $C_{16}CN$ concentration was further increased, with a ratio of 3.1 ± 0.9 (see Fig. 4.23). As for hydrogen- and methyl-capped polyynes, 1064 nm provided a greater increase in BPO solutions also for cyano-capped polyynes, indeed all ratios were above unity. $C_{10}CN$ ratio was 1.1 ± 0.2, while $C_{12}CN$ had a ratio of 1.3 ± 0.3 and $C_{14}CN$ ratio was 1.7 ± 0.6. The highest gain was reached for $C_{16}CN$ in 1064 nm solutions, with a ratio of 6 ± 2 (see Fig. 4.23). This big ratio is also related to the fact that in pure ACN ablations I did not record the presence of $C_{16}CN$, while with BPO solutions $C_{16}CN$ was always measurable. An example of the chromatograms at 326 nm from ablations in pure ACN and 5 mM BPO solution is reported in Fig. 4.24. As it is shown, the chromatographic peak of $C_{16}CN$ in pure ACN was barely visible (see Fig. 4.24a), while in the ablation with BPO (see Fig. 4.24b) the peak is slightly smaller than the peak of $C_{16}CH_3$ (the chromatographic peak at around 28 min).

All these experimental results show a different effect of BPO in the ablations with ACN

(a)

(b)
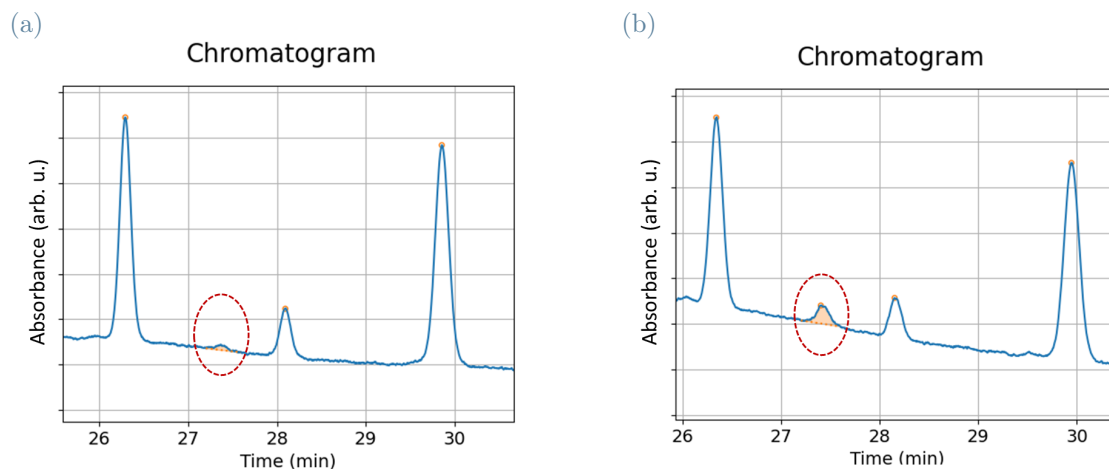
Figure 4.24:   Comparison between two chromatograms at 326 nm of ablations with 532 nm for 15 min in (a) pure ACN and (b) 5 mM BPO solution. In orange is depicted the peak of $C_{16}CN$, almost invisible in (a) pure ACN.

as liquid environment compared to those with alcohols. One of the reasons for this difference could be related to the higher stability of BPO in ACN rather than in MeOH and EtOH [104]. Hence, less BPO may react in ACN solutions, i.e. far from the plasma plume. However, this hypothesis does not explain the difference between 1064 nm and 532 nm in ACN. Therefore, the different behaviour of the two wavelengths may be an indicator of the presence of different coexisting phenomena as proposed in section 4.1.6. Moreover, for both wavelengths, the presence of BPO seems to favour longer cyano-capped polyynes. This effect could be related to the depletion of hydrogen- and methyl-endgroups. Indeed, BPO reacts with hydrogen and methyl groups forming BA and MeBA, leaving a higher concentration of cyano-groups around the plasma plume, thus inducing more cyano-termination processes. However, the main effect of BPO is related to the increase of the polymerization process, and thus the increase of the synthesis yield of cyano-capped polyynes is more relevant for longer chains.

5 | Conclusions and future developments

The investigation of the effects of a radical initiator on the synthesis of polyynes via PLAL was the main aim of this thesis work. The experimental results showed that Benzoyl Peroxide (BPO) contributes to the synthesis of polyynes, increasing the concentration of polyynes. Indeed, when BPO is dissolved in isopropyl alcohol (IPA) an increase in the concentrations of hydrogen-capped polyynes was obtained with respect to ablations in the pure solvent. The improvement in the synthesis yield was shown also to be dependent on the amount of BPO in the ablated solutions. For example, in the 5 mM and 7.5 mM solutions, increases up to 80% were obtained for C_{20} chains when employing the 532 nm laser. The effect of BPO was shown to be more favoured by the 532 nm laser rather than the 1064 nm one, when ablating for 15 min. On the contrary for long ablation times (120 min), ablations with the 1064 nm laser featured larger growths of polyyne synthesis yield due to the presence of BPO. The effect of BPO on the formation of methyl-capped polyynes is controversial, since their concentration increases when ablating with 532 nm, while for 1064 nm there is no a clear tendency. Besides IPA, I studied the effect of BPO in ablations in other solvents, as methanol (MeOH), ethanol (EtOH) and acetonitrile (ACN). Both in MeOH and EtOH, the effect of BPO was similar to that in IPA, i.e. larger improvements in the synthesis yield by ablation with the 532 nm laser compared to slightly increases with the 1064 nm laser. In acetonitrile, I recorded an opposite effect compared to alcohols. Indeed, ablations with the 532 nm laser was detrimental for BPO solutions leading to lower concentration of hydrogen-capped polyynes compared to ablations in pure ACN. On the contrary, greater gains were reached for ablations with the 1064 nm laser. An interesting result was obtained considering cyano-capped polyynes synthesized in ACN. The presence of BPO favoured the formation of long cyano-capped polyynes up to $C_{16}CN$ for ablations with both 532 nm and 1064 nm lasers. An increase of $C_{16}CN$ concentration of 310% was observed in 532 nm ablations and even higher up to 600% in 1064 nm ablations.

From these results, I suggested an explanation of the effect of BPO on the synthesis of

polyynes via PLAL. The main cause of the increase in polyyne productivity could be related to the dissociation of BPO in benzoate radicals during the ablations. Indeed, I recorded the presence of benzoic acid (BA), methyl benzoate (MeBA) and ethyl benzoate (EtBA) as degradation products after the ablations, obtained by the cleavage of the O−O bond of the peroxide. After the homolytic cleavage, BPO radicals subproducts could capture free hydrogen atoms around the plasma plume forming BA and depleting the hydrogen concentration. Hence, the hydrogenation process of polyynes should be less probable and longer chains could grow. The enhancement of methyl-capped and cyano-capped polyynes could be related to the same process: by depleting the hydrogen content, termination through methyl- or cyano-endgroups becomes more probable. However, the different behaviour obtained with different ablation laser wavelengths is not completely understood. Therefore, different process could occur in parallel to that described before, as ring-opening mechanism of the phenyl groups of BPO, and generate other effects on the synthesis of polyynes.

The effect of BPO showed to be beneficial to the concentration of the synthesized polyynes, hence the use of radical initiators for polyyne synthesis via PLAL should be further studied. Indeed, many different thermally activated molecules could be employed as other diacyl peroxides or diazocompounds. The use of diacyl peroxides with no aromatic groups could be employed to study the effect of free radicals without having the presence of ring-opening processes. Moreover, bulky free radicals, as phenyl radicals, near the plasma plume could also act as terminations for the growing chains. Other hydrogen-capturing compounds could also be employed to study the effect of the hydrogen depletion on the synthesis of polyynes. Since BPO is commonly employed as a thermally activated radical initiator, further investigations by changing the temperature of the solvent could be interesting. Another class of compounds that could be studied is photo-initiators, which produce free radicals through dissociation induced by UV light.

I also compared the synthesis of polyynes via PLAL in different solvents and with different wavelengths. The highest production in pure solvent was obtained for IPA employing the 1064 nm laser. Regarding the three employed alcohols, I recorded the highest production in pure IPA both with 532 nm and 1064 nm, followed by EtOH and MeOH. These results confirm the role of viscosity and C/H ratio of the solvent in the synthesis of polyynes. Higher viscosities and C/H ratios promote the formation of polyynes and allow to synthesize longer chains [32, 78]. The effect of laser wavelength in alcohols was in agreement with the result obtained in literature [79, 80], as longer wavelengths corresponded to higher concentration of polyynes. However, I reported a different behaviour when ablating ACN. Ablations with the 532 nm laser produced more polyynes than with the 1064 nm laser.

Therefore, further effects affect the formation of polyynes in ACN. Increasing the ablation time in IPA corresponded to higher productivity of polyynes. Indeed, by increasing the ablation time to 30 min and 120 nm, both C_{24} and C_{26} hydrogen-capped polyynes were detected in IPA for ablations with 1064 nm laser. The combined effects of solvent and laser wavelength are not completely clear. Therefore, further investigations on these solvents should be considered.

Bibliography

[1] C. S. Casari et al. "Carbon–atom wires: 1–D systems with tunable properties". In: *Nanoscale* 8 (8 Feb. 2016), pp. 4414–4435. ISSN: 20403372. DOI: 10.1039/c5nr06175j (cit. on pp. 3, 4, 6–8, 13–19).

[2] C. S. Casari and A. Milani. "Carbyne: From the elusive allotrope to stable carbon atom wires". In: *MRS Communications* 8 (2 June 2018), pp. 207–219. ISSN: 21596867. DOI: 10.1557/mrc.2018.48 (cit. on pp. 3, 13, 15, 17, 20).

[3] M. C. McCarthy and P. Thaddeus. "Microwave and laser spectroscopy of carbon chains and rings". In: *Chemical Society Reviews* 30 (3 Jan. 2001), pp. 177–185. ISSN: 03060012. DOI: 10.1039/B006648F (cit. on p. 3).

[4] L. Ravagnan et al. "Cluster–Beam Deposition and in situ Characterization of Carbyne–Rich Carbon Films". In: *Physical Review Letters* 89 (28 Dec. 2002), pp. 1–4. ISSN: 10797114. DOI: 10.1103/PHYSREVLETT.89.285506 (cit. on p. 3).

[5] Carlo S. Casari. "Carbon Atomic Wires: from stars to nanotechnology". In: *Istituto Lombardo – Accademia di Scienze e Lettere – Rendiconti di Scienze* (Dec. 2012). ISSN: 2384–986X. DOI: 10.4081/SCIE.2012.130 (cit. on pp. 3, 4, 7, 13–15, 17).

[6] Annabelle L.K. Shi Shun and Rik R. Tykwinski. "Synthesis of Naturally Occurring Polyynes". In: *Angewandte Chemie International Edition* 45 (7 Feb. 2006), pp. 1034–1057. ISSN: 1521–3773. DOI: 10.1002/ANIE.200502071 (cit. on p. 3).

[7] C. Glaser. "Beiträge zur Kenntniss des Acetenylbenzols". In: *Berichte der deutschen chemischen Gesellschaft* 2 (1 Jan. 1869), pp. 422–424. ISSN: 0365–9496. DOI: 10.1002/CBER.186900201183 (cit. on p. 3).

[8] A M Sladkov and Yu P Kudryavtsev. "Polyynes". In: *Russ. Chem. Rev* 32 (1963), p. 229 (cit. on p. 3).

[9] H. W. Kroto et al. "C60: Buckminsterfullerene". In: *Nature* 318 (1985), pp. 162–163 (cit. on pp. 3, 9).

[10] Andreas Hirsch. *The era of carbon allotropes*. 2010. DOI: 10.1038/nmat2885 (cit. on pp. 3, 7, 9).

[11] Sumio Iijima. "Helical microtubules of graphitic carbon". In: *Nature 1991 354:6348* 354 (6348 1991), pp. 56–58. ISSN: 1476–4687. DOI: 10.1038/354056a0 (cit. on p. 3).

[12] A K Geim and K S Novoselov. "The rise of graphene". In: *Nature Materials* 6 (Mar. 2007), pp. 183–191 (cit. on pp. 3, 10).

[13] Salisu Nasir et al. *Carbon–based nanomaterials/allotropes: A glimpse of their synthesis, properties and some applications*. Feb. 2018. DOI: `10.3390/ma11020295` (cit. on pp. 3, 5, 6, 8, 9, 13).

[14] Hugh O. Pierson. *Handbook of Carbon, graphite, diamond and fullerenes*. Chapter 1–2. Noyes Publications, 1993, pp. 1–42 (cit. on pp. 3, 5).

[15] Yueze Gao et al. "The loss of endgroup effects in long pyridyl–endcapped oligoynes on the way to carbyne". In: *Nature Chemistry 2020 12:12* 12 (12 Nov. 2020), pp. 1143–1149. ISSN: 1755–4349. DOI: `10.1038/s41557-020-0550-0` (cit. on pp. 4, 16–18).

[16] Lei Shi et al. "Confined linear carbon chains as a route to bulk carbyne". In: *Nature Materials 2016 15:6* 15 (6 Apr. 2016), pp. 634–639. ISSN: 1476–4660. DOI: `10.1038/nmat4617` (cit. on pp. 4, 13, 17).

[17] Martin Weller et al. *Inorganic chemistry*. 7th edition. Oxford University Press, 2018, p. 943. ISBN: 9780198768128 (cit. on pp. 4, 8, 9, 13, 20, 21).

[18] Peter William Atkins, Julio de Paula, and James Keeler. *Atkins' Physical Chemistry*. 11th edition. Oxford University Press, 2018, p. 908. ISBN: 9780198769866 (cit. on pp. 4–6).

[19] Guozhong Cao. *Nanostructures and Nanomaterials*. IMPERIAL COLLEGE PRESS, WORLD SCIENTIFIC PUBLISHING CO., Apr. 2004. DOI: `10.1142/P305` (cit. on pp. 6, 9, 11, 25).

[20] K. S. Novoselov. "Nobel Lecture: Graphene: Materials in the Flatland". In: *Reviews of Modern Physics* 83 (3 Aug. 2011), pp. 837–849. ISSN: 00346861. DOI: `10.1103/RevModPhys.83.837` (cit. on p. 8).

[21] Dimitrios G. Papageorgiou, Ian A. Kinloch, and Robert J. Young. "Mechanical properties of graphene and graphene–based nanocomposites". In: *Progress in Materials Science* 90 (Oct. 2017), pp. 75–127. ISSN: 0079–6425. DOI: `10.1016/J.PMATSCI.2017.07.004` (cit. on pp. 8, 9).

[22] J. C. Charlier et al. "Electron and Phonon Properties of Graphene: Their Relationship with Carbon Nanotubes". In: *Topics in Applied Physics* 111 (2007), pp. 673–709. ISSN: 03034216. DOI: `10.1007/978-3-540-72865-8_21` (cit. on p. 8).

[23] K. I. Bolotin et al. "Ultrahigh electron mobility in suspended graphene". In: *Solid State Communications* 146 (9–10 June 2008), pp. 351–355. ISSN: 0038–1098. DOI: `10.1016/J.SSC.2008.02.024` (cit. on p. 8).

[24] Caterina Soldano, Ather Mahmood, and Erik Dujardin. "Production, properties and potential of graphene". In: *Carbon* 48 (8 July 2010), pp. 2127–2150. ISSN: 0008–6223. DOI: 10.1016/J.CARBON.2010.01.058 (cit. on p. 8).

[25] Yijian Ouyang, Youngki Yoon, and Jing Guo. "Scaling behaviors of graphene nanoribbon FETs: A three–dimensional quantum simulation study". In: *IEEE Transactions on Electron Devices* 54 (9 Sept. 2007), pp. 2223–2231. ISSN: 00189383. DOI: 10.1109/TED.2007.902692 (cit. on p. 8).

[26] V. Parasuk and J. Almlöf. "C20: the smallest fullerene?" In: *Chemical Physics Letters* 184 (1–3 Sept. 1991), pp. 187–190. ISSN: 00092614. DOI: 10.1016/0009-2614(91)87185-E (cit. on p. 9).

[27] I. V. Davydov, A. I. Podlivaev, and L. A. Openov. "Anomalous thermal stability of metastable C20 fullerene". In: *Physics of the Solid State 2005 47:4* 47 (4 2005), pp. 778–784. ISSN: 1090–6460. DOI: 10.1134/1.1913997 (cit. on p. 9).

[28] M S Dresselhaus. "Future directions in Carbon science". In: *Annu. Rev. Mater. Sci* 27 (1997), pp. 1–34 (cit. on pp. 9, 12).

[29] Nicole Grobert. "Carbon nanotubes – becoming clean". In: *Materials Today* 10 (1–2 Jan. 2007), pp. 28–35. ISSN: 1369–7021. DOI: 10.1016/S1369-7021(06)71789-8 (cit. on p. 12).

[30] Riccardo Alberto Lotti. "Sp–carbon chains by pulsed laser ablation in liquid: synthesis and stability". Politecnico di Milano, Dec. 2019 (cit. on p. 13).

[31] Alberto Milani et al. "Raman spectroscopy as a tool to investigate the structure and electronic properties of carbon–atom wires". In: *Beilstein Journal of Nanotechnology* 6 (1 2015), pp. 480–491. ISSN: 21904286. DOI: 10.3762/bjnano.6.49 (cit. on pp. 16, 20, 21).

[32] Sonia Peggiani et al. "Solvent–dependent termination, size and stability in polyynes synthesized: Via laser ablation in liquids". In: *Physical Chemistry Chemical Physics* 22 (45 Dec. 2020), pp. 26312–26321. ISSN: 14639076. DOI: 10.1039/d0cp04132g (cit. on pp. 17, 19, 22–24, 35–39, 61, 75, 84).

[33] Franco Cataldo. "Synthesis of polyynes in a submerged electric arc in organic solvents". In: *Carbon* 42 (1 2004), pp. 129–142. ISSN: 00086223. DOI: 10.1016/j.carbon.2003.10.016 (cit. on p. 17).

[34] Tomonari Wakabayashi et al. "Isotope scrambling in the formation of cyanopolyynes by laser ablation of carbon particles in liquid acetonitrile". In: vol. 50. Jan. 2012, pp. 47–56. DOI: 10.1016/j.carbon.2011.07.053 (cit. on pp. 17, 19, 38, 39).

[35] Slawomir Szafert and J. A. Gladysz. "Carbon in one dimension: Structural analysis of the higher conjugated polyynes". In: *Chemical Reviews* 103 (11 Nov. 2003), pp. 4175–4205. ISSN: 00092665. DOI: 10.1021/CR030041O (cit. on p. 17).

[36] Franco Cataldo et al. "One–pot synthesis and characterization of polyynes end–capped by biphenyl groups (α,ω–biphenylpolyynes)". In: *Carbon* 126 (Jan. 2018), pp. 232–240. ISSN: 00086223. DOI: `10.1016/j.carbon.2017.09.098` (cit. on pp. 17, 18, 24).

[37] Franco Cataldo et al. "Synthesis, characterization, and modeling of naphthyl–terminated sp carbon chains: Dinaphthylpolyynes". In: *Journal of Physical Chemistry B* 114 (46 Nov. 2010), pp. 14834–14841. ISSN: 15205207. DOI: `10.1021/JP104863V` (cit. on pp. 17, 18, 24).

[38] N. R. Agarwal et al. "Structure and chain polarization of long polyynes investigated with infrared and Raman spectroscopy". In: *Journal of Raman Spectroscopy* 44 (10 Oct. 2013), pp. 1398–1410. ISSN: 1097–4555. DOI: `10.1002/JRS.4300` (cit. on p. 17).

[39] Wesley A. Chalifoux and Rik R. Tykwinski. "Synthesis of polyynes to model the sp–carbon allotrope carbyne". In: *Nature Chemistry* 2 (11 Nov. 2010), pp. 967–971. ISSN: 17554330. DOI: `10.1038/nchem.828` (cit. on p. 17).

[40] Sonia Peggiani et al. "In situ synthesis of polyynes in a polymer matrix via pulsed laser ablation in a liquid". In: *Materials Advances* 1 (8 2020), pp. 2729–2736. ISSN: 2633–5409. DOI: `10.1039/d0ma00545b` (cit. on p. 17).

[41] Kang An et al. "Stability improvement of C8H2 and C10H2 embedded in poly(vinyl alcohol) films with adsorption on gold nanoparticles". In: *Chemical Physics Letters* 637 (Sept. 2015), pp. 71–76. ISSN: 0009–2614. DOI: `10.1016/J.CPLETT.2015.07.051` (cit. on p. 17).

[42] Ryutaro Matsutani et al. "Preparation of polyynes up to C22H2 by liquid–phase laser ablation and their immobilization into SiO2 gel". In: *Carbon* 47 (7 June 2009), pp. 1659–1663. ISSN: 0008–6223. DOI: `10.1016/J.CARBON.2009.02.026` (cit. on p. 17).

[43] Enlai Gao, Ruishan Li, and Ray H. Baughman. "Predicted Confinement–Enhanced Stability and Extraordinary Mechanical Properties for Carbon Nanotube Wrapped Chains of Linear Carbon". In: *ACS Nano* 14 (12 Dec. 2020), pp. 17071–17079. ISSN: 1936086X. DOI: `10.1021/ACSNANO.0C06602` (cit. on p. 17).

[44] Franco Cataldo. "Polyynes Production in a Solvent-Submerged Electric Arc Between Graphite Electrodes. III. Chemical Reactivity and Stability Toward Air, Ozone, and Light". In: *http://dx.doi.org/10.1081/FST–200026951* 12 (3 Aug. 2007), pp. 633–646. ISSN: 1536383X. DOI: `10.1081/FST-200026951` (cit. on p. 17).

[45] Wesley A. Chalifoux and Rik R. Tykwinski. "Synthesis of extended polyynes: Toward carbyne". In: *Comptes Rendus Chimie* 12 (3–4 Mar. 2009), pp. 341–358. ISSN: 1631–0748. DOI: `10.1016/J.CRCI.2008.10.004` (cit. on p. 18).

[46] Franco Cataldo. "Synthesis of Polyynes with Electric Arc Part 5: Detection of PAHs as Minor Products". In: *Fullerenes, Nanotubes, and Carbon Nanostructures* 13 (1 Jan. 2006), pp. 21–30. ISSN: 1536383X. DOI: `10.1081/FST-200040750` (cit. on p. 18).

[47] Sonia Peggiani et al. "Size–selected polyynes synthesised by submerged arc discharge in water". In: *Chemical Physics Letters* 740 (Feb. 2020). ISSN: 00092614. DOI: `10.1016/j.cplett.2019.137054` (cit. on pp. 19, 24).

[48] Franco Cataldo. "Polyynes and cyanopolyynes synthesis from the submerged electric arc: about the role played by the electrodes and solvents in polyynes formation". In: *Tetrahedron* 60 (19 May 2004), pp. 4265–4274. ISSN: 0040–4020. DOI: `10.1016/J.TET.2004.03.033` (cit. on p. 19).

[49] Yangliu Wu et al. "Effects of precursor molecules on polyyne formation by arc discharge between two copper electrodes". In: *Chemical Physics Letters* 730 (Sept. 2019), pp. 64–69. ISSN: 0009–2614. DOI: `10.1016/J.CPLETT.2019.05.040` (cit. on p. 19).

[50] Ali Ramadhan et al. "Synthesis of hydrogen– and methyl–capped long–chain polyynes by intense ultrashort laser pulse irradiation of toluene". In: *Carbon* 118 (July 2017), pp. 680–685. ISSN: 00086223. DOI: `10.1016/J.CARBON.2017.03.096` (cit. on pp. 24, 35, 36, 38).

[51] Vincenzo Amendola and Moreno Meneghetti. "What controls the composition and the structure of nanomaterials generated by laser ablation in liquid solution?" In: *Physical Chemistry Chemical Physics* 15 (9 Feb. 2013), pp. 3027–3046. ISSN: 1463–9084. DOI: `10.1039/C2CP42895D` (cit. on pp. 25–33, 36, 70).

[52] P. P. Patil et al. "Pulsed–laser–induced reactive quenching at liquid–solid interface: Aqueous oxidation of iron". In: *Physical Review Letters* 58 (3 Jan. 1987), p. 238. ISSN: 00319007. DOI: `10.1103/PhysRevLett.58.238` (cit. on p. 25).

[53] Hajar Sadeghi, Elmira Solati, and Davoud Dorranian. "Producing graphene nanosheets by pulsed laser ablation: Effects of liquid environment". In: *Journal of Laser Applications* 31 (4 Sept. 2019), p. 042003. ISSN: 1042–346X. DOI: `10.2351/1.5109424` (cit. on pp. 25, 26).

[54] G. W. Yang. "Laser ablation in liquids: Applications in the synthesis of nanocrystals". In: *Progress in Materials Science* 52 (4 May 2007), pp. 648–698. ISSN: 0079–6425. DOI: `10.1016/J.PMATSCI.2006.10.016` (cit. on pp. 26, 29, 32).

[55] William T. Nichols, Takeshi Sasaki, and Naoto Koshizaki. "Laser ablation of a platinum target in water. III. Laser–induced reactions". In: *Journal of Applied Physics* 100 (11 Dec. 2006), p. 114913. ISSN: 0021–8979. DOI: `10.1063/1.2390642` (cit. on p. 26).

[56] William T. Nichols, Takeshi Sasaki, and Naoto Koshizaki. "Laser ablation of a platinum target in water. I. Ablation mechanisms". In: *Journal of Applied Physics* 100 (11 Dec. 2006), p. 114911. ISSN: 0021–8979. DOI: 10.1063/1.2390640 (cit. on pp. 26, 30).

[57] William T. Nichols, Takeshi Sasaki, and Naoto Koshizaki. "Laser ablation of a platinum target in water. II. Ablation rate and nanoparticle size distributions". In: *Journal of Applied Physics* 100 (11 Dec. 2006), p. 114912. ISSN: 0021–8979. DOI: 10.1063/1.2390641 (cit. on pp. 26, 31, 32).

[58] R. Fabbro et al. "Physical study of laser-produced plasma in confined geometry". In: *Journal of Applied Physics* 68 (2 June 1998), p. 775. ISSN: 0021–8979. DOI: 10.1063/1.346783 (cit. on p. 26).

[59] Carsten Momma et al. "Short–pulse laser ablation of solid targets". In: *Optics Communications* 129 (1–2 Aug. 1996), pp. 134–142. ISSN: 0030–4018. DOI: 10.1016/0030-4018(96)00250-7 (cit. on pp. 28, 31, 32).

[60] Daniel Werner et al. "Femtosecond laser–induced size reduction of aqueous gold nanoparticles: In situ and pump–probe spectroscopy investigations revealing coulomb explosion". In: *Journal of Physical Chemistry C* 115 (17 May 2011), pp. 8503–8512. ISSN: 19327447. DOI: 10.1021/JP112262U (cit. on p. 28).

[61] Philipp Wagener et al. "Pulsed laser ablation of zinc in tetrahydrofuran: Bypassing the cavitation bubble". In: *Journal of Physical Chemistry C* 114 (17 May 2010), pp. 7618–7625. ISSN: 19327447. DOI: 10.1021/JP911243A (cit. on pp. 28, 31, 32).

[62] Danny Perez et al. "Numerical study of the thermal ablation of wet solids by ultrashort laser pulses". In: *Physical Review B – Condensed Matter and Materials Physics* 77 (1 Jan. 2008), p. 014108. ISSN: 10980121. DOI: 10.1103/PHYSREVB.77.014108 (cit. on p. 28).

[63] Takeshi Tsuji et al. "Microsecond–resolved imaging of laser ablation at solid–liquid interface: investigation of formation process of nano–size metal colloids". In: *Applied Surface Science* 229 (1–4 May 2004), pp. 365–371. ISSN: 0169–4332. DOI: 10.1016/J.APSUSC.2004.02.013 (cit. on pp. 29, 30, 32, 38).

[64] Leonid V. Zhigilei, Zhibin Lin, and Dmitriy S. Ivanov. "Atomistic Modeling of Short Pulse Laser Ablation of Metals: Connections between Melting, Spallation, and Phase Explosion†". In: *Journal of Physical Chemistry C* 113 (27 July 2009), pp. 11892–11906. ISSN: 19327447. DOI: 10.1021/JP902294M (cit. on pp. 29–31).

[65] A. De Giacomo et al. "From single pulse to double pulse ns–Laser Induced Breakdown Spectroscopy under water: Elemental analysis of aqueous solutions and submerged solid samples". In: *Spectrochimica Acta – Part B Atomic Spectroscopy* 62

(8 Aug. 2007), pp. 721–738. ISSN: 05848547. DOI: `10.1016/J.SAB.2007.06.008` (cit. on p. 29).

[66] Zijie Yan and Douglas B. Chrisey. "Pulsed laser ablation in liquid for micro–/nanostructure generation". In: *Journal of Photochemistry and Photobiology C: Photochemistry Reviews* 13 (3 Sept. 2012), pp. 204–223. ISSN: 13895567. DOI: `10.1016/j.jphotochemrev.2012.04.004` (cit. on p. 29).

[67] Zijie Yan et al. "Hollow particles formed on laser–induced bubbles by excimer laser ablation of Al in liquid". In: *Journal of Physical Chemistry C* 114 (26 July 2010), pp. 11370–11374. ISSN: 19327447. DOI: `10.1021/JP104884X` (cit. on p. 30).

[68] Vincenzo Amendola and Moreno Meneghetti. "Laser ablation synthesis in solution and size manipulation of noble metal nanoparticles". In: *Physical Chemistry Chemical Physics* 11 (20 Apr. 2009), pp. 3805–3821. ISSN: 14639076. DOI: `10.1039/B900654K` (cit. on pp. 30–32).

[69] Fumitaka Mafuné et al. "Formation of Gold Nanoparticles by Laser Ablation in Aqueous Solution of Surfactant". In: *Journal of Physical Chemistry B* 105 (22 June 2001), pp. 5114–5120. ISSN: 10895647. DOI: `10.1021/JP0037091` (cit. on pp. 32, 33).

[70] Zijie Yan et al. "Excimer Laser Production, Assembly, Sintering, and Fragmentation of Novel Fullerene–like Permalloy Particles in Liquid". In: *Journal of Physical Chemistry C* 114 (9 Mar. 2010), pp. 3869–3873. ISSN: 19327447. DOI: `10.1021/JP911566A` (cit. on p. 32).

[71] Gabriele C. Messina et al. "Pulsed laser ablation of a continuously–fed wire in liquid flow for high–yield production of silver nanoparticles". In: *Physical Chemistry Chemical Physics* 15 (9 Feb. 2013), pp. 3093–3098. ISSN: 14639076. DOI: `10.1039/C2CP42626A` (cit. on p. 32).

[72] Fumitaka Mafuné et al. "Structure and Stability of Silver Nanoparticles in Aqueous Solution Produced by Laser Ablation". In: *The Journal of Physical Chemistry B* 104 (35 Sept. 2000), pp. 8336–8337. ISSN: 15206106. DOI: `10.1021/JP001803B` (cit. on p. 33).

[73] J R Heath et al. "The formation of long Carbon chain molecules during Laser vaporization of Graphite". In: *J. Am. Chem. Soc.* 109 (2 1987), p. 167 (cit. on p. 34).

[74] Akihiro Wakisaka et al. "Growth of carbon clusters. The simplest process, 2C 1 $\rightarrow$ C 2 , observed via spectrometry and chemical reaction". In: *Journal of the Chemical Society, Faraday Transactions* 89 (7 Jan. 1993), pp. 1001–1005. ISSN: 09565000. DOI: `10.1039/FT9938901001` (cit. on pp. 34–36).

[75] J. J. Gaumet et al. "Formation of carbon clusters Cn by laser vaporization of graphite and a study of their chemical reactivity by gas chromatography–mass spectrometry". In: *Journal of the Chemical Society, Faraday Transactions* 92 (11 1996), pp. 1831–1834 (cit. on pp. 34–36).

[76] Masaharu Tsuji et al. "Formation of hydrogen–capped polyynes by laser ablation of graphite particles suspended in solution". In: *Chemical Physics Letters* 355 (2002), pp. 101–108 (cit. on pp. 34–38).

[77] Giuseppe Compagnini et al. "Spectroscopic study of polyynes obtained by laser ablation in liquids". In: *Journal of Raman Spectroscopy* 39 (2 Feb. 2008), pp. 177–181. ISSN: 1097–4555. DOI: 10.1002/JRS.1837 (cit. on pp. 35, 36, 38).

[78] Ryutaro Matsutani et al. "Preparation of long–chain polyynes of C28H2 and C30H2 by liquid–phase laser ablation". In: *Journal of Photochemistry and Photobiology A: Chemistry* 240 (July 2012), pp. 1–4. ISSN: 1010–6030. DOI: 10.1016/J.JPHOTOCHEM.2012.05.004 (cit. on pp. 35–37, 39, 66, 84).

[79] Young Eun Park, Seung Keun Shin, and Seung Min Park. "The physical effects on the formation of polyynes by laser ablation". In: *Chemical Physics Letters* 568–569 (May 2013), pp. 112–116. ISSN: 0009–2614. DOI: 10.1016/J.CPLETT.2013.03.016 (cit. on pp. 35, 36, 38, 65, 66, 84).

[80] Ryutaro Matsutani et al. "Wavelength dependence of polyyne preparation by liquid–phase laser ablation using pellet targets". In: *Chemical Communications* 47 (20 May 2011), pp. 5840–5842. ISSN: 1364548X. DOI: 10.1039/C1CC00102G (cit. on pp. 35–38, 63, 65, 84).

[81] Masaharu Tsuji et al. "Formation of hydrogen–capped polyynes by laser ablation of C60 particles suspended in solution". In: *Carbon* 41 (11 Jan. 2003), pp. 2141–2148. ISSN: 0008–6223. DOI: 10.1016/S0008-6223(03)00241-0 (cit. on pp. 35, 37, 38).

[82] A. A. Zaidi et al. "Femtosecond laser ablation of solid methane". In: *International Journal of Mass Spectrometry* 376 (Jan. 2015), pp. 32–34. ISSN: 1387–3806. DOI: 10.1016/J.IJMS.2014.11.009 (cit. on pp. 35, 37).

[83] A. Hu et al. "Direct synthesis of polyyne molecules in acetone by dissociation using femtosecond laser irradiation". In: *Carbon* 46 (13 Nov. 2008), pp. 1823–1825. ISSN: 0008–6223. DOI: 10.1016/J.CARBON.2008.07.036 (cit. on pp. 35, 36).

[84] Young Eun Park, Seung Keun Shin, and Seung Min Park. "Power Dependence on Formation of Polyynes by Laser Ablation in Water". In: *Bulletin of the Korean Chemical Society* 34 (4 Apr. 2013), pp. 1039–1042. ISSN: 0253–2964. DOI: 10.5012/BKCS.2013.34.4.1039 (cit. on pp. 35, 36).

[85] A. A. Zaidi et al. "Femtosecond laser irradiation of liquid alkanes: Mechanism of polyyne formation". In: *Chemical Physics Letters* 723 (May 2019), pp. 151–154. ISSN: 0009–2614. DOI: 10.1016/J.CPLETT.2019.01.036 (cit. on p. 36).

[86] Y. Sato et al. "Synthesis of polyyne molecules from hexane by irradiation of intense femtosecond laser pulses". In: *Carbon* 48 (5 Apr. 2010), pp. 1673–1676. ISSN: 0008–6223. DOI: 10.1016/J.CARBON.2009.12.036 (cit. on pp. 36, 38).

[87] A Santagata et al. "Carbon–Based Nanostructures Obtained in Water by Ultrashort Laser Pulses". In: *J. Phys. Chem. C* 115 (2011), pp. 5160–5164. DOI: 10.1021/jp1094239 (cit. on p. 36).

[88] H. Tabata, M. Fujii, and S. Hayashi. "Synthesis of polyynes by laser ablation of diamond nanoparticles suspended in solution". In: *The European Physical Journal D – Atomic, Molecular, Optical and Plasma Physics 2005 34:1* 34 (1 July 2005), pp. 223–225. ISSN: 1434–6079. DOI: 10.1140/EPJD/E2005-00147-0 (cit. on pp. 36–38, 66).

[89] Giuseppe Compagnini et al. "Short polyyne chains produced by pulsed laser ablationof graphite in water". In: *Carbon* 45 (2007), pp. 2456–2458 (cit. on pp. 37, 38).

[90] Junwei Zhao et al. "Synthesis of polyynes by intense femtosecond laser irradiation of SWCNTs suspended in methanol". In: *Chemical Physics Letters* 682 (Aug. 2017), pp. 96–100. ISSN: 0009–2614. DOI: 10.1016/J.CPLETT.2017.05.063 (cit. on p. 37).

[91] Michal J. Wesolowski et al. "Synthesis of Polymer–like Hydrogenated Amorphous Carbon by fs–pulsed Laser Induced Plasma Processing of Solid Hexane". In: *Plasma Processes and Polymers* 9 (7 July 2012), pp. 701–708. ISSN: 1612–8869. DOI: 10.1002/PPAP.201100206 (cit. on p. 37).

[92] Ryutaro Matsutani et al. "Preparation of long–chain polyynes C18H2 and C20H2 by laser ablation of pellets of graphite and perylene derivative in liquid phase". In: *Carbon* 46 (7 June 2008), pp. 1103–1106. ISSN: 0008–6223. DOI: 10.1016/J.CARBON.2008.03.009 (cit. on p. 37).

[93] Marco Benoliel. "Investigation of naphthalene and its hydrogenated derivatives in the formation process of polyynes by Pulsed Laser Ablation in Liquid". Politecnico di Milano, 2021 (cit. on pp. 37, 38, 40).

[94] Seung Keun Shin, Jae Kyu Song, and Seung Min Park. "Preparation of polyynes by laser ablation of graphite in aqueous media". In: *Applied Surface Science* 257 (12 Apr. 2011), pp. 5156–5158. ISSN: 0169–4332. DOI: 10.1016/J.APSUSC.2010.10.074 (cit. on pp. 38–40).

[95] G. Forte et al. "The effects of liquid environments on the optical properties of linear carbon chains prepared by laser ablation generated plasmas". In: *Applied Surface*

Science 272 (May 2013), pp. 76–81. ISSN: 0169–4332. DOI: `10.1016/J.APSUSC.2012.03.156` (cit. on pp. 38, 39).

[96] Ryutaro Matsutani et al. "Preparation of polyynes by liquid–phase laser ablation using different irradiation target materials and solvents". In: *Carbon* 49 (1 Jan. 2011), pp. 77–81. ISSN: 0008–6223. DOI: `10.1016/J.CARBON.2010.08.044` (cit. on pp. 38, 39).

[97] Natalia R. Arutyunyan et al. "Resonant Effects in SERS Spectra of Linear Carbon Chains". In: *physica status solidi (b)* 255 (1 Jan. 2018), p. 1700254. ISSN: 1521–3951. DOI: `10.1002/PSSB.201700254` (cit. on p. 38).

[98] Kenji Hanamura et al. "Surface–enhanced Raman scattering of size–selected polyynes (C8H2) adsorbed on silver colloidal nanoparticles". In: *Chemical Physics Letters* 503 (1–3 Feb. 2011), pp. 118–123. ISSN: 0009–2614. DOI: `10.1016/J.CPLETT.2010.12.078` (cit. on p. 38).

[99] Seung Keun Shin and Seung Min Park. "Preparation of Polyynes by the Laser Ablation of Graphite in Water and Organic Solvents". In: *Bulletin of the Korean Chemical Society* 33 (2 Feb. 2012), pp. 597–600. ISSN: 0253–2964. DOI: `10.5012/BKCS.2012.33.2.597` (cit. on pp. 38, 40).

[100] M. J. Wesolowski et al. "Polyyne synthesis and amorphous carbon nano–particle formation by femtosecond irradiation of benzene". In: *Carbon* 49 (2 Feb. 2011), pp. 625–630. ISSN: 0008–6223. DOI: `10.1016/J.CARBON.2010.10.008` (cit. on p. 38).

[101] Kohei Inoue et al. "Preparation of long–chain polyynes of C24H2 and C26H2 by liquid–phase laser ablation in decalin". In: *Carbon* 48 (14 Nov. 2010), pp. 4209–4211. ISSN: 0008–6223. DOI: `10.1016/J.CARBON.2010.07.020` (cit. on p. 38).

[102] Y. Wada et al. "Photoinduced reaction of methylpolyynes H(CC)nCH3 (n = 5–7) and polyyne H(CC)5H with I2 molecules". In: *The European Physical Journal D 2012 66:12* 66 (12 Dec. 2012), pp. 1–6. ISSN: 1434–6079. DOI: `10.1140/EPJD/E2012-30545-X` (cit. on p. 39).

[103] Kirk and Othmer. "Peroxides and Peroxide Compounds, Organic Peroxides". In: *Kirk–Othmer Encyclopedia of Chemical Technology* 18 (), pp. 1–86 (cit. on p. 43).

[104] Toshio Hongo, Sakari Hikage, and Atsushige Sato. "Stability of Benzoyl Peroxide in Methyl Alcohol". In: *Dental Materials Journal* 25 (2 2006), pp. 298–302 (cit. on pp. 43, 44, 69, 75, 82).

[105] G G Makarov et al. "Kinetic study of thermal decomposition of Benzoyl Peroxide in Polyamide and degradation of polymer macromolecules". In: *Polymer Science U.S.S.R* 20 (1979), pp. 2882–2888 (cit. on p. 43).

[106] F Severini and R Gallo. *Differential scanning calorimetry study of thermal decomposition of Benzoyl Peroxide and 2,2' – Azobisisobutyronitrile mixtures*. 1984, pp. 561–566 (cit. on p. 43).

[107] T. W. Graham Solomons Craig B. Fryhle and Scott A. Snyder. *Organic Chemistry*. 12th. Wiley, Jan. 2016, p. 1124. ISBN: 978–1–118–87576–6 (cit. on p. 43).

[108] Eric M. Chellquist and William G. Gorman. "Benzoyl Peroxide Solubility and Stability in Hydric Solvents". In: *Pharmaceutical Research* 9 (10 1992), pp. 1341–1346 (cit. on pp. 43, 44, 46).

[109] Paul D. Bartlett and Kenzie Nozaki. "The Decomposition of Benzoyl Peroxide in Solvents. II. Ethers, Alcohols, Phenols and Amines". In: *Journal of the American Chemical Society* 69 (10 1947), pp. 2299–2306 (cit. on pp. 43, 44).

[110] W. E. Cass. "Kinetics of Decomposition of Benzoyl Peroxide in Solvents". In: *Journal of the American Chemical Society* 68 (1946), pp. 1976–1982 (cit. on p. 44).

[111] Kenzie Nozaki and Paul D Bartlett. "The Kinetics of Decomposition of Benzoyl Peroxide in Solvents. I". In: *Journal of the American Chemical Society* 86 (9 1946), pp. 1686–1692. DOI: 10.1021/ja01213a002 (cit. on p. 44).

[112] Ankush Gupta, Monica Gulati, and Narendra Kumar Pandey. "A validated UV spectrophotometric method for simultaneous estimation of Tretinoin and Benzoyl Peroxide in bulk and semi solid dosage form". In: *Rasayan Journal of Chemistry* 2 (3 2009), pp. 649–654. ISSN: 0974–1496 (cit. on p. 44).

[113] Herbert E Ungnade and Robert W Lamb. "Spectra of Benzoic Acid The Absorption Spectra of Benzoic Acid and Esters". In: *Journal of the American Chemical Society* 74 (15 1952), pp. 3789–3794 (cit. on pp. 44, 46).

[114] Ana Menéndez–Manjón, Philipp Wagener, and Stephan Barcikowski. "Transfer–matrix method for efficient ablation by pulsed laser ablation and nanoparticle generation in liquids". In: *Journal of Physical Chemistry C* 115 (12 Mar. 2011), pp. 5108–5114. ISSN: 19327447. DOI: 10.1021/JP109370Q (cit. on p. 49).

[115] A. Kanitz et al. "Review on experimental and theoretical investigations of the early stage, femtoseconds to microseconds processes during laser ablation in liquid–phase for the synthesis of colloidal nanoparticles". In: *Plasma Sources Science and Technology* 28 (10 Oct. 2019), p. 103001. ISSN: 0963–0252. DOI: 10.1088/1361-6595/AB3DBE (cit. on p. 70).

List of Figures

List of Tables

Acknowledgements

At the end of this thesis work, I would like to express my deep gratitude to Professor Carlo S. Casari, my advisor, for the great opportunity given to me with this work. I would also like to thank him and my co-advisor, Pietro Marabotti, for their patient guidance, for sharing their experience and for the useful critiques of this research, but also for the help in finalizing this work. I wish to extend my special thanks to the people of the EspLORE group for their enthusiastic encouragement and valuable suggestions, and to all the staff of the NanoLab for making the time of this thesis so enjoyable.

Finally, I would like to thank my family, my parents and my sister, for their support and for always giving me the opportunity to follow my passions.